Title
Sunlight inactivation of fecal indicator bacteria in open-water unit process wetlands

Author
Nguyen, Mi T.

Publication Date
2015

Peer reviewed|Thesis/dissertation

Sunlight inactivation of fecal indicator bacteria in open-water unit process wetlands

By

Mi Tra Nguyen

A dissertation submitted in partial satisfaction of

the requirements for the degree of

Doctor of Philosophy

in

Engineering - Civil and Environmental Engineering

in the

Graduate Division

of the

University of California, Berkeley

Committee in charge:

Professor Kara L. Nelson, Chair

Professor David L. Sedlak

Professor John D. Coates

Spring 2015

Sunlight inactivation of fecal indicator bacteria in open-water unit process wetlands

Mi Tra Nguyen

Abstract

Sunlight inactivation of fecal indicator bacteria in open-water unit process wetlands

by

Mi Tra Nguyen

Doctor of Philosophy in Engineering - Civil and Environmental Engineering

University of California, Berkeley

Professor Kara L. Nelson, Chair

Constructed wetlands harness natural processes to provide a low cost and energy technology for wastewater treatment. Although not the primary goal of wetland design, wetlands may remove and inactivate pathogens via a number of mechanisms including sunlight inactivation, predation, and sorption coupled to sedimentation. The contribution of sunlight inactivation is generally insignificant in vegetated wetlands due to light screening by emergent macrophytes and deep water. A novel wetland design, termed open-water wetlands, utilizes geotextile fabrics on the wetland bottom to prevent the growth of emergent vegetation. This allows sunlight to penetrate the shallow water column (<30 cm), thereby enhancing sunlight inactivation of pathogens. The goal of this research was to evaluate the potential of open-water wetlands to inactivate pathogens in secondary municipal wastewater effluent. To this end, indicator organism inactivation was monitored in a pilot-scale open-water wetland. In addition, to gain insight into inactivation mechanisms (e.g., endogenous versus exogenous inactivation), laboratory experiments were conducted using photosensitizer-free water, wetland water and simulated sunlight. These studies resulted in a descriptive model that predicts inactivation rates of bacteria in open-water wetlands and other sunlit water bodies.

As a first step towards developing a complete photoinactivation model for bacteria, a model was developed for a simpler organism (MS2 coliphage) considering only endogenous inactivation (Chapter 2; published in Environmental Science and Technology, 2014). The objective of the model was to account for wavelength specificity of photoinactivation, using a photoaction spectrum (PAS), and accounting for changes in the light spectrum due to season and attenuation in the water column. Experiments were set up to measure inactivation rates of MS2 in photosensitizer-free water in under natural sunlight in different seasons (one summer and one winter day), and in a wetland water column under simulated sunlight. The PAS model successfully predicted MS2 inactivation rates based on natural sunlight irradiances throughout the year, as well as in different water column depths. One of the challenges in developing and applying the PAS model was the uncertainty in measuring and predicting (using a radiative transfer model) sunlight irradiance in the range of 280 – 300 nm. The possibility of using total UVB as a simplified model parameter for estimating rates of endogenous inactivation was also tested using the experimental results. Although the total UVB model has a major limitation (it values each wavelength in the range of 280 – 320 nm equally), this simplified model can be used

for estimating endogenous inactivation rates of organisms whose photoaction spectra have not yet been measured.

To evaluate the performance of open-water wetlands in removing pathogens, fecal indicator bacteria concentrations were monitored in a pilot-scale open-water wetland over a one-year period (Chapter 3). The pilot-scale wetland provided effective inactivation of fecal indicator bacteria (up to 3-log and 2-log removal of *E. coli* and enterococci, respectively), primarily via sunlight inactivation. A novel model to predict endogenous and exogenous inactivation rates of fecal indicator bacteria in the wetland was developed and validated using data from laboratory experiments and field data. Endogenous inactivation was predicted using a total UV (sum of UVA and UVB irradiance) model. Exogenous inactivation was significant only for enterococci, and was modeled as a function of steady-state concentration of singlet oxygen in the bulk aqueous phase. The model was also applied to predict the land area required to achieve 3-log removal of fecal indicator bacteria throughout the year. Results suggested that during summer conditions in central California, open-water cells can provide greater than 3-log removal of non-pigmented fecal indicator bacteria in an area comparable to existing full-scale wetland systems.

To provide further insight into the role of dissolved organic matter (DOM) in the exogenous inactivation of indicator organisms, wetland DOM isolates from different wetland types (open-water, bulrush, and cattail) were prepared using solid-phase extraction and were tested for inactivation potential (Chapter 4). Inactivation of MS2 was enhanced by all wetland DOM isolates, as well as by two standard DOM isolates [Suwannee River Fulvic Acid (SRFA) and Pony Lake Fulvic Acid (PLFA)]. The steady-state concentration of singlet oxygen in the bulk phase of the DOM isolate solutions was positively correlated with the MS2 exogenous inactivation rate. For *Ent. faecalis*, inactivation was enhanced in solutions of wetland DOM isolates and PLFA; however, for the SRFA solution light screening dominated any photosensitizing effect. The degree of association of *Ent. faecalis* with DOM varied among the isolates, and a positive trend was observed between greater association and inactivation rate. Similar inactivation rates were observed in solutions of DOM isolates and their parent whole wetland water samples for *Ent. faecalis*, whereas for MS2, much lower inactivation rates were observed with the isolates than in the whole wetland water samples.

To quantify the effect of photosensitizer association on exogenous inactivation of fecal indicator bacteria, experiments were conducted measuring inactivation of *Ent. faecalis* (gram-positive) and *E. coli* (gram-negative) in the presence of a natural DOM and a model photosensitizer [Rose Bengal (RB)] at different Mg^{2+} concentrations (Chapter 5). Due to differences in cell wall structure, *Ent. faecalis* associated more strongly with DOM than *E. coli*. Inactivation of *Ent. faecalis* was enhanced by photosensitizer adsorption onto bacterial cells. Despite RB and EfOM association with *E. coli* cells, *E. coli* inactivation rates were not enhanced by adsorbed photosensitizers, likely due to the protection offered by the outer membrane. Inactivation of *Ent. faecalis* was not enhanced in irradiated solutions of polymer beads coated with RB (compared to sensitizer-free solutions), which were used to generate singlet oxygen in the absence of bacteria-sensitizer association, suggesting that association with photosensitizers is a prerequisite requirement for exogenous inactivation of *Ent. faecalis.*

A significant output of this research is the descriptive model to predict sunlight inactivation of fecal indicator bacteria, which can be used to evaluate designs for future applications of open-water wetlands. This research also produced several important outcomes.

First, the monitoring data of the pilot-scale open-water provided evidence that open-water unit process wetlands can achieve significant inactivation of fecal indicator bacteria. This finding can be used to promote the adoption of the novel open-water wetland design for pathogen removal, as a component of multi-barrier approaches to control pathogen transmission, or to reduce the use of chemical disinfectants. Second, insight into the exogenous mechanism of fecal indicator bacteria inactivation suggested that the association between photosensitizers and bacterial cells plays a key role in exogenous inactivation for the gram positive model species *Ent. faecalis*. Third, lab-cultured bacteria were inactivated significantly more rapidly than indigenous wastewater indicator bacteria, emphasizing that lab-cultured indicators should not be used to determine inactivation rate constants for indigenous bacteria.

TABLE OF CONTENTS

TABLE OF CONTENTS ..... **II**

LIST OF FIGURES ..... **V**

LIST OF TABLES ..... **VIII**

ACKNOWLEDGMENTS ..... **IX**

CHAPTER 1. INTRODUCTION **1**

1.1 MOTIVATION 2

1.2 TREATMENT WETLANDS 2

1.3 REMOVAL AND INACTIVATION OF PATHOGENS AND INDICATORS IN TREATMENT WETLANDS 4

1.4 RESEARCH OBJECTIVES 6

1.4.1 Objective 1. Evaluate models for predicting endogenous inactivation of MS2 coliphage in photosensitizer-free water *6*

1.4.2 Objective 2. Evaluate sunlight inactivation of fecal indicator bacteria in open-water wetlands *6*

1.4.3 Objective 3. Determine the effects of natural photosensitizers in different cells of unit process wetlands on exogenous inactivation of fecal indicator bacteria and virus *7*

1.4.4 Objective 4. Evaluate the effects of association between photosensitizers and indicator organisms to exogenous sunlight inactivation *7*

CHAPTER 2. SUNLIGHT INACTIVATION OF MS2 COLIPHAGE IN THE ABSENCE OF PHOTOSENSITIZERS: MODELING THE ENDOGENOUS INACTIVATION RATE USING A PHOTOACTION SPECTRUM AND TOTAL UVB IRRADIANCE. **8**

2.1 INTRODUCTION 9

2.2 MATERIALS AND METHODS 10

2.2.1 MS2 Propogation and Enumeration *10*

2.2.2 Experimental approach *10*

2.2.3 Data analysis *12*

2.2.4 Statistical tests *17*

2.3 RESULTS AND DISCUSSION 17

2.3.1 Comparison of observed and modeled inactivation of MS2 using PAS model in photosensitizer-free water under natural sunlight *17*

2.3.2 Comparison of observed and modeled inactivation rates of MS2 using PAS model in photosensitizer-free water in wetland water under simulated sunlight *27*

2.3.3 Comparison of observed and modeled inactivation rates of MS2 using PAS model in photosensitizer-free water under simulated sunlight from previous studies *28*

2.3.4 Limitations and challenges of using the PAS model to predict endogenous inactivation rate of an organism *29*

2.3.5 Possibility of using the tUVB model to predict endogenous inactivation rate of an organism *31*

CHAPTER 3. SUNLIGHT INACTIVATION OF FECAL INDICATOR BACTERIA IN OPEN-WATER UNIT PROCESS TREATMENT WETLANDS: MODELING ENDOGENOUS AND EXOGENOUS INACTIVATION RATES **34**

3.1 INTRODUCTION 35

3.2 MATERIALS AND METHODS 35

3.2.1 Experiments at the pilot-scale open-water wetland *36*

3.2.2 Lab experiments *43*

3.2.3 Modelling inactivation of FIB in in-situ batch reactors and the open-water wetland *45*

3.2.4 Comparison of modeled and measured inactivation *49*

3.2.5 Statistical tests *49*

3.3 RESULTS 50

3.3.1 Removal of the FIB in the open-water wetland *50*

3.3.2 Inactivation of lab-cultured bacteria under simulated sunlight *52*

3.3.3 Sunlight inactivation of lab-cultured FIB versus indigenous wastewater FIB *54*
3.3.4 Modeling inactivation of the FIB in open-water wetland *57*
3.4 DISCUSSION 62
3.4.1 Contribution of endogenous and exogenous mechanisms to sunlight inactivation of lab-cultured bacteria under simulated sunlight *62*
3.4.2 Lab-cultured bacteria as indicators for indigenous bacteria and pathogens in open-water wetlands receiving wastewater *63*
3.4.3 Comparison with High Rate Algal Ponds *63*
3.4.4 Modeling the inactivation of the FIB in the open-water wetland *64*
3.4.5 Estimation of wetland area necessary for inactivation of the FIB *64*

CHAPTER 4. NATURAL PHOTOSENSITIZERS IN CONSTRUCTED UNIT PROCESS WETLANDS: SPECTROSCOPIC CHARACTERIZATION, PRODUCTION OF REACTIVE SPECIES AND EFFECT ON INACTIVATION OF INDICATOR ORGANISMS 66
4.1 INTRODUCTION 67
4.2 MATERIALS AND METHODS 68
4.2.2 Field site and sampling. *68*
4.2.3 Concentration and isolation of DOM from unit process wetlands. *69*
4.2.4 Spectroscopic characterization of wetland waters, wetland DOM isolates and standard DOM solutions. *69*
4.2.6 Formation of reactive species and calculation of quantum yields. *71*
4.2.7 Inactivation of pathogen indicators. *72*
4.2.8 Association between Ent. faecalis and the DOM isolates. *73*
4.3 RESULTS AND DISCUSSION 73
4.3.1 Isolation and spectroscopic characterization of the wetland DOM isolates. *73*
4.3.2 Photochemical reactive species formation in wetland waters and wetland DOM isolates. *76*
4.3.3 Role of DOM in sunlight inactivation of MS2 ..... *79*
4.3.4 Role of DOM in sunlight inactivation of Ent. faecalis. *83*
4.3.5 Implications for unit process wetlands design. *88*

CHAPTER 5. EFFECTS OF ASSOCIATION BETWEEN PHOTOSENSITIZERS AND INDICATOR ORGANISMS TO EXOGENOUS INACTIVATION. 89
5.1 INTRODUCTION 90
5.2 MATERIALS AND METHODS 91
5.2.1 Chemicals and analytical instruments *91*
5.2.2 Synthesis of RB-immobilized beads *91*
5.2.3 Isolation of EfOM *92*
5.2.4 Indicators for sunlight inactivation experiments *92*
5.2.5 Irradiation experiments *93*
5.2.6 Measuring bulk-phase steady-state concentration of singlet oxygen *94*
5.2.7 Measuring association between the indicators and RB-Beads *94*
5.2.8 Association of bacterial cells to photosensitizers *94*
5.2.9 Data analysis *95*
5.3 RESULTS AND DISCUSSION 95
5.3.1 Association between dissolved photosensitizers and bacterial cells *95*
5.3.2 Effect of association between dissolved photosensitizers and bacterial cells to sunlight inactivation *97*
5.3.3 Inactivation of indicator microorganisms in clear water with addition of RB-Beads *99*
5.3.4 Implication for exogenous inactivation of bacteria *103*

CHAPTER 6. CONCLUSIONS 104
6.1 SUMMARY 105
6.2 SUNLIGHT INACTIVATION OF INDICATORS IN OPEN-WATER WETLANDS 105
6.3 EFFECTS OF PHOTOSENSITIZERS TO EXOGENOUS INACTIVATION 106
6.4 FUTURE RESEARCH 107

REFERENCES 109

LIST OF FIGURES

Figure 1.1. Plan-view diagram of the pilot-scale unit process wetlands and photograph of the open-water cell in Discovery Bay, CA. 4

Figure 1.2. Removal efficiency of fecal indicator microorganisms and pathogens in free water surface wetlands receiving non-disinfected influent. 5

Figure 2.1. UVB irradiance of simulated sunlight measured by spectroradiometer, and natural sunlight at noon on June 27, 2012 in Berkeley 11

Figure 2.2. Wetland water absorbance and scalar simulated sunlight irradiance at various depths in the wetland water column. 12

Figure 2.3. Inactivation of MS2 under simulated sunlight in quartz tubes and open beakers 13

Figure 2.4. Inactivation of MS2 under natural sunlight as a function of time during a winter day and a summer day 18

Figure 2.5. Observed and modeled inactivation rates of MS2 under natural sunlight in winter and summer. . 19

Figure 2.6. Solar UV irradiance during the winter experiment 20

Figure 2.7. Solar UV irradiance during the summer experiment 22

Figure 2.8. MS2 photodamage coefficients during the winter experiment 24

Figure 2.9. MS2 of photodamage coefficients during the summer experiment 25

Figure 2.10. Irradiance of simulated sunlight measured in this study, and reported by the reviewed MS2 inactivation publications 25

Figure 2.11. Computed time needed for 1-log removal of MS2 in clear water under clear sky conditions at different latitudes over the course of a year. 27

Figure 2.12. Observed and modeled endogenous inactivation rates of MS2 at different depths in wetland water. 28

Figure 2.13. Comparison of observed and modeled inactivation rates of MS2 in photosensitizer-free water 29

Figure 2.14. Comparison between observed and modeled inactivation rates of MS2 in photosensitizer-free solution at different depths in wetland water under simulated sunlight. 32

Figure 2.15. Relationship between total UVB irradiance and MS2 k_{obs} in photosensitizer-free solution. 33

Figure 3.1. Recorded data of temperature, pH, and dissolved oxygen over 84 hours at the inlet and outlet of the open-water wetland cell during clear skies. 38

Figure 3.2. Average DOC concentrations and UV-VIS absorbance of water collected from different locations at the open-water wetland. 39

Figure 3.3. 24-hour averaged solar irradiance on the 21st day of each month throughout the year at Discovery Bay, CA. 39

Figure 3.4. Estimated scalar solar irradiance at summer noon at different depths 40

Figure 3.5. Measured inactivation rate constants of the FIB in in-situ batch reactors fed with 100% influent and 50% influent+50% effluent of the open-water wetland. 41

Figure 3.6. Solar simulator outputs in lab inactivation experiments with atmospheric attenuation filter and UVB-blocking filter. 45

Figure 3.7. Concentrations of the FIB at different locations in the wetland cell in different months throughout the year 51

Figure 3.8. Concentrations of pigmented and non-pigmented enterococci determined from pigmentation test results 52

Figure 3.9. Inactivation rate constants of lab-cultured and field isolated FIB in clear water and wetland water under full spectrum and UVB-blocked simulated sunlight 53

Figure 3.10. Inactivation rate constants as functions of time and as functions of photon fluence of indigenous wastewater FIB in comparison with lab-cultured FIB 55

Figure 3.11. Comparison between observed and modeled inactivation rate constants of the FIB in in-situ batch reactors 56

Figure 3.12. Log removal values based on monitoring data and the best-fit line for *E. coli* in different months at Discovery Bay open-water wetland. 58

Figure 3.13. Log removal values based on monitoring data and the best-fit line for pigmented enterococci in different months at Discovery Bay open-water wetland. 59

Figure 3.14. Log removal values based on monitoring data and the best-fit line for non-pigmented enterococci in different months at Discovery Bay open-water wetland. 60

Figure 3.15. Comparison between observed and modeled inactivation rate constants of the FIB in the open-water wetland in different months of the year 61

Figure 3.16. Area predicted from model to provide 3-log removal of the FIB from 1 MGD of wastewater effluent in open-water treatment wetlands during different seasons 65

Figure 4.1. Specific absorption coefficient spectra of whole water samples and DOM isolates in comparison with standard DOMs. 74

Figure 4.2. $SUVA_{254}$ and spectral slopes of whole water samples, wetland DOM isolates, and total SPE discharges in comparison to standard DOMs 75

Figure 4.3. Specific absorption coefficient spectra of cattail wetland effluent as an example for wetland water samples subject to SPE.. 76

Figure 4.4. Steady-state concentration of singlet oxygen in the bulk phase and TMP depletion rate constants of cattail wetland effluent samples as an example for wetland water samples during SPE 77

Figure 4.5. Linear regression relationship between steady-state concentration of singlet oxygen in the bulk phase and DOC concentration 78

Figure 4.6. Singlet oxygen quantum yields and TMP quantum yield coefficients of wetland water samples, DOM isolates and standard DOMs 79

Figure 4.7. Inactivation rates of MS2 in DOM isolates as a function of [DOC] under UVB- blocked simulated sunlight 80

Figure 4.8. The observed inactivation rates of MS2 as a function of steady-state concentration of singlet oxygen in the bulk phase 82

Figure 4.9. Inactivation rates of MS2 in wetland waters, total SPE discharges, and total SPE discharges with addition of DOM isolates..... 83

Figure 4.10. Inactivation rates of *Ent. faecalis* in solutions of DOM isolates as a function of [DOC] under UVB-blocked simulated sunlight..... 84

Figure 4.11. The observed inactivation rates of *Ent. faecalis* as a function of steady-state concentration of singlet oxygen in the bulk phase..... 85

Figure 4.12. Inactivation rates of *Ent. faecalis* in whole wetland waters and total SPE discharges..... 85

Figure 4.13. Normalized mass of DOM adsorbed onto *Ent. faecalis* cells..... 87

Figure 5.1. Normalized mass of adsorbed photosensitizer onto *Ent. faecalis* and *E. coli* in the absence and presence of Mg^{2+}..... 97

Figure 5.2. Observed inactivation rates of *Ent. faecalis* and *E. coli* in RB solutions and the EfOM solutions with or without the addition of Mg^{2+} 99

Figure 5.3. Steady-state concentration of singlet oxygen produced in clear water with addition of RB-Beads or uncoated beads under UVB-blocked simulated sunlight or dark condition..... 101

Figure 5.4. Number of microorganisms associated with membrane filter and RB-Beads in clear water. 102

LIST OF TABLES

Table 2.1. Photoaction spectrum sensitivity coefficients for MS2 14

Table 2.2. Inputs to the SMARTS model..... 14

Table 2.3. Total UVB irradiance and its distribution from different light sources in MS2 inactivation experiments. 30

Table 3.1. Summary of experiments conducted in Chapter 3. 36

Table 3.2. 16S rRNA sequences of two chosen enterococcal isolates used in this study. 43

Table 3.3. Lab-cultured bacteria used in Chapter 3. 44

Table 3.4. Values of solar zenith angle at Discovery Bay, CA at noon on the 21st of each month..... 46

Table 3.5. Data from lab experiments used to calculate k_2 values for lab-cultured pigmented and non-pigmented enterococcal isolates. 54

Table 3.6. Partition of pigmented and non-pigmented enterococci in the open-water wetland at different locations and in in-situ batch reactors at different time points.. 57

Table 3.7. Measured and modeled inactivation rate constants of FIB in in-situ batch reactors..... 57

Table 3.8. Modeled inactivation rate constants of indigenous wastewater FIB in the open-water wetland in different months.. 62

Table 4.1. Characteristics of wetland water samples, DOM isolates and solid phase extraction discharges..... 70

Table 4.2. Concentration of TOC in initial samples and SPE discharge. 76

Table 4.3. Linear regression of MS2 observed inactivation rates and steady-state concentration of singlet oxygen in the bulk phase produced in the DOM isolates..... 82

Table 4.4. Linear regression slope from the k_{photon} vs. [DOC] as a function of the mass of adsorbed DOM. 87

ACKNOWLEDGMENTS

Thank you, Prof. Kara Nelson, for being a great advisor and supporter. I have learnt so much from you during this journey.

Thank you, Prof. David Sedlak, for your help and support.

Thank you, Justin Jasper, Samantha Bear, and Andrea Silverman, for being amazing friends.

Thank you, Ariel Grostern, Jannis Wenk, Anh Pham, Rong Chao Bi, Iris Schilling, Brie Webber, Rabia Chaudhry, Andy Torkelson, Negassi Hadgu, Carsten Prasse, Yujie Men, Xinwei Mao, Tom Bruton, Wei Zhuang, and Shan Yi, for helping me with my tedious labwork.

And thank you, my family, for always being with me!

CHAPTER 1. Introduction

1.1 Motivation

Constructed wetlands, through a combination of natural processes (e.g., sunlight inactivation, attachment and sedimentation, and predation), have the potential to remove pathogens from wastewater. They can potentially be used to provide safe effluent for discharge or reuse, to reduce chemical or UV disinfection requirements, and to lower operation costs and energy usage compared to mechanical wastewater treatment. Alternatively, constructed wetlands used as a polishing step in combination with chemical or UV disinfection have the advantage of providing multiple barriers for pathogen removal, enhancing the removal of pathogens resistant to chlorine or UV. However, to provide efficient and reliable inactivation of pathogens, treatment wetlands must be designed based on a thorough understanding of pathogen inactivation mechanisms.

Unit process wetlands consist of a series wetland cells that are specialized to treat specific contaminants via different mechanisms. A shallow, open-water cell integrated in unit process wetlands is designed to promote sunlight inactivation, which is normally insignificant in conventional treatment wetlands due to shading of the water column by emergent vegetation and deep water. This research evaluated sunlight inactivation of pathogens in open-water wetlands receiving municipal wastewater effluent and quantified important sunlight inactivation mechanisms, allowing for the design and management of effective wetland cells which can be integrated into unit process wetland systems.

1.2 Treatment wetlands

The application of constructed wetlands as a natural treatment system for wastewater effluent has been practiced for at least five decades (Vymazal, 2011). As a biologically productive ecosystem, treatment wetlands can remove nutrients and transform pollutants [e.g., nitrate, biological oxygen demand (BOD), metals] from wastewater effluent (Kadlec and Wallace, 2009). The operation of treatment wetlands also provides a number of ancillary benefits including green space for recreational opportunities, wildlife viewing, and habitat creation (Fleming-Singer and Horne, 2006).

Two common designs of treatment wetlands are free water surface and subsurface flow wetlands (Kadlec and Wallace, 2009). Free water surface wetlands contain above-ground flow of water through vegetation of open ponds, whereas subsurface flow wetlands have water flow beneath a media bed that may be planted with vegetation (Kadlec and Wallace, 2009). Subsurface flow wetlands are employed especially in cases where the risk of water exposure associated with human or wildlife needs to be minimized (e.g., industrial wastewater). Operational performance, size, and cost are commonly used to determine the wetland type for wastewater treatment (Kadlec, 2009). Subsurface flow wetlands are generally more expensive than free water surface wetlands due to the cost of additional material for filter media (Kadlec, 2009). Decentralized treatment wetlands are normally subsurface wetlands due to their small size and the ability to be embedded in building architecture (US EPA, 2001). Free water surface wetlands with larger sizes are commonly chosen as a centralized wastewater treatment technology to remove nutrients in pretreated wastewater effluents or river water (Jasper et al., 2013). Besides treating nutrients, BOD, and metals, both free water surface and subsurface flow wetlands have the potential to reduce concentrations of other contaminants, including pathogens and trace organic chemicals (Kadlec and Wallace, 2009).

To enhance the removal of pathogens and other contaminants, a novel approach for treatment wetland design is unit process wetlands, in which each wetland cell is designed to treat a specific contaminant or group of contaminants (Horne and Fleming-Singer, 2005; Jasper et al., 2013). With the design and operation of wetlands as a sequence of cells, it is expected that unit process wetlands can provide more effective and reliable removal of pathogens and other contaminants than conventional treatment wetlands (Jasper et al., 2013).

To demonstrate the ability of treatment wetlands to operate as unit processes to remove contaminants from wastewater effluent, a pilot-scale unit process wetland system was constructed in Discovery Bay, CA (Figure 1.1). The wetland system consisted of four different cells, including a shallow, open-water cell that lacks emergent macrophytes, and three vegetated wetlands [two bulrush (*Scirpus* spp.) cells and one cattail (*Typha* spp.) cell]. All wetlands received non-disinfected nitrified wastewater from an adjacent oxidation ditch at the Discovery Bay wastewater treatment plant. The bulrush and cattail wetlands were designed for denitrification, metal sequestration, and biotransformation of trace organic contaminants. The shallow, open-water wetland was designed to enable sunlight to penetrate the whole water column and to allow algae to grow on the cell bottom to produce dissolved oxygen. These conditions were hypothesized to promote photolysis of trace organic contaminants and sunlight inactivation of pathogens in wastewater, processes which are generally insignificant in vegetated wetlands due to shading of vegetation.

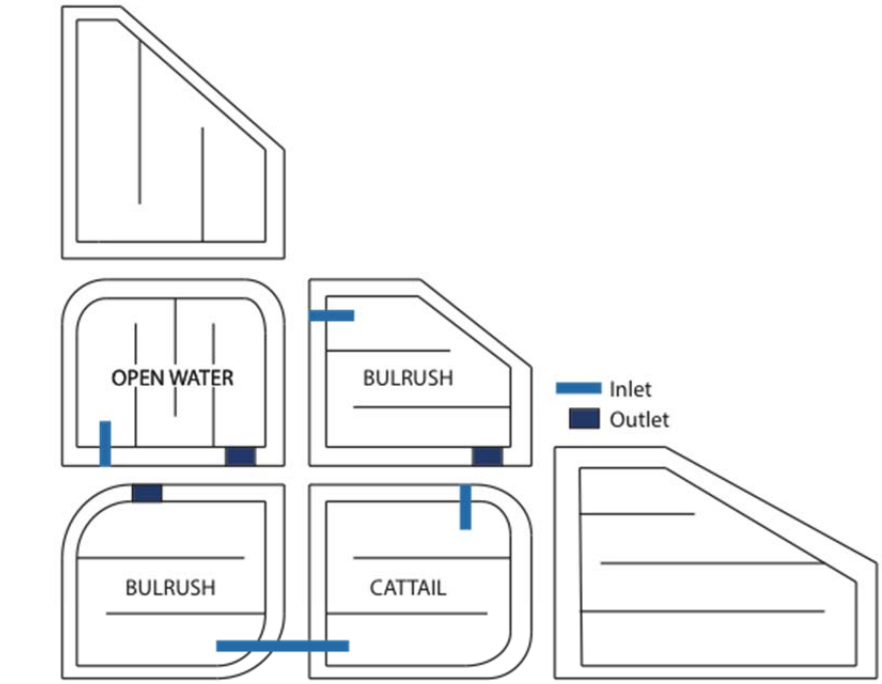

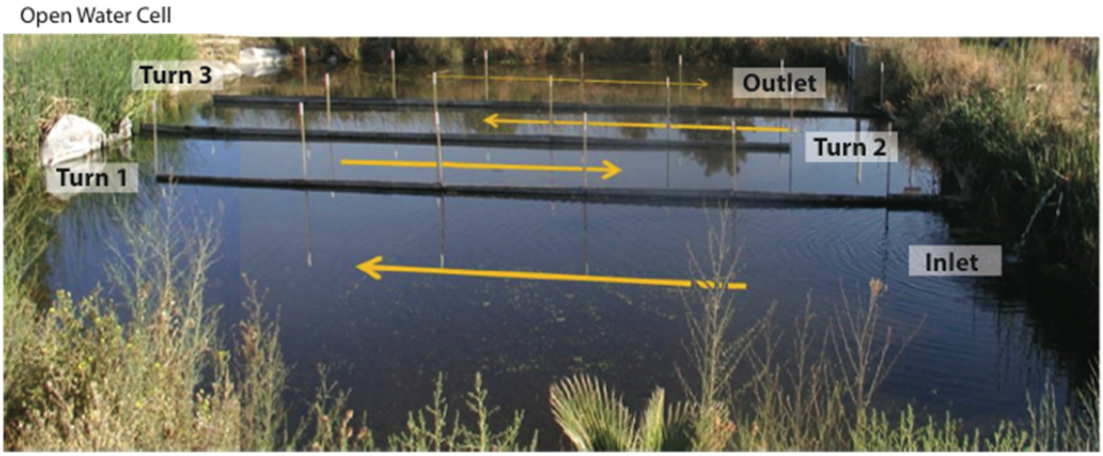

Figure 1.1. Plan-view diagram of the pilot-scale unit process wetlands and photograph of the open-water cell in Discovery Bay, CA. Arrows demonstrate flow direction and sampling points are indicated (i.e., inlet, turns 1, 2, 3, and outlet). Photo credit: Justin Jasper.

1.3 Removal and inactivation of pathogens and indicators in treatment wetlands

Wastewater effluent contains potentially infectious microorganisms, including viruses, bacteria, protozoan (oo)cysts, and helminth eggs. Removal or inactivation of pathogens is therefore necessary before treated wastewater effluent is discharged or reused. It has been shown that free water surface wetlands designed to treat other contaminants (e.g., BOD, nutrients, metals) are capable of providing modest removal [i.e., ~1-log (90%)] of fecal indicator organisms as well as human pathogens (Figure 1.2).

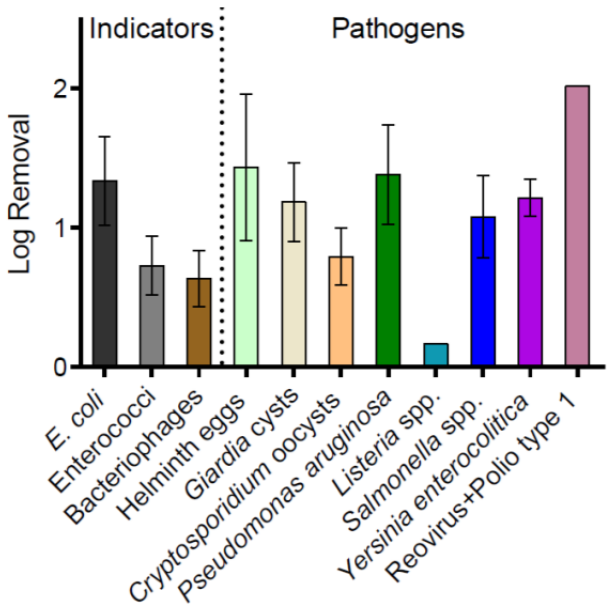

Figure 1.2. Removal efficiency of fecal indicator microorganisms and pathogens in free water surface wetlands receiving non-disinfected influent. Reproduced from data collected by Kadlec and Wallace (Kadlec and Wallace, 2009).

Most studies on the removal of pathogens in treatment wetlands have employed measurements of indicator organisms (e.g., fecal indicator bacteria, bacteriophage) rather than actual pathogens. Indicators are used to study the fate of pathogens due to the high cost and technical challenges in measuring concentrations of human pathogens in environmental samples (Bonde, 1963; Maier et al., 2009). The reduction of pathogen and indicator concentrations in treatment wetlands with emergent macrophytes is caused by natural cell die-off, predation, attachment and sedimentation, and sunlight inactivation (Kadlec and Wallace, 2009). Among four types of pathogens, helminth eggs and protozoa (oo)cysts are larger in size and mainly removed via attachment and sedimentation (Quiñónez-Díaz et al., 2001; Sengupta et al., 2011), while viruses and bacteria are subject to a wider range of removal and inactivation mechanisms.

Sunlight inactivation, an important mode of disinfection in waste stabilization ponds (Davies-Colley, 2005) and other sunlit waters (Boehm et al., 2009; McGuigan et al., 2012; Sinton et al., 1999), can occur via three mechanisms: direct inactivation, indirect endogenous inactivation, and indirect exogenous inactivation (Davies-Colley et al., 1999; Silverman et al., 2013). Direct and indirect endogenous mechanisms occur when a component in the microorganism absorbs sunlight, and causes damage to itself or other essential cell components. Exogenous inactivation involes sunlight absorption by photosensitizers in the water column that generate reactive intermediates, which subsequently cause damage to the microorganism. Important reactive intermediates include singlet oxygen ($^1O_2$), hydrogen peroxide (H_2O_2), superoxide (O_2^-), and hydroxyl radical (•OH) (Cooper et al., 1989). In a shallow, open-water wetland, direct and indirect endogenous mechanisms are important because solar UV light is able to penetrate throughout the water column. Exogenous inactivation is enhanced by natural photosensitizers present in nitrified wastewater or produced by plants and microbes in the

wetland. The contribution of each mechanism to sunlight inactivation of pathogens is expected to vary based on water quality and pathogens' physiology.

1.4 Research objectives

The main goal of this research was to study sunlight inactivation of fecal indicator bacteria in open-water unit process wetlands. *Escherichia coli* and *Enterococcus* spp. representing gram-negative and gram-positive bacteria, respectively, were used as fecal indicator bacteria in this research. Additionally, MS2 coliphage was used as an indicator for human viruses in some experiments in the laboratory. Concentrations of the indicator bacteria in a pilot-scale, open-water wetland were monitored over a year to evaluate the performance of pathogen removal in the wetland. Experiments were conducted in the laboratory to investigate the susceptibility of each indicator organism to sunlight inactivation in the open-water wetland. Results from laboratory and field experiments, along with knowledge of modeling sunlight inactivation of indicator viruses were used to develop a descriptive model for prediction of sunlight inactivation of fecal indicator bacteria in open-water wetlands. The exogenous inactivation mechanism was further studied with DOM isolated from different cells in the pilot-scale unit process wetlands. The effects of association between photosensitizers and indicators on their exogenous inactivation were also investigated. The specific objectives of the research are as follows:

1.4.1 Objective 1. Evaluate models for predicting endogenous inactivation of MS2 coliphage in photosensitizer-free water

To evaluate the accuracy of a photoaction spectrum (PAS) model to predict endogenous inactivation rates of microorganisms in sunlit water areas, experiments with MS2 coliphage in sensitizer-free water were conducted. The first set of experiments was conducted under natural sunlight on a winter and a summer day to test the accuracy of the PAS model to predict the diurnal and seasonal effects of natural sunlight on inactivation rates. The second set of experiments was conducted to determine whether the model could accurately predict the effects of light screening on inactivation rates at different water depths. The possibility of using a simplified total UVB model to estimate endogenous inactivation rates of microorganisms for which a PAS has not yet been measured was also investigated.

1.4.2 Objective 2. Evaluate sunlight inactivation of fecal indicator bacteria in open-water wetlands

The ability of open-water wetlands to enhance sunlight inactivation was evaluated by monitoring concentrations of fecal indicator bacteria at different locations in a pilot-scale open-water wetland for one year. In addition, laboratory experiments were conducted with lab-cultured indicator bacteria and wetland water under different light conditions to provide a better understanding of the sunlight inactivation mechanisms in the open-water wetland. A novel modeling approach was developed based on results from laboratory experiments to predict endogenous and exogenous inactivation rates of indicator organismss in the wetland. The model accuracy was evaluated using the monitoring data from the wetland. Using the model, the open-water wetland area necessary for efficient removal of the indicators ($A^{1}_{3-\log}$) was estimated. To explain the low removal of enterococci in the open-water wetland, pigmentation tests were carried out to test for the presence of pigmented enterococci, which were shown to be more

resistant to sunlight inactivation. A side-by-side experiment was conducted with lab-cultured and indigenous wastewater bacteria to determine the difference between lab and field conditions.

1.4.3 Objective 3. Determine the effects of natural photosensitizers on exogenous inactivation of fecal indicator bacteria and viruses

DOM in the influent and effluents of the open-water wetland and two vegetated wetlands (bulrush and cattail) was isolated to study the effects of natural photosensitizers on exogenous inactivation of fecal indicators (*Ent. faecalis* and MS2). Spectroscopic properties and light-induced formation of reactive species ($^1O_2$, •OH and $^3DOM^*$) of the DOM were quantified to determine the characteristics of the wetland DOM isolates and were related to indicator organism inactivation rates. Results from characterization and inactivation experiments were used to determine the role of the wetland DOM isolates in exogenous inactivation of the indicators. Two standard DOMs (Suwannee River Fulvic Acids and Pony Lake Fulvic Acids) were included in the study for comparison.

1.4.4 Objective 4. Evaluate the effects of association between photosensitizers and indicator organisms on exogenous sunlight inactivation

The role of association between indicator bacteria and photosentisitizers (Rose Bengal and EfOM) in exogenous sunlight inactivation of indicator bacteria was studied. *Ent. faecalis* and *E. coli* were used as indicators for gram-negative and gram-positive bacteria, respectively. Inactivation experiments with photosensitizer solutions in the absence and presence of the divalent cation Mg^{2+}, which enhances association, were conducted to determine if greater association increased inactivation. Correlation tests were performed to evaluate the relationship between photosensitizer association and bacterial inactivation rates. To determine whether inactivation could occur in the absence of association between photosensitizers and indicator bacteria, inactivation experiments were conducted using synthesized polymer beads coated with Rose Bengal as a source of exogenous singlet oxygen.

CHAPTER 2. Sunlight inactivation of MS2 coliphage in the absence of photosensitizers: Modeling the endogenous inactivation rate using a photoaction spectrum and total UVB irradiance

Reproduced with permission from Mi T. Nguyen[1]; Andrea I. Silverman[2]; and Kara L. Nelson[3]. Effects of association between photosensitizers and indicator organisms to exogenous inactivation. *Environ. Sci. Technol.* **2014**, *48* (7), 3891–3898.

[1]Primary author and researcher

[2]Author and researcher of the total UVB model

[3]Editor and advisor

2.1 Introduction

Sunlight disinfection is an important process contributing to inactivation of viruses in natural and engineered sunlit waters, including waste stabilization ponds (Davies-Colley et al., 2000, 1999), seawater (Boehm et al., 2009; Sinton et al., 1999), and solar disinfection of drinking water (SODIS) (Fisher et al., 2012; Reed, 2004). Viruses can be inactivated via three possible mechanisms (Silverman et al., 2013). The first two – the direct and indirect endogenous mechanisms – involve photon absorption by the virus itself; the direct mechanism causes damage to the virus component that absorbed the photon (i.e., nucleic acids or proteins) (Davies and Truscott, 2001; Jagger, 1985), while the indirect endogenous mechanism occurs if photosensitizers located within the virus absorb photons and form reactive intermediates (e.g., excited state species and radicals) (Davies and Truscott, 2001; Davies, 2003) that cause damage to other components of the virus. The third mechanism, the exogenous mechanism, differs in that it relies on the absorption of photons by photosensitizers present in the water column [e.g., natural organic matter (NOM)] that form reactive intermediates [i.e., excited triplet states or reactive oxygen species (ROS)], which can damage virus components (Kohn and Nelson, 2007; Rosado-Lausell et al., 2013). All three mechanisms are wavelength dependent. While exogenous photosensitizers can absorb light in the UVB (280–320 nm), UVA (320–400 nm), and visible light regions, nucleic acids and proteins have negligible absorption at wavelengths above 320 nm, such that the waterborne non-enveloped viruses studied to date have negligible inactivation from wavelengths above 320 nm (Love et al., 2010; Silverman et al., 2013).

Models that predict the inactivation rates of viruses in surface waters can be used to design natural wastewater treatment systems and manage recreational water quality. As a step towards developing a model for virus inactivation in sunlit waters, Fisher et al. (2011) determined photoaction spectra (PAS) for the endogenous inactivation (combined direct and indirect) of two bacteriophages, MS2 and PRD1, based on their responses to polychromatic simulated sunlight in clear water containing no exogenous photosensitizers. PAS, which consist of wavelength-specific spectral sensitivity coefficients [$P(\lambda)$, $m^2\ W^{-1}\ h^{-1}$], allow for the estimation of endogenous inactivation rates under different sunlight conditions (Fisher et al., 2011). To date, the accuracies of the PAS model of the viruses have only been tested in clear water using a solar simulator.

The main objective of this study was to evaluate the ability of the PAS model to predict the endogenous inactivation rate of MS2 under natural sunlight and in waters containing light-attenuating substances, which more accurately reflect environmental conditions. We compared MS2 endogenous inactivation rates predicted using the PAS model with those measured experimentally under two conditions: (1) in clear water under natural sunlight in the winter and summer, to capture diurnal and seasonal changes in solar irradiance; and (2) in wetland water under simulated sunlight to capture the effects of light attenuation by NOM in the water column. Evaluating the accuracy of the PAS model is an important step towards developing models that estimate total inactivation rates of viruses in sunlit environments (i.e., endogenous and exogenous photoinactivation, as well as dark processes). In addition, we investigated the possibility of using a simplified model, which was developed based on the linear relationship between total UVB (tUVB) irradiance and observed inactivation rates for predicting MS2 endogenous inactivation rates under the two experimental conditions mentioned above. The

tUVB model option was considered to estimate the endogenous inactivation rates of organisms for which no PAS currently exist.

2.2 Materials and Methods

2.2.1 MS2 Propogation and Enumeration

Detailed virus propagation, purification and enumeration methods have been described elsewhere (Fisher et al., 2011; Love et al., 2010). Briefly, MS2 (ATCC 15597-B1) was propagated by broth enrichment using the *E. coli* F_{amp} host (ATCC 700891). To remove broth constituents, crude MS2 stocks were chloroform extracted (1:3 vol/vol) and precipitated overnight in polyethylene glycol solution (8% PEG 6000, wt/vol; 0.3 M NaCl) at 4 °C. The solution was centrifuged at 23,000×g for 30 min to produce virus pellets, which were resuspended in phosphate buffered saline (PBS: 4 mM NaH_2PO_4, 16 mM Na_2HPO_4, and 10 mM NaCl; pH 7.5), chloroform extracted as above, and filtered through a 0.22 μm filter. Purified bacteriophage stocks were stored at -80 °C. Bacteriophage were assayed using the double agar layer (DAL) method with 100-μL sample inocula, and modified Luria Burtani (LB) top and bottom agar. Modified LB agar includes the following ingredients: Bacto Agar [0.75% (top) or 1.5% (bottom) wt/vol; BD], 10 g L^{-1} Bacto Tryptone (BD), 0.137 M NaCl, 1 g L^{-1} yeast extract (EMD Chemicals), 0.0055 M dextrose (EMD Chemicals), 0.002 M $CaCl_2$ (Fisher). DAL plates were incubated at 37 °C for 18–24 h and plaque forming units (PFU) were counted.

2.2.2 Experimental approach

Experiments were conducted either under natural sunlight (to capture the effects of diurnal and seasonal variation in solar irradiance) or simulated sunlight (to determine the ability of the model to account for spectral light attenuation with depth in a sample of wetland water). All experiments were conducted with MS2 in photosensitizer-free water, thus the observed inactivation rates are a result of endogenous inactivation mechanisms only. MS2 stock solution was diluted in PBS to initial concentrations of 10^6 PFU mL^{-1} for experiments under natural sunlight, and 10^4 PFU mL^{-1} for light attenuation experiments. Quartz tubes (10.5 mm inner diameter, 12.75 mm outer diameter, 100 mm length; Technical Glass Products, Inc.; Painesville Township, OH) were filled with 8.4 mL of MS2 in PBS and closed with polyethylene chloride caps (Polyethylene Press snap cap; Fisher Scientific) with minimal headspace. Quartz tubes were used to allow light transmission at all sunlight wavelengths. During all experiments, triplicate samples were collected at each time point: three tubes were collected sacrificially, and sub-samples from the collected tubes were frozen at -80°C until analysis by DAL plaque assay (within 2 d). Dark controls were maintained under the same conditions as light samples, but wrapped in aluminum foil.

Experiments under natural sunlight. Quartz tubes containing MS2 in PBS were placed on an aluminum tray that was painted black and submerged in a water bath maintained around 20°C. The tubes were exposed to sunlight in Berkeley, California (37°52’27”, -122°15’32”) from 9:30 to 15:30 on a sunny winter day (01/28/2012) and 8:00 to 18:00 on a sunny summer day (06/27/2012). Solar irradiance was measured every 30 minutes throughout the day using a spectroradiometer with a cosine detector (EPP2000-HR, CR2; StellarNet Inc.; Tampa, FL) positioned in a parallel plane to the quartz tubes. The cosine detector was covered by a 10% aperture to allow measurement of light that is 10 times brighter than the detector limit.

Light attenuation experiments under simulated sunlight. Quartz tubes containing MS2 in PBS were placed at different depths (2, 5, and 10 cm) in a 19 L acrylic tank filled with wetland water (15 cm deep); the tank was wrapped on the outside with black plastic to reduce light reflection. The rationale for using PBS-filled quartz tubes submerged in wetland water was to prevent contact between MS2 and exogenous photosensitizers in the wetland water, while allowing for light attenuation in the water column; this experimental design allowed us to model the effects of light attenuation on endogenous inactivation without the contribution of the exogenous mechanism. Wetland water was collected the day before the experiment at the outlet of an open-water treatment wetland fed with nitrified wastewater effluent (Discovery Bay, CA) (Jasper and Sedlak, 2013). The tank was irradiated for 24 hours using an ozone-free 1000 W Xe arc lamp housed in a solar simulator (Oriel, model number 91194; Newport; Irvine, CA) fitted with a 1.5:G:A global air mass filter (Newport, part number 81388) and an atmospheric attenuation filter (Newport, part number 81017) to mimic the solar spectrum. A comparison of the simulated sunlight irradiance with natural sunlight irradiance at noon on June 27, 2012 [measured by the spectroradiometer and also predicted using the SMARTS radiative transfer model (Gueymard, 2005)] is provided in Figure 2.1. The wetland water column was well-mixed using magnetic stir bars, and the temperature was maintained at around 20 °C. Wetland water instead of distilled water was added periodically (~0.7 L in total) to compensate for photobleaching and water loss due to evaporation. However, photobleaching was still evident, as the absorption spectrum (280 nm to 700 nm) of the wetland water decreased from the beginning to the end of the experiment (Figure 2.2a), which reduced the spectral light attenuation by wetland water throughout the experiment (Figure 2.2b). To account for photobleaching, the average of the initial and final absorption coefficients was used for calculations.

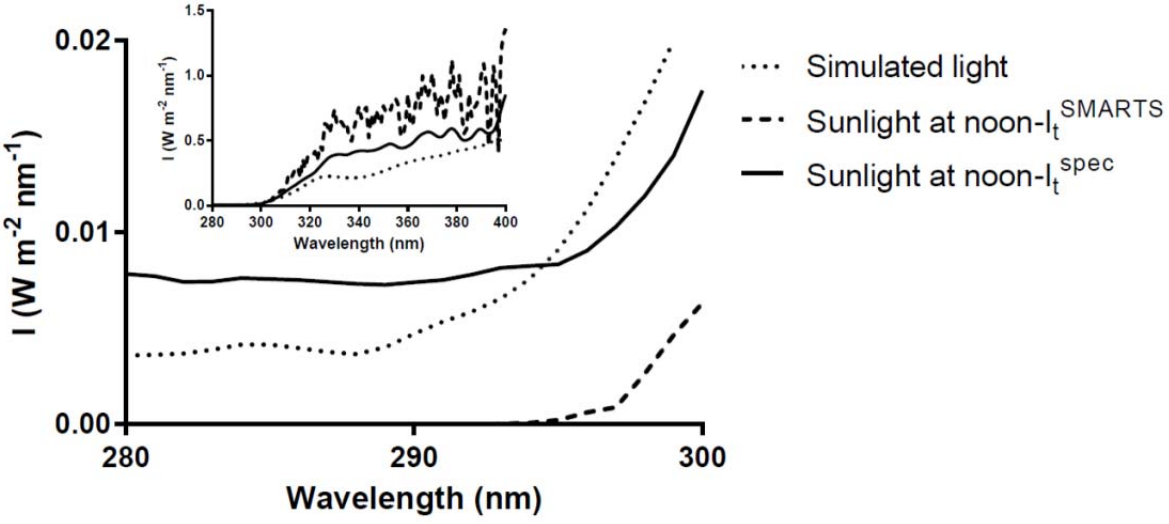

Figure 2.1. UVB irradiance of simulated sunlight measured by spectroradiometer, and natural sunlight at noon on June 27, 2012 in Berkeley predicted by SMARTS and measured by spectroradiometer. Inset is the same data with wavelengths ranging from 280 to 400 nm.

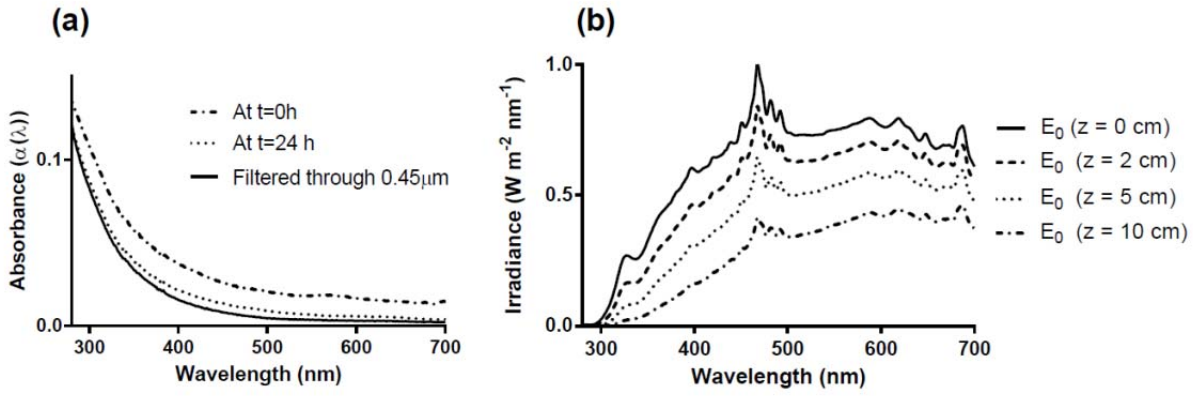

Figure 2.2. (a) Wetland water absorbance (measured using 1-cm cuvette) and (b) scalar simulated sunlight irradiance at various depths in the wetland water column.

2.2.3 Data analysis

Observed inactivation rates. First-order, observed inactivation rate constants (k_{obs}; h^{-1}) were calculated as the negative slope of the linear regression trend line of $\ln(C_t/C_0)$ versus time, where C_0 is the initial MS2 concentration and C_t is the concentration measured in samples collected at time t.

The geometry effects of quartz tubes on inactivation rates. Sunlight degradation rates measured in quartz tubes have been found to be faster than those in open beakers due to the ability of light to enter tubes from all sides (Dulin and Mill, 1982; Haag and Hoigne, 1986), and a longer light pathlength in quartz tubes resulting from internal reflection off tube walls (Zepp and Cline, 1977). The effect of geometric amplification on MS2 inactivation rates in quartz tubes, as compared to the open beakers that were used in Fisher et al. (2011) must be accounted for to apply the results from the previous study. Simulated sunlight experiments were conducted to compare MS2 inactivation rates measured in quartz tubes with those in open beakers; resulting data were used to calculate a ratio (r) between inactivation rates in quartz tubes and open beakers. Briefly, quartz tubes and glass beakers containing MS2 in PBS (initial concentration of 10^6 PFU mL^{-1}) were exposed to simulated sunlight for 10 h. The beakers and a tray (both painted black) holding quartz tubes were submerged in the same water bath maintained at 20°C with a recirculating chiller (Thermo Electron). Quartz tubes were sacrificially collected every 2 h, at the same time that 0.5-mL sub-samples were collected from beakers. Water samples were immediately frozen at -80 °C until analysis for MS2. Experiments were performed in quadruplicate on two different days. The inactivation rates of MS2 in the tubes and beakers are presented in Figure 2.3 ($k_{obs}^{tube} = 0.73 \pm 0.03$ h^{-1}, $k_{obs}^{beaker} = 0.22 \pm 0.01$ h^{-1}), and r was calculated to be 3.3. To correct for quartz tube geometry effects, all k_{obs} derived experimentally using quartz tubes were divided by r to convert them to the equivalent value in open beakers.

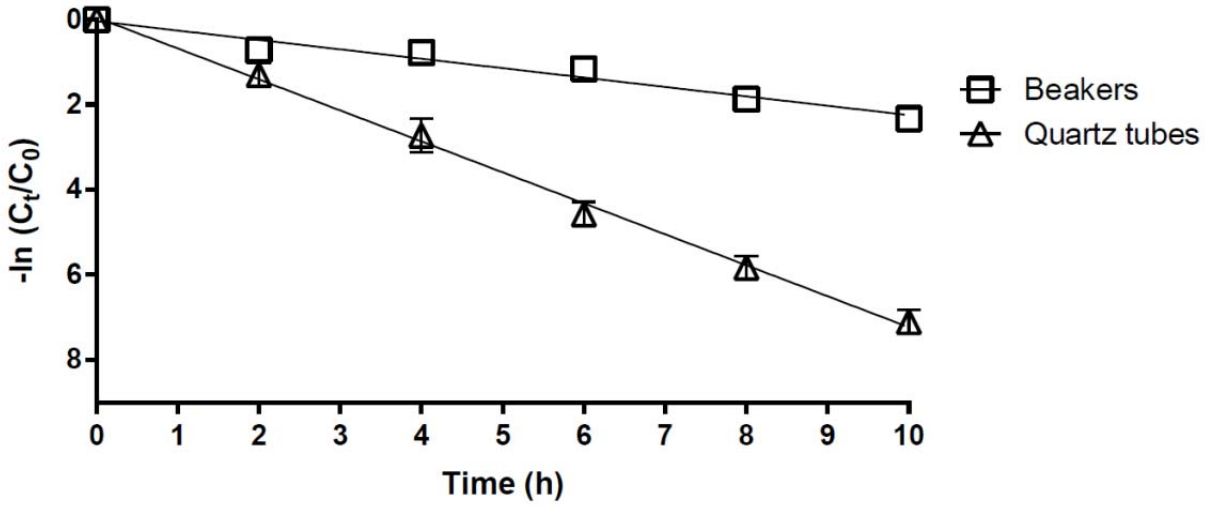

Figure 2.3. Inactivation of MS2 under simulated sunlight in quartz tubes and open beakers. Error bars indicate ± one standard error. The solid lines indicate the linear regression lines of $\ln(C_t/C_0)$ and time ($k_{obs}^{beakers} = 0.22\pm0.01$ h^{-1}, $R^2 = 0.92$; $k_{obs}^{tubes} = 0.73\pm0.03$ h^{-1}, $R^2 = 0.96$).

Modeled inactivation rates in natural sunlight experiments.

Using PAS model. Photodamage coefficients at time t [$D_t^i(\lambda)$] were calculated at 1-h intervals as irradiance-weighted spectral sensitivity coefficients:

$$D_t^i(\lambda) = I_t^i(\lambda) \times P(\lambda) \tag{2.1}$$

where $I_t^i(\lambda)$ is the spectral irradiance of sunlight (W m^{-2} nm^{-1}), either measured by a spectroradiometer (i = spec) or predicted by the SMARTS radiative transfer model (Gueymard, 2005) (i = SMARTS), and $P(\lambda)$ is the spectral sensitivity coefficient (m^2 W^{-1} h^{-1}); $P(\lambda)$ values for MS2 exist in the 280 – 496 nm range, at 3-nm resolution (Fisher et al., 2011) (Table 2.1). Values input to the SMARTS model are listed in Table 2.2.

The modeled, first-order inactivation rates of MS2 at each time t (k_{mod}^i) were calculated by taking the summation of the irradiance-weighted photodamage spectrum over the wavelength range 280 – 496 nm (Fisher et al., 2011):

$$k_{mod}^i = \sum_{\lambda} D_t^i(\lambda) \times \Delta\lambda = \sum_{\lambda} I_t^i(\lambda) \times P(\lambda) \times \Delta\lambda \tag{2.2}$$

where $\Delta\lambda$ is the wavelength interval ($\Delta\lambda$ = 3 nm). The inactivation rate predicted at each time point was used to calculate log inactivation during the previous hour:

$$-\log\left(\frac{C_t}{C_{t-1}}\right) = \frac{k_{mod}^i \times \Delta t}{2.303} \tag{2.3}$$

where Δt is the time interval (Δt =1 h).

Table 2.1. Photoaction spectrum sensitivity coefficients [P(λ)] for MS2 (Fisher et al., 2011). Note that these values are larger than those reported in Fisher et al. in Figure 3 (Fisher et al., 2011) by a factor of 2.303 to account for the fact that Fisher et al. determined the inactivation rate constants (k_{obs}) from the inverse slope of $\log(C_t/C_0)$ rather than $\ln(C_t/C_0)$, as used herein.

Wavelength (nm)	P(λ) (m^2 W^{-1} h^{-1})	Wavelength	P(λ)	Wavelength	P(λ)
281	2.882	356	0	431	0
284	1.281	359	0	434	0
287	0.320	362	0	437	0
290	0	365	0	440	0
293	0	368	0	443	0
296	0.067	371	2.65E-06	446	0
299	0.183	374	9.6E-04	449	0
302	0.299	377	0.002	452	0
305	0.281	380	0.003	455	0
308	0.165	383	0.002	458	0
311	0.049	386	0.001	461	0
314	0	389	0	464	0
317	0	392	0	467	0
320	0	395	0	470	0
323	0	398	0	473	0
326	0	401	0	476	0
329	0	404	0	479	0
332	0	407	0	482	0
335	0	410	0	485	0
338	0	413	0	488	0
341	0	416	0	491	0
344	0	419	0	494	0
347	0	422	0	496	0
350	0	425	0		
353	0	428	0		

Table 2.2. Inputs to the SMARTS model

Parameter	Input	Unit
Site pressure	1005.035	millibars
Altitude	0.06	km
Height	0.01	km
Atmosphere*	US standard Atmosphere 1976	
Water vapor	Calculate from reference atmosphere and altitude	
Columnar ozone abundance	Use default from reference atmosphere	
Gaseous absorption and pollution	Use defaults from selected atmosphere	

Carbon dioxide	370	ppmv
Extraterrestrial spectrum*	Gueymard 2004	
Aerosol model*	Shettle & Fenn Urban	
Atmospheric turbidity	Turbidity value: 130 Meterological range (km)	
Regional albedo	Manmade material: Concrete slab	
Tilted Surface and Local Albedo	Bypass tilt calculations	
Spectral Range	280 – 700	nm
Solar Constant	1366.1	W m^{-2}
Circumsolar Calculations	Bypass	
Extra scanning/smoothing	Bypass	
Extra illuminance calculations	Bypass	
Extra UV calculations	Bypass	
Solar Position and Air Mass	Latitude: 37.874278 Longitude: -122.258976 Time zone: -8	

(*) Suggested by SMARTS

Using tUVB model. The inactivation rates MS2 in sensitizer-free water under natural sunlight can be estimated using the tUVB model as follows:

$$k^{i}_{mod,tUVB} = \gamma^{i} \times \sum_{\lambda=280}^{320} I^{i}_{t}(\lambda) \quad (2.4)$$

where γ^{i} is the correlation factor between total UVB irradiance of natural sunlight (measured by a spectroradiometer or predicted by the SMARTS) and the observed MS2 inactivation rates k^{i}_{obs}.

Modeled t_{90} at different latitudes. Solar irradiances at different latitudes on the 21st day of each month were predicted for clear sky conditions using SMARTS (Gueymard, 2005), and averaged over 24 h. As the shortest and longest days of the year occur on approximately the 21st day of June and December, respectively, we chose the 21st day as the representative day for predicting solar irradiance of each month. The action spectrum and 24-h averaged solar irradiances were used to predict k^{SMARTS}_{mod} (h^{-1}) in clear water using Equation 2.2. The time for 1-log inactivation of MS2 (t_{90}, d) was calculated based on k^{SMARTS}_{mod}:

$$t_{90} = \frac{2.303}{24 \times k^{SMARTS}_{mod}} \quad (2.5)$$

Modeled inactivation rates accounting for light attenuation.

Using PAS model. The light attenuation experiment was conducted under simulated sunlight. The inactivation rate of MS2 at each depth was modeled similarly to Equation 2.2, but using scalar irradiance at depth z [$E_0(z,\lambda)$] instead of $I^{i}_{t}(\lambda)$:

$$k_{mod}(z) = \sum_{\lambda} E_0\ (z, \lambda) \times P(\lambda) \times \Delta\lambda \tag{2.6}$$

$E_0\ (z, \lambda)$ was calculated using the following relationship between light irradiance and water depth (Kirk, 2010):

$$E_0(z, \lambda) = E_d(z, \lambda) = E_d(\lambda, 0)\ e^{-\psi \cdot K_d(\lambda) \cdot z} \tag{2.7}$$

where $E_d\ (0, \lambda)$ is the irradiance just below the water surface, $K_d(\lambda)$ is the vertical attenuation coefficient for downward irradiance, and ψ is a pathlength correction factor used to correct the light-path geometry for the value of z. Given that the light source was a collimated beam (i.e., no light was reflected by the water surface), it is assumed that $\psi = 1$, and $E_d\ (0, \lambda)$ can be measured just above the water surface.

$K_d(\lambda)$ of a particular water depends on its absorption and scattering coefficients, $a(\lambda)$ and $b(\lambda)$, respectively. The absorption coefficient $a(\lambda)$ (m^{-1}) was calculated using the decadic absorption coefficient [$\alpha(\lambda)$] (Kirk, 2010):

$$a(\lambda) = \frac{2.303\alpha(\lambda)}{l} \tag{2.8}$$

where $\alpha(\lambda)$ was measured using a UV-VIS spectrophotometer (PerkinElmer, Waltham, MA), with a pathlength (l) equal to 0.01 m.

The scattering coefficient $b(\lambda)$ (m^{-1}) was estimated indirectly via nephelometric turbidity, using an average ratio of turbidity T_n (NTU) to $b(\lambda)$ of 2.03 ± 0.26 determined for a range of inland surface waters for the wavelength range 400 to 700 nm (Kirk, 1980). Wetland water $T_n$was measured before and after the experiment using a Hach 2100N turbidimeter; the average T_n was 8 NTU. Using the T_n to $b(\lambda)$ ratio, $b(\lambda)$ was calculated to be 3.93 m^{-1}. Combined with the average $a(\lambda)$ value in the range of 400 to 700 nm (Figure 2.2a), the ratio of $b(\lambda)$ to $a(\lambda)$ had the value of 0.63.

$K_d(\lambda)$ in the range of 400 to 700 nm was determined using the equation (Kirk, 1981):

$$K_d\ (\lambda) = a(\lambda) \times \left[1 + 0.256\frac{b(\lambda)}{a(\lambda)}\right]^{1/2} \tag{2.9}$$

The calculated values of $K_d(\lambda)$ were approximately equal to $a(\lambda)$, suggesting that the contribution of light scattering in the wetland water for visible light (400 – 700 nm) was minor. Scattering in the wavelength range of interest is dominated by particles, which has only a weak wavelength dependence (Kirk, 2010); thus, it was considered reasonable to assume that $K_d(\lambda)$ was equal to $a(\lambda)$ at all wavelengths (280 – 700 nm).

Using tUVB model. The tUVB model was introduced to estimate the MS2 endogenous inactivation rate under simulated sunlight as follows (Silverman et al., 2015):

$$k_{mod,tUVB}(z) = \beta \times \sum_{\lambda=280}^{320} E_d(z,\lambda) \quad (2.10)$$

where β is the correlation factor between total UVB irradiance of the downward simulated sunlight irradiance at depth z and $k_{mod,tUVB}(z)$. The β value of 0.12±0.02 $m^2 W^{-1} h^{-1}$ (R^2=0.89) was determined by Silverman et al. (Silverman et al., 2015) from compiled data on MS2 inactivation rates in sensitizer-free water under simulated sunlight from previous publications (Fisher et al., 2011; Kohn and Nelson, 2007; Love et al., 2010; Silverman et al., 2015, 2013).

2.2.4 Statistical tests

Statistical tests were performed using GraphPad Prism 6.0.1 (GraphPad Software, La Jolla, CA). Linear regression analysis was performed to determine observed inactivation rates from measured $\ln(C_t/C_0)$ data. For natural sunlight experiments, non-linear regression analysis (four parameter logistic model for sigmoidal curve fit) was performed to construct the best-fit line for $\log(C_t/C_0)$ data versus time (6 points in Figure 2.4a, and 11 points in Figure 2.4b), and the F-test was used to compare the best-fit lines of observed and predicted $\log(C_t/C_0)$ versus time. Two-way ANOVA analysis was conducted to compare observed and modeled inactivation rate constants in natural sunlight and light attenuation experiments. A correlation test was performed to evaluate the relationship between k_{obs} and k_{mod}.

2.3 Results and Discussion

2.3.1 Comparison of observed and modeled inactivation of MS2 using PAS model in photosensitizer-free water under natural sunlight

Observed and modeled inactivation curves for MS2 in clear water under natural sunlight during winter and summer are presented in Figure 2.4. No significant change in MS2 concentration occurred in dark controls (k_{dark} = -0.012 ± 0.005 h^{-1}). Endogenous inactivation rates were modeled using solar irradiance spectra that were either measured using a spectroradiometer (k_{mod}^{spec}) or predicted using SMARTS (k_{mod}^{SMARTS}). There was good agreement between modeled and observed inactivation of MS2 on both days using both types of irradiance data (F-test, p > 0.1; correlation coefficient r = 0.97, R^2 = 0.94), and the action spectrum model accurately predicted higher inactivation of MS2 in the summer compared to the winter.

The diurnal variation in MS2 inactivation rates was also captured by the action spectrum model, as demonstrated by an increase and then decrease in predicted inactivation rate constants over the course of the day for both experiments (Figure 2.5). Although there was no statistically significant difference between k_{obs} and either k_{mod}^{spec} or k_{mod}^{SMARTS} values (ANOVA, Tukey's post test, p > 0.1), k_{mod}^{SMARTS} values were observed to be lower than k_{mod}^{spec} in winter and at the beginning (9:00) and the end (15:00 to 17:00) of the summer experiment. The discrepancy between k_{mod}^{SMARTS} and $k_{mod}^{spec}$was due to differences in the two sources of solar irradiance data. Although $I_t^{SMARTS}(\lambda)$ was often higher than $I_t^{spec}(\lambda)$ for wavelengths greater than 300 nm (Figure 2.6a and 2.7a), $I_t^{spec}(\lambda)$ was larger than $I_t^{SMARTS}(\lambda)$ for the 280 to 300 nm range (Figure 2.6b and 2.7b) at many time points. Although the irradiance below 300 nm was very low, $P(\lambda)$

values are extremely high between 280 and 290 nm (Table 2.1), such that even very low irradiance in this range makes a large contribution to k_{mod}^{spec}; this effect can be seen in graphs of the photodamage spectra (Figure 2.8 and 2.9). In some cases, the areas under $D_t^{spec}(\lambda)$ and $D_t^{SMARTS}(\lambda)$ curves were similar (the areas under the curves are equal to k_{mod}^{spec} and k_{mod}^{SMARTS}, respectively) but k_{mod}^{spec} was influenced more by wavelengths less than 290 nm and $k_{mod}^{SMARTS}$was influenced more by wavelengths between 295 and 315 nm.

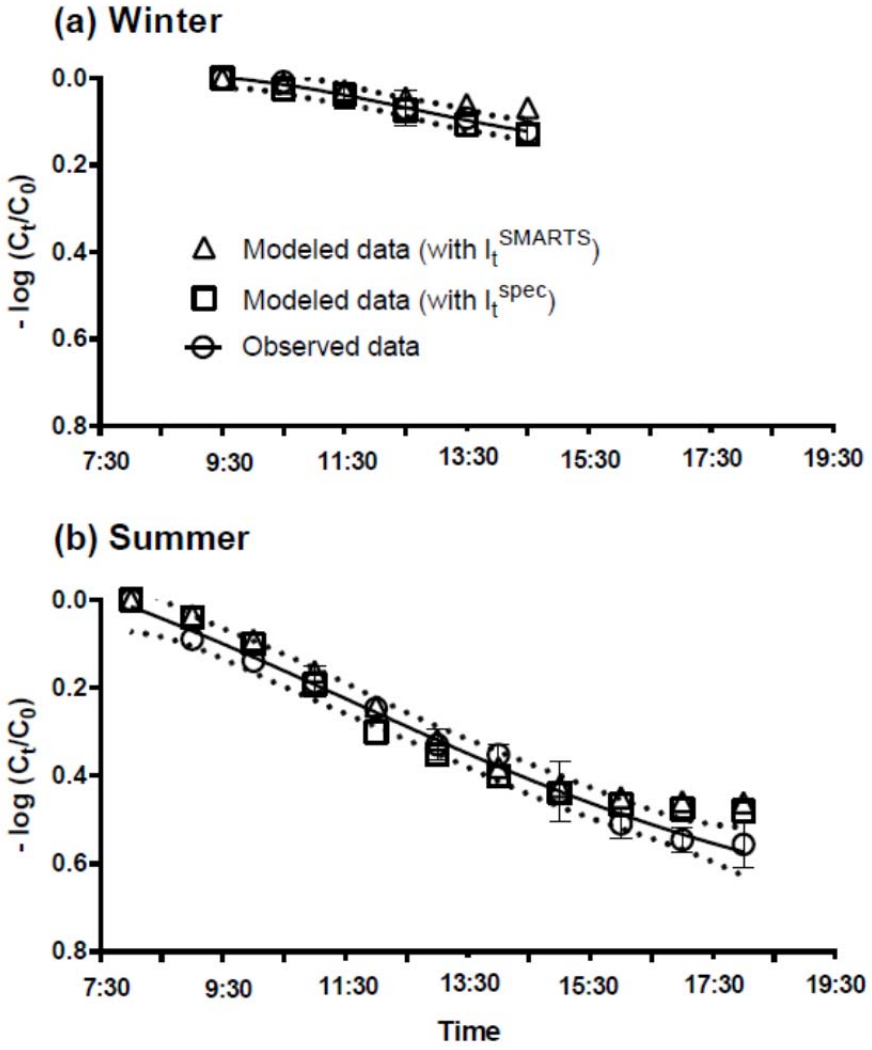

Figure 2.4. Inactivation of MS2 under natural sunlight as a function of time during (a) a winter day and (b) a summer day. Modeled data was calculated from irradiance measured by spectroradiometer (I_t^{spec}) or predicted by the SMARTS model (I_t^{SMARTS}). Error bars indicate ± one standard error. The solid lines indicate best-fit lines for the observed data [$R^2 = 0.81$ for (a), $R^2 = 0.93$ for (b)], dotted lines indicate 95% confidence interval of the best-fit lines.

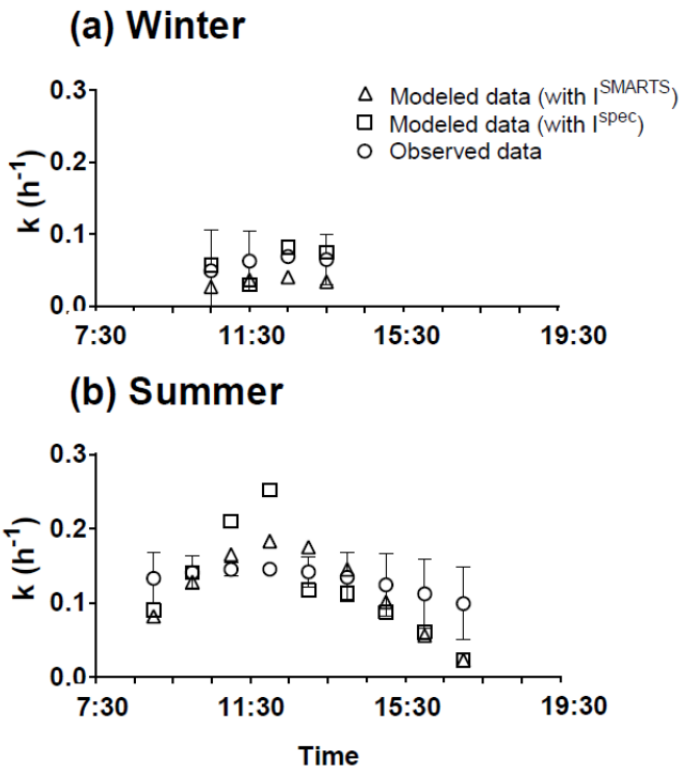

Figure 2.5. Observed and modeled inactivation rates (k_{obs} and k_{mod}) of MS2 under natural sunlight in (a) winter and (b) summer. Observed inactivation rates at each time, t, were calculated from $\ln(C_t/C_0)$ data at three time points: (t – 1), t, and (t +1). Error bars indicate ± one standard error for the observed data.

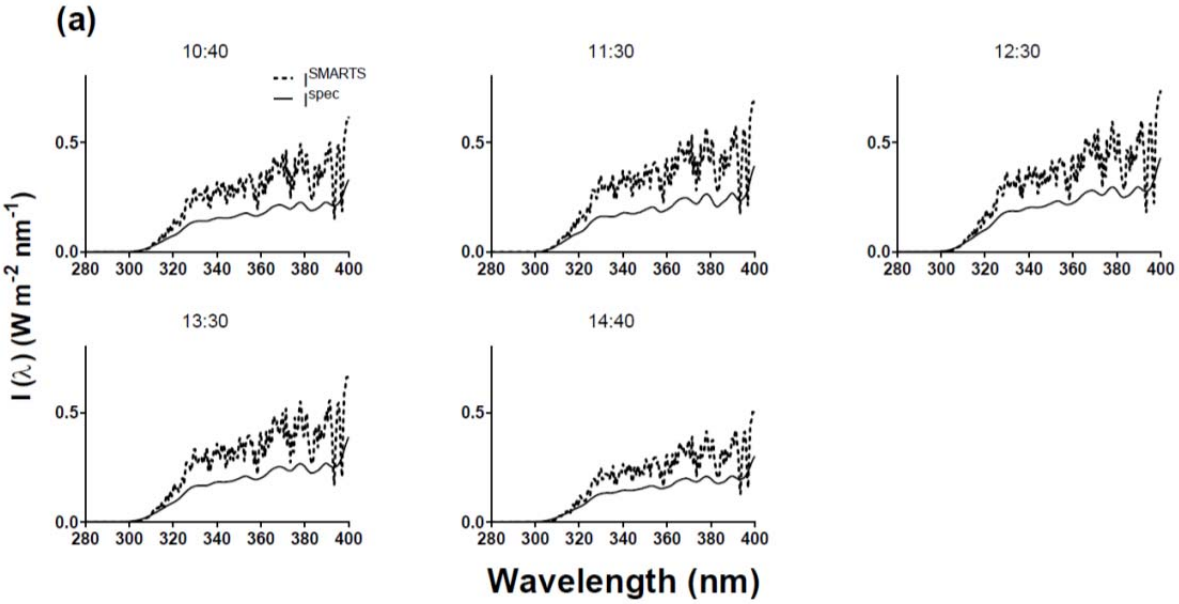

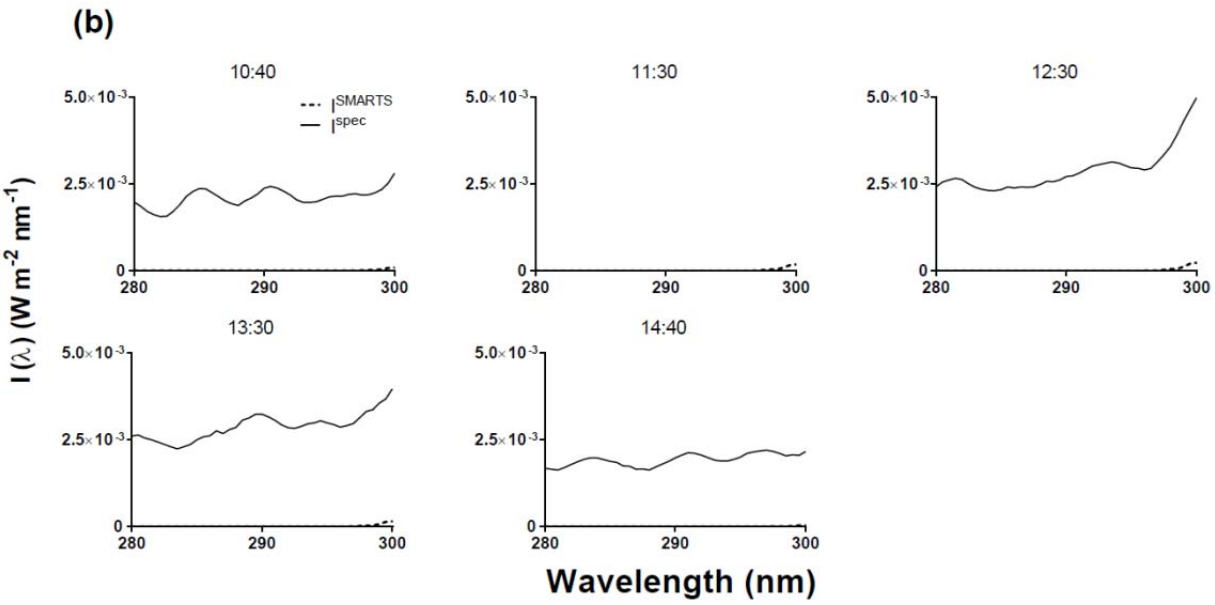

Figure 2.6. Solar UV irradiance during the winter experiment (01/28/2012) with wavelengths ranging from (a) 280 to 400 nm, and from (b) 280 to 300 nm. Note that values of $I_t^{SMARTS}(\lambda)$ or $I_t^{spec}(\lambda)$ cannot be seen at some time points in (b) due to their small values compared to the scale of the y-axis.

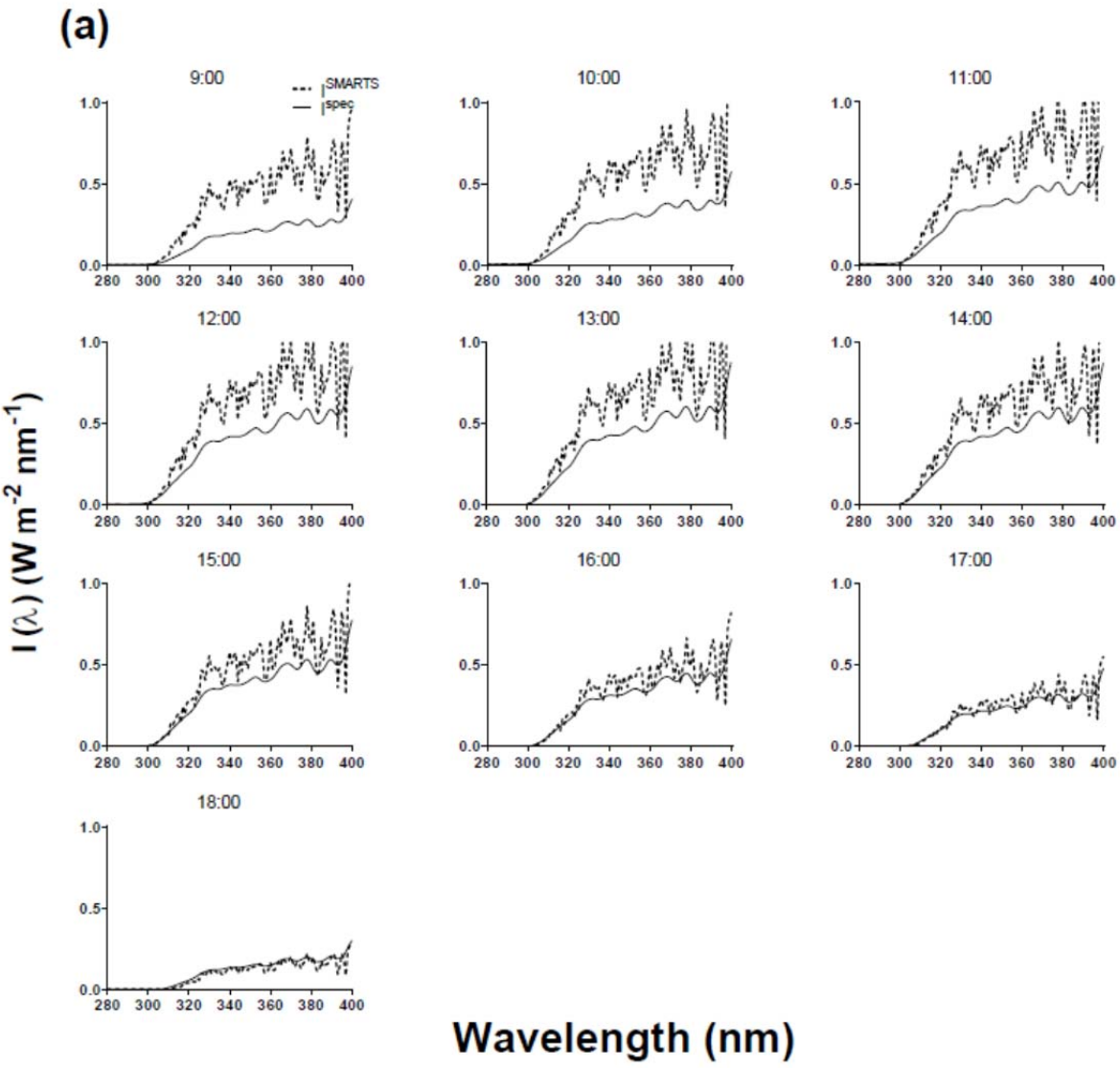
(a)
9:00
10:00
11:00
12:00
13:00
14:00
15:00
16:00
17:00
18:00
SMARTS
spec
I (λ) (W m-2 nm-1)
Wavelength (nm)

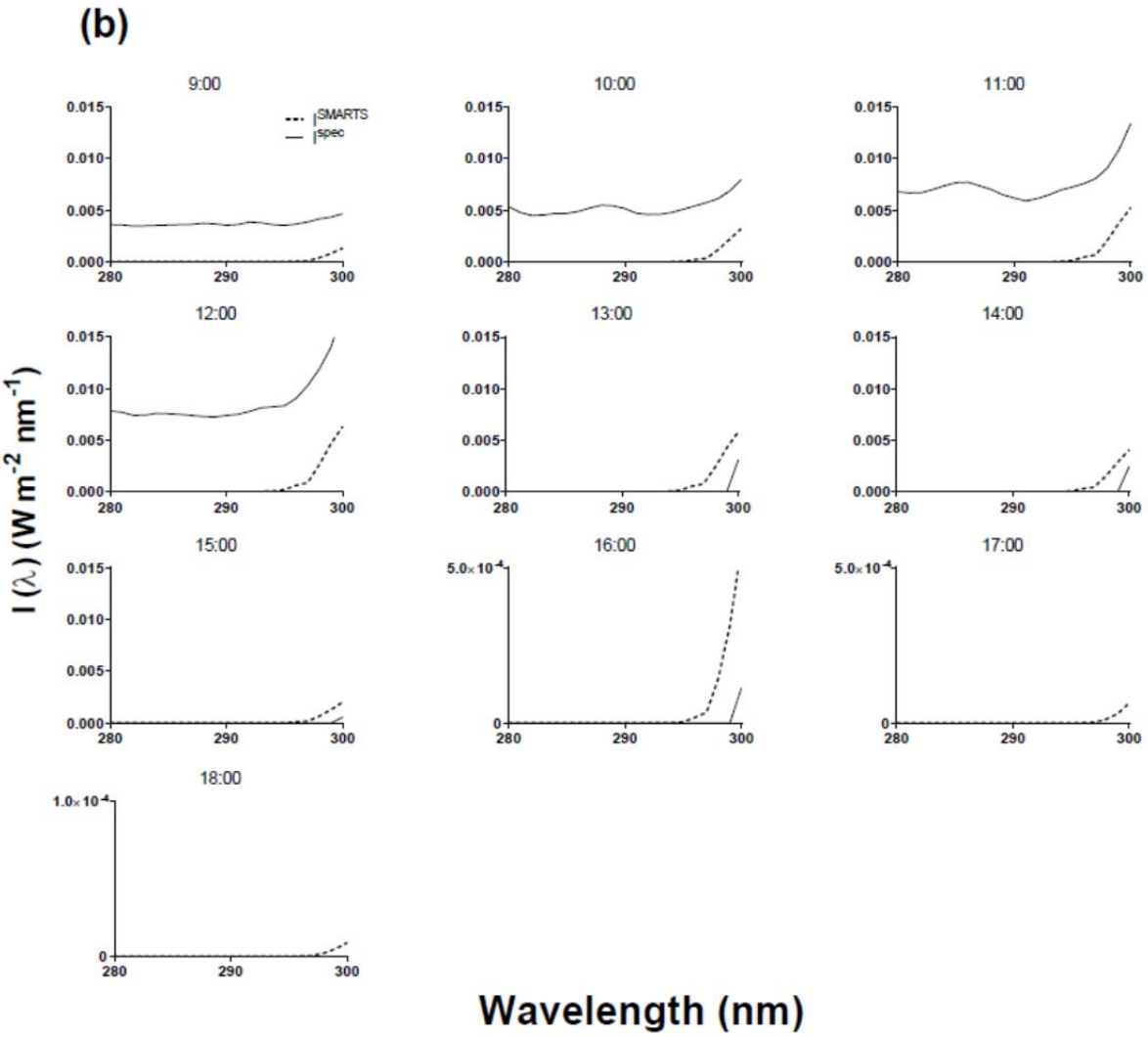

Figure 2.7. Solar UV irradiance during the summer experiment (06/27/2012) with wavelengths ranging from (a) 280 to 400 nm, and (b) from 280 to 300 nm. Note that the scale of the y-axis in (b) is different for each time point; and values of $I_t^{SMARTS}(\lambda)$ or $I_t^{spec}(\lambda)$ cannot be seen at some time points due to their small values compared to the scale of the y-axis.

There are a few possible explanations for why the $I_t^{SMARTS}(\lambda)$ and $I_t^{spec}(\lambda)$ spectra differ. At wavelengths below 300 nm there is very low light irradiance and the spectroradiometer measurements may be inaccurate (Bernhard and Seckmeyer, 1999). The fairly constant irradiance reported by the spectroradiometer below about 295 nm for many time points in Figure 2.7b suggests that these values represent noise. From inspection of Figures 2.1 and 2.10, it appears that reporting of noise is also an issue with spectroradiometer measurements of simulated sunlight, including the values used by Fisher et al. (Fisher et al., 2011) to determine $P(\lambda)$, which is further discussed below. Additionally, the detector is sensitive to temperature (pers. comm. with StellarNet, Inc.), and the absence of light below 300 nm at some time points may be attributed to the sensor overheating. Measurement error associated with overheating of the detector can be avoided in future research by placing the spectroradiometer under sunlight for

short intervals when taking measurements, and storing it in a cool location between measurements. It is also possible that irradiance values predicted by SMARTS are inaccurate because we used default input values for some model parameters (e.g., ozone concentration, precipitable water, aerosol optical depth). All input data used for predicting solar irradiance in this study were recommended in the SMARTS user guidelines (Gueymard, 2003). Nonetheless, a more accurate way to use the SMARTS model would be to measure these parameters (Gueymard, 2008).

The difficulty in both measuring (e.g., with a spectroradiometer) and predicting (e.g., with SMARTS) UVB irradiance, in particular below 300 nm, is a significant limitation to the ability to accurately predict inactivation of MS2 by sunlight. Importantly, the $P(\lambda)$ values reported by Fisher et al. (Fisher et al., 2011) need to be re-examined; if the true solar simulator irradiance below 295 nm was lower than the measured values that were used (as shown in Figure 2.10), then $P(\lambda)$ for contributing wavelengths above 295 nm would have to be higher to compensate for the loss of the photodamage peak between 280 and 290 nm. A similar issue exists with respect to $P(\lambda)$ values centered around 380 nm. Fisher et al. noted that the peak in $D_t\ (\lambda)$ at 380 nm for MS2 could be an artifact of the method used to develop the action spectrum (Fisher et al., 2011). The contribution of the peak at 380 nm is likely to be negligible (less than 5% of inactivation) under typical sunlight conditions (Fisher et al., 2011), given that previous studies found MS2 k_{obs} in photosensitizer-free water to be insignificant with exposure to simulated sunlight with the UVB region removed by a UVB-blocking filter (Love et al., 2010; Silverman et al., 2013). Nonetheless, during natural sunlight experiments in the present study, the apparent contribution of $D_t\ (380)$ in MS2 inactivation was not negligible. $D_t\ (380)$ accounted for 6 to 15% of k_{mod}^{spec}, and 11% to 30% of k_{mod}^{SMARTS} between the hours of 11:00 and 14:00 (Figure 2.8 and 2.9). Thus, while it is likely that the $D_t\ (380)$ peak is an artifact, and did not actually contribute to MS2 endogenous inactivation, if it was not included in the estimates of k_{mod} in this current study, the total inactivation rate would be underestimated.

To address these issues, we recommend that a new action spectrum be developed, with (1) validation of irradiance measurements and the contribution of wavelengths below 295 nm, and (2) a determination of whether the values around 380 nm are authentic or artifactual. In the meantime, the action spectrum from Fisher et al. (2011) can be used but its limitations should be recognized.

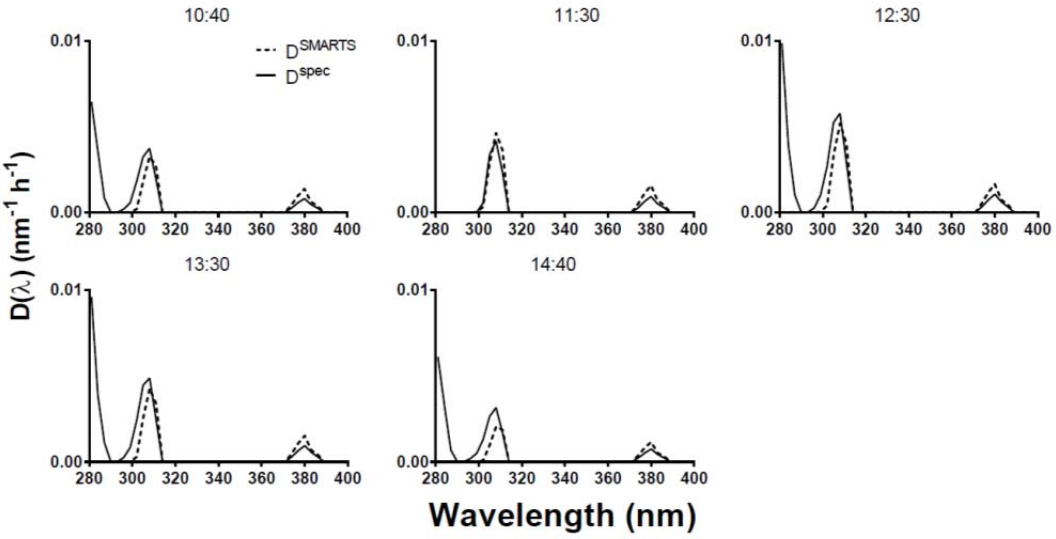

Figure 2.8. MS2 photodamage coefficients during the winter experiment (01/28/2012).

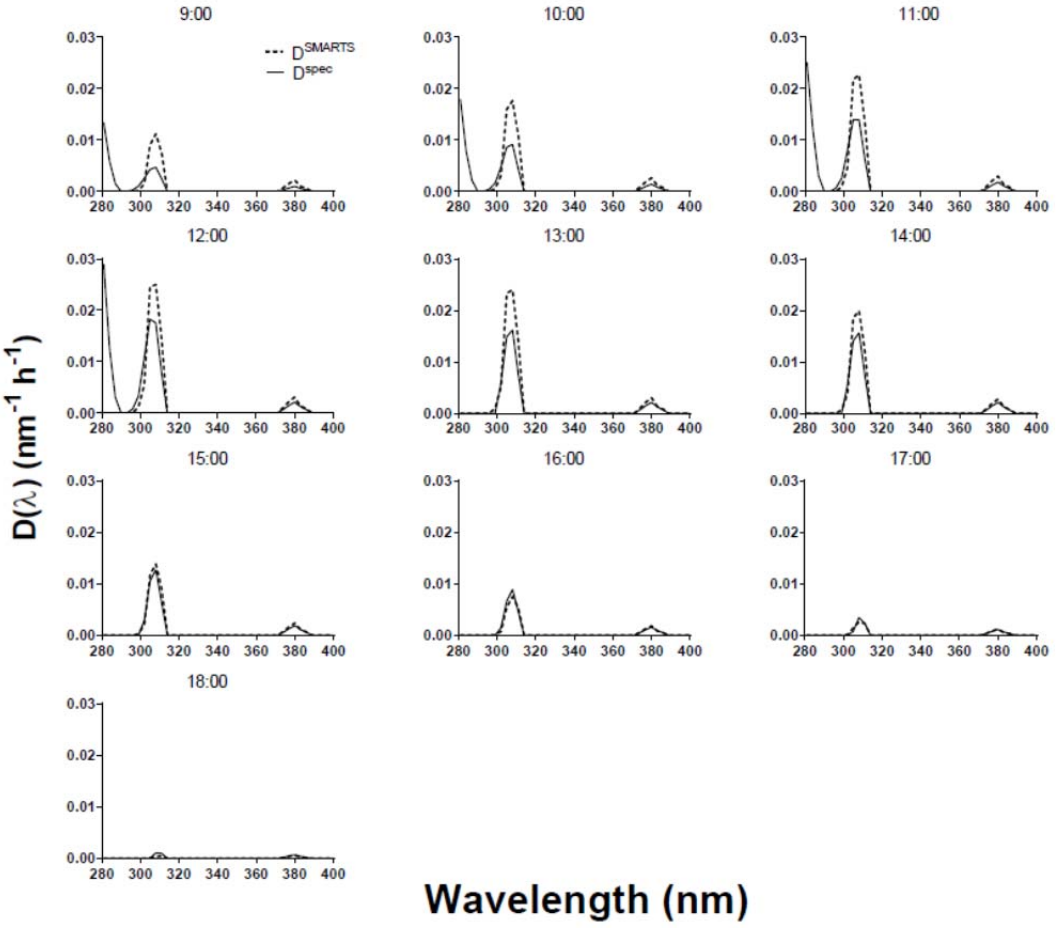

Figure 2.9. MS2 of photodamage coefficients during the summer experiment (06/27/2012).

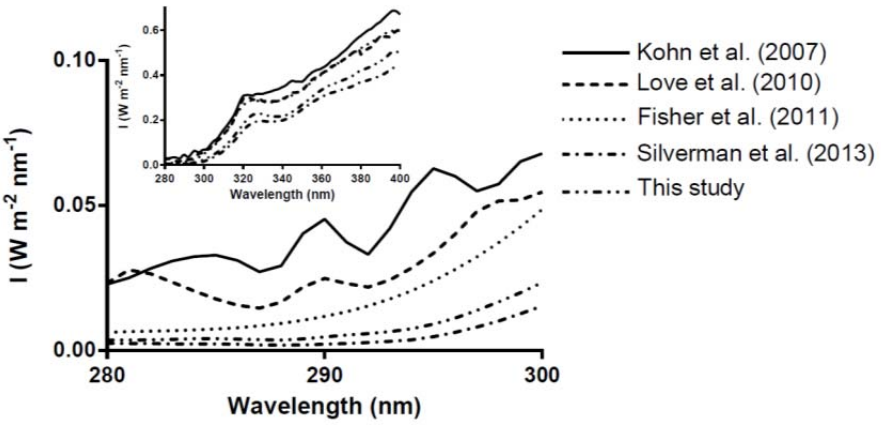

Figure 2.10. Irradiance of simulated sunlight measured in this study, and reported by the reviewed MS2 inactivation publications (Fisher et al., 2011; Kohn and Nelson, 2007; Love et al., 2010; Silverman et al., 2013). Inset is the same data with wavelengths ranging from 280 to 400 nm.

Predicted t_{90} at different latitudes. To illustrate an application of the action spectrum approach for predicting inactivation, we used Equations 2.2 and 2.5, with solar irradiance spectra predicted by SMARTS as input, to calculate the time for 1-log removal of MS2 (t_{90}) in clear water (i.e., without light attenuation or exogenous inactivation) under sunlight at different latitudes throughout the year (Figure 2.11). It should be noted that t_{90} estimates do not include seasonal atmospheric conditions (e.g., humidity, cloud cover, precipitation, particulates and pollutants), which could increase t_{90} values due to a decrease in UVB irradiance (Jablonski and Chaplin, 2010). Also, longer inactivation times might be required if significant light attenuation occurs in the water column, although the same substances that attenuate light may also serve as sensitizers for exogenous inactivation of MS2 (Kohn and Nelson, 2007), and the action spectrum does not account for these effects. The inactivation rate is normalized over the entire day, so that the rate takes into account seasonal changes in the length of the solar day.

Solar UVB irradiance on the Earth's surface is much lower than UVA irradiance, and its distribution is more variable due to solar altitude and scattering and absorption by aerosols in the atmosphere (Jablonski and Chaplin, 2010). As UVB irradiance varies by location and season, and MS2 inactivation rates in clear water depend on UVB, t_{90} exhibits strong association with latitude and season. At the equator (0°) and within the tropics (< 23°), average UVB irradiance is high with two seasonal peaks at the equinoxes (March 20 and September 22) (Chaplin and Jablonski, 2009); these peaks can be observed in Figure 2.11 as the two lowest t_{90} values, which occur in March and September. Nonetheless, the variation is small, resulting in similar t_{90} values (between 2 and 4 d) for 0° and 10° throughout the year. Outside of the tropics, average UVB irradiances are generally lower and, in the northern hemisphere, exhibit a single peak during the summer solstice (June 20 or 21) (Chaplin and Jablonski, 2009); this pattern is observed in the t_{90} curves for 30°N and 40°N latitudes, which have minima in June. The seasonal UVB variation is higher outside the tropics, resulting in t_{90} values at 30°N and 40°N latitudes ranging from 2 d in summer up to 24 d in winter.

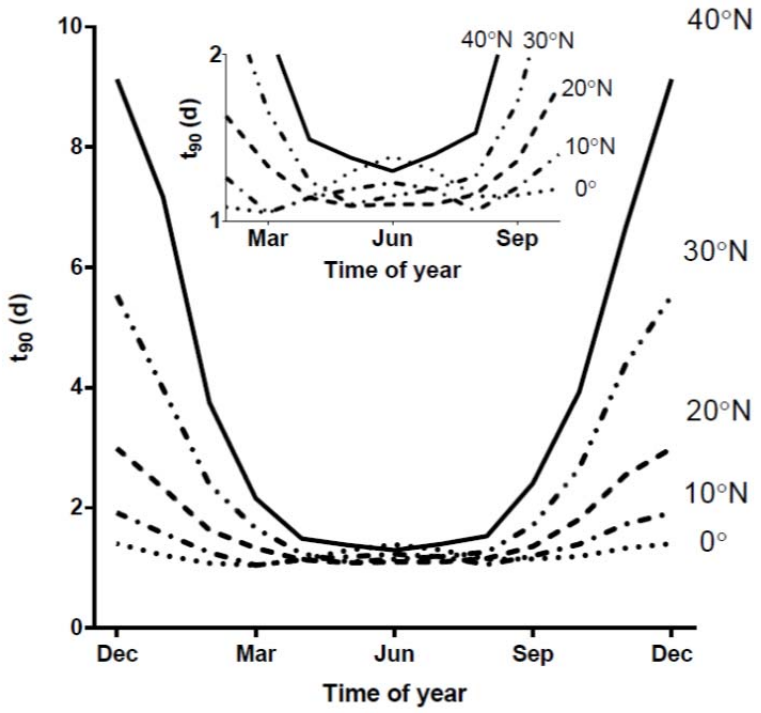

Figure 2.11. Computed time needed for 1-log removal of MS2 (t_{90}) in clear water under clear sky conditions at different latitudes over the course of a year. 24-h averaged solar irradiance predicted using SMARTS was used as the input irradiance spectrum. Inset is the same data with t_{90} in the range of 1 to 2 d.

2.3.2 Comparison of observed and modeled inactivation rates of MS2 using PAS model in photosensitizer-free water in wetland water under simulated sunlight

To measure endogenous inactivation in the absence of photosensitized exogenous mechanisms, quartz tubes containing MS2 in sensitizer-free water were submerged at different depths (z = 2, 5, and 10 cm) in wetland water and exposed to simulated sunlight for 24 h; results of this experiment are presented in Figure 2.12. No significant changes in MS2 concentration were observed in dark controls over 24 hours ($k_{dark} = 0.003 \pm 0.004$ h^{-1}). The irradiance spectra at each depth in the water column ($E_0\ (z, \lambda)$, calculated using Equations 2.7, 2.8, and 2.9) decreased with increasing depth in the water column (Figure 2.2b). $E_0\ (z, \lambda)$ values were used in Equation 2.6 to compute the predicted inactivation rate of MS2 at 1-cm intervals over the depth of the water column (Figure 2.12). There was no statistically significant difference between k_{obs} and k_{mod} at the four experimental depths in the wetland water column (ANOVA, Sidak's post test, $p > 0.1$), and the two data sets were in good agreement (correlation coefficient $r = 0.97$, $R^2 = 0.94$). However, compared to k_{obs} values, k_{mod} values were higher at 2 cm and lower at 10 cm. Given that k_{obs} and k_{mod} were in close agreement at the two other depths (0 and 5 cm), the discrepancies between k_{obs} and k_{mod} may be related to experimental variability, as it was challenging to ensure that all quartz tubes had the identical orientation to the light source and that there was no shading. Thus, the action spectrum model was able to account for wavelength-

specific light attenuation with depth in the water column, and can be used to predict endogenous inactivation of MS2 in water containing light-attenuating compounds.

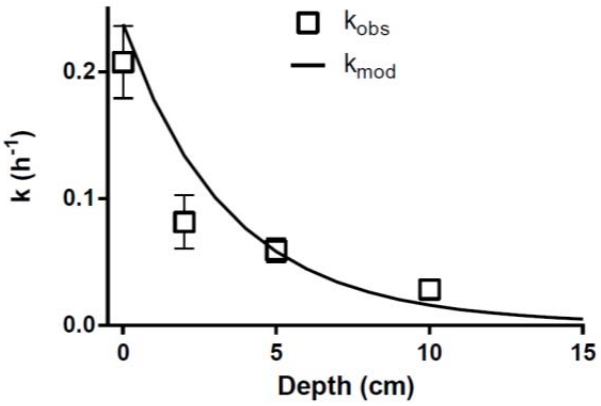

Figure 2.12. Observed (k_{obs}) and modeled (k_{mod}) endogenous inactivation rates of MS2 at different depths (z = 0, 2, 5, and 10 cm) in wetland water. The irradiance at each depth was calculated using Equation 2.7, and used in combination with $P(\lambda)$ in Equation 2.6 to calculate inactivation rates. Dotted lines are when $k_{obs} = k_{mod}$. Error bars indicate ± one standard error.

2.3.3 Comparison of observed and modeled inactivation rates of MS2 using PAS model in photosensitizer-free water under simulated sunlight from previous studies

The k_{obs} values of MS2 measured in this study, as well as k_{obs} measured in four previous publications from our laboratory (Fisher et al., 2011; Kohn and Nelson, 2007; Love et al., 2010; Silverman et al., 2013), were compared to k_{mod} calculated using the action spectrum model and I^{spec} measured during each of the studies. It should be noted that all of these experiments were conducted in same laboratory, with the same solar simulator, using the same MS2 purification protocols. Light irradiance was measured with International Light RPS 200 and 380 spectroradiometers in Kohn et al. (Kohn and Nelson, 2007), Love et al. (Love et al., 2010), and Fisher et al. (Fisher et al., 2011), whereas the StellarNet spectroradiometer was used for irradiance measurements in Silverman et al. (Silverman et al., 2013) and the present study; reported light irradiance data are presented in Figure 2.10. The shape of the spectra produced by the solar simulator was roughly the same for all studies, but the irradiance values were different. The differences in the solar simulator output reported in the different papers are primarily due to aging of the simulator lenses and surfaces (such that more light is lost to absorption and scattering), the use of different Xenon lamps, and the power settings. In addition, different radiometers have been found to report different measurements of the same light source (Bernhard and Seckmeyer, 1999). It should be noted that the irradiance reported by Fisher et al. (Fisher et al., 2011) in the wavelength range of 280 to 300 nm is lower than that in Kohn et al. (Kohn and Nelson, 2007) and Love et al. (Love et al., 2010), despite the same instruments being used, because it was corrected to reduce noise. However, as discussed in the previous section, we now suspect that even the very low irradiance reported below 295 nm may produce artifacts in the action spectrum.

The comparisons of k_{mod} and k_{obs} data collected from previous studies (Fisher et al., 2011; Kohn and Nelson, 2007; Love et al., 2010; Silverman et al., 2013), and from experiments in this study are shown in Figures 2.13a and b, respectively. Despite the challenges associated with quantifying irradiance of the lowest wavelengths, there was good agreement between k_{mod} and k_{obs} for most datasets (Pearson's correlation coefficient $r = 0.96$, $p < 0.05$ for data in Figure 2.13a; $r = 0.95$, $p < 0.001$ for data in Figure 2.13b). The higher k_{mod} than k_{obs} values in Kohn et al. (2007) and Love et al. (2010) are likely due to erroneously high irradiance measurements between 280 and 300 nm (Fisher et al., 2011).

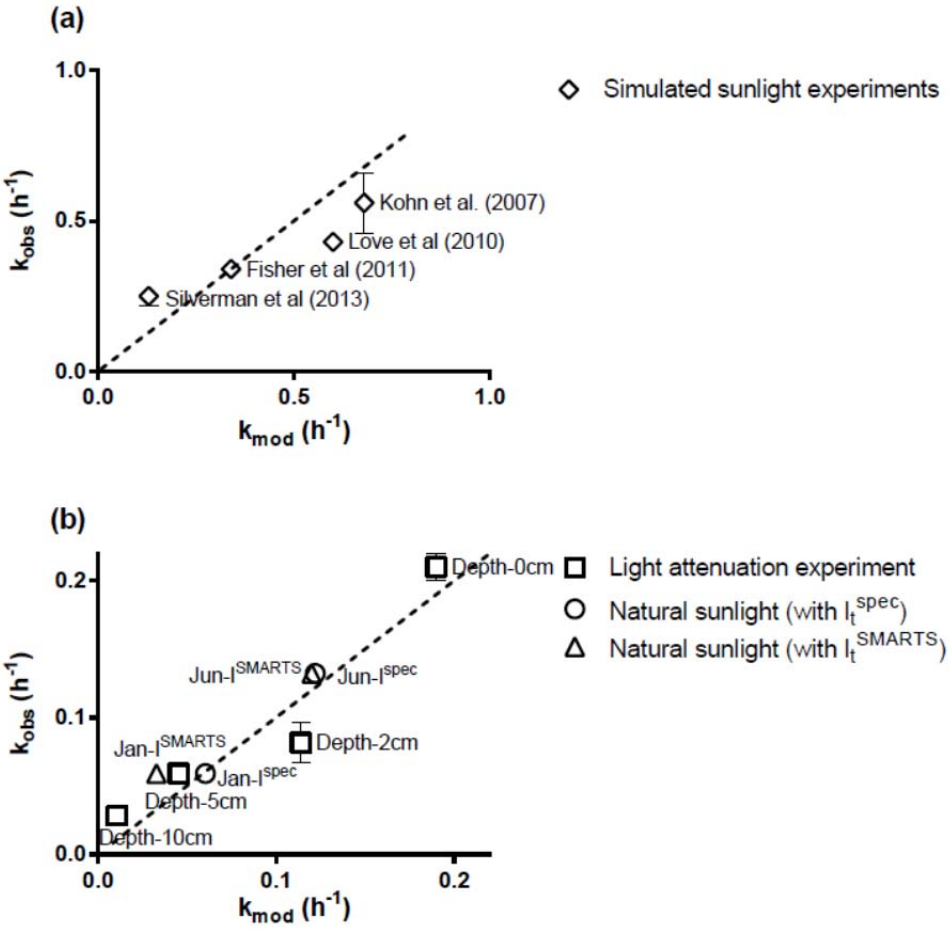

Figure 2.13. Comparison of observed (k_{obs}) and modeled (k_{mod}) inactivation rates of MS2 in photosensitizer-free water from (a) previous studies (Fisher et al., 2011; Kohn and Nelson, 2007; Love et al., 2010; Silverman et al., 2013) and (b) this study. The dotted lines indicate $k_{obs} = k_{mod}$. k_{obs} data from experiments under natural sunlight were calculated as first-order rate constants from observed inactivation data in Figure 2.4.

2.3.4 Limitations and challenges of using the PAS model to predict endogenous inactivation rate of an organism

The theory behind using an PAS, or biological weighting function, to predict inactivation of viruses is to accurately account for the unequal contribution of photons of different

wavelengths to inactivation. Therefore, differences in the shape of the contributing portion of the solar spectrum at different locations, times, or depths in a water body can be explicitly accounted for. We demonstrated the application of this approach to predict sunlight inactivation of MS2 under winter and summer sunlight, and to account for light attenuation in wetland water. Although the predictions were reasonable, we found that a major limitation to this approach was uncertainty about sunlight irradiance in the range 280 to 300 nm measured using a spectroradiometer or predicted using SMARTS; because MS2 is extremely sensitive to photons in this range, they have a disproportionate effect on the overall inactivation rate. Importantly, we cannot determine if $I_t^{spec}(\lambda)$ values in the UVB range used by Fisher et al. (Fisher et al., 2011) to develop the action spectra sensitivity coefficients were accurate enough. If actual irradiance values below 300 nm were lower than the measured values used to develop the action spectrum, then weighting of the other wavelengths needs to be adjusted.

Solar simulators are widely used in virus inactivation experiments to produce light of constant irradiance, such that the same experimental conditions can be produced for extended periods of time, on different days, and in different laboratories. However, we documented that measured UVB light irradiance outputs – as well as the ratios of irradiance of shorter, more damaging, wavelength UVB to longer wavelength UVB $\left(\frac{I_{280-300nm}}{I_{300-320nm}}\right)$ – vary between experiments (Table 2.3) and likely differ between laboratories, solar simulator models, and spectroradiometer instruments used to measure irradiance. PAS make it possible to account for these differences by weighting each wavelength appropriately. However, better measurement of UVB light irradiance in the 280 to 300 nm range in simulated and natural sunlight is needed, as well as a better understanding of the discrepancy between irradiance measured by spectroradiometers and predicted by the widely used radiative transfer model SMARTS. Chemical actinometry (Leifer, 1988) combined with spectral cutoff filters should be explored in future research as an approach for making more accurate measurements of light irradiance and validating spectroradiometer measurements.

Table 2.3. Total UVB irradiance and its distribution $\frac{\sum_{\lambda=280}^{300} I}{\sum_{\lambda=300}^{320} I}$(%) from different light sources (simulated sunlight versus natural sunlight) in MS2 inactivation experiments. Results listed without citation are from the present study.

Light source	**Study**		$\sum_{\lambda=280}^{320} I$ **(W m^{-2})**	$\frac{\sum_{\lambda=280}^{300} I}{\sum_{\lambda=300}^{320} I}$(%)
Simulated sunlight	Kohn et al. (2007)		4.30	25
	Love et al. (2010)		3.71	19
	Fisher et al. (2011)		3.37	12
	Silverman et al. (2013)		1.57	6
	Depth-0 cm		1.98	9
	Depth-2 cm		1.84	8
	Depth-5 cm		1.32	7
	Depth-10 cm		0.77	6

	Season	Time	Spec	SMARTS	Spec	SMARTS
Natural sunlight	Summer	9:00	0.89	1.98	9.66	0.14
		10:00	1.48	2.75	8.13	0.27
		11:00	2.09	3.32	8.23	0.38
		12:00	2.57	3.58	7.79	0.43
		13:00	2.28	3.47	0.14	0.41
		14:00	2.22	3.02	0.11	0.32
		15:00	1.89	2.31	0.03	0.19
		16:00	1.43	1.49	0.01	0.07
		17:00	0.78	0.73	0.00	0.02
	Winter	9:30	0.04	0.40	9.68	0.01
		10:30	0.67	0.81	6.41	0.02
		11:30	0.74	1.03	0.00	0.03
		12:30	0.96	1.12	6.18	0.03
		13:30	0.84	0.98	7.06	0.02

2.3.5 Possibility of using the tUVB model to predict endogenous inactivation rate of an organism

The tUVB model was developed with the recognition that endogenous inactivation of MS2 and other viruses (e.g., Poliovirus type 3) only occurs with exposure to UVB irradiance (Kohn and Nelson, 2007; Love et al., 2010; Silverman et al., 2013). The tUVB model which weighs all UVB wavelengths equally can be used as a simplified model to estimate the endogenous inactivation rates of organisms for which their PAS do not exist. For other organisms that are sensitive to both UVB and UVA (e.g., *Ent. faecalis* and *E. coli*) (Davies-Colley et al., 1997; Kadir and Nelson, 2014; Sinton et al., 2002), all wavelengths in the UV range (280 – 400 nm) are included.

In the depth experiment under simulated sunlight, the linear regression slope of k_{obs} and total UVB irradiance was 0.09 ± 0.03 $m^2 W^{-1} h^{-1}$ ($R^2 = 0.86$, Figure 2.14), not significantly different than the β value of 0.12 ± 0.02 $m^2 W^{-1} h^{-1}$ estimated in a previous study (Silverman et al., 2015). This result suggested that the tUVB model was able to roughly estimate the observed inactivation rates of MS2 in sensitizer-free water at different depths in wetland water column under simulated sunlight. Under natural sunlight, linear regression slopes of k_{obs} and total UVB irradiance measured by spectroradiometer and predicted using SMARTS were similar to each other but only about one third of the β value [$\gamma^{spec} = 0.03 \pm 0.01$ $m^2 W^{-1} h^{-1}$ ($R^2 = 0.64$), $\gamma^{SMARTS} = 0.04 \pm 0.01$ $m^2 W^{-1} h^{-1}$ ($R^2 = 0.77$), Figure 2.15]. Given that shorter wavelengths in the UVB range are likely to cause more damage to MS2 than longer wavelengths, different light sources with the same total UVB irradiance but various $\frac{I_{280-300nm}}{I_{300-320nm}}$ ratios can cause different inactivation rates. The difference in the ratios of irradiance of shorter wavelength UVB to longer wavelength UVB between simulated sunlight and natural sunlight (Table 2.3) is likely result in the discrepancy between γ^i and β values. This result revealed the major limitation of the simplied tUVB model, which weighs damage from all UVB wavelengths equally.

In conclusion, the strong linear correlation between k_{obs} and total UVB irradiance observed from the experimental results suggested that the tUVB model might be used as a simplified model to

estimate sunlight inactivation rates of viruses and other organisms for which no PAS are available. Nonetheless, the modeled results need to be interpreted carefully if the tUVB model is developed and used under different light sources.

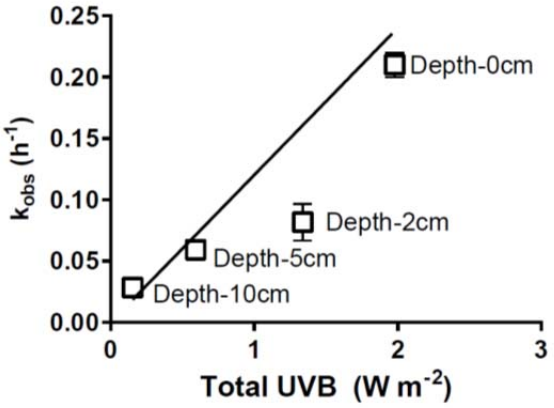

Figure 2.14. Comparison between $k_{obs}(z)$ and $k_{mod,tUVB}(z)$ of MS2 in sensitizer-free solution at different depths in wetland water under simulated sunlight. Error bar indicate ± one standard error of replicates. Line is the total UVB model with $\beta = 0.12 \pm 0.02$ m^2 W^{-1} h^{-1}. Labels next to data points designate the depth of the samples.

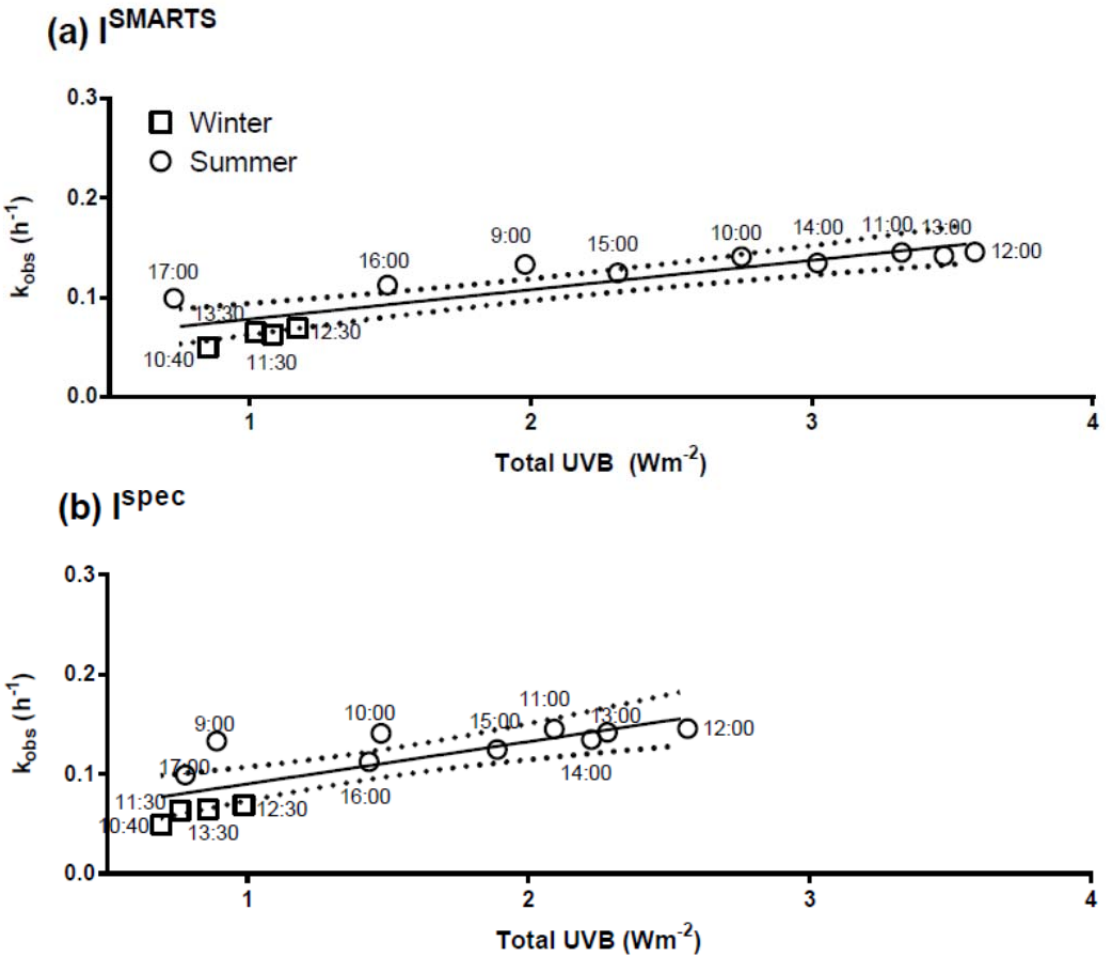

Figure 2.15. Relationship between total UVB irradiance and MS2 kobs in clear, sensitizer-free solution for 1 h intervals with exposure to natural sunlight in Berkeley, CA. Solid lines are the linear regression lines [(a) $\gamma^{\mathrm{SMARTS}} = 0.04 \pm 0.01$ m^2 W^{-1} h^{-1}; $R^2 = 0.77$; (b) $\gamma^{\mathrm{spec}} = 0.03 \pm 0.01$ m^2 W^{-1} h^{-1}; $R^2 = 0.64$]. Dotted lines show 95% confidence intervals of the linear regression lines. Labels next to data points designate the time of day the sample and irradiance spectrum were taken.

CHAPTER 3. Sunlight inactivation of fecal indicator bacteria in open-water unit process treatment wetlands: Modeling endogenous and exogenous inactivation rates

Reproduced with permission from Mi T. Nguyen[1]; Justin T. Jasper[2]; Alexandria B. Boehm[3]; and Kara L. Nelson[4]. Sunlight inactivation of fecal indicator bacteria in open-water unit process treatment wetlands: Modeling the endogenous and exogenous inactivation rates. In preparation for submission to *Water Research.*

[1]Primary author and researcher

[2,3]Editor

[4]Editor and advisor

3.1 Introduction

Constructed wetlands dominated by emergent macrophytes are capable of providing modest removal of fecal indicator bacteria (FIB) (e.g., up to 80% removal of total and fecal coliforms and 99% removal of fecal streptococci) via cell die-off, attachment-sedimentation, and predation processes (Kadlec and Wallace, 2009). Sunlight inactivation, an important mode of disinfection in waste stabilization ponds (Davies-Colley et al., 1997) and other sunlit waters (Boehm et al., 2009; McGuigan et al., 2012), is usually insignificant in vegetated wetlands due to shading by emergent macrophytes and floating vegetation. Unit process wetlands, consisting of individual cells that are designed to treat specific contaminants, can promote sunlight inactivation in shallow, open-water cells (Horne and Fleming-Singer, 2005; Jasper et al., 2013).

Three mechanisms of sunlight inactivation can affect bacteria in shallow, open-water wetlands: direct and indirect endogenous mechanisms and indirect exogenous mechanism (Davies-Colley et al., 1999; Silverman et al., 2013). Direct endogenous inactivation is caused by damage to bacterial components that absorb solar irradiation (e.g., nucleic acids) (Jagger, 1985). Indirect endogenous inactivation occurs when solar irradiation is absorbed by endogenous photosensitizers (e.g., NADH/NADPH, flavins, porphyrins) to form reactive intermediates which can damage other components of the bacterium (Cunningham et al., 1985). Exogenous inactivation occurs when photosensitizers in the water absorb solar irradiation and produce exogenous reactive intermediates [e.g., singlet oxygen ($^1O_2$), hydrogen peroxide (H_2O_2), superoxide (O_2^-), and hydroxyl radical (•OH)] (Cooper et al., 1989). The contribution of each mechanism to sunlight inactivation is expected to vary for different bacteria, depending on their susceptibility to each mechanism and the water quality conditions. Despite the growing understanding of sunlight inactivation mechanisms of bacteria, modeling approaches have not yet been developed that account separately for endogenous and exogenous inactivation mechanisms. Two recent papers presented approaches for modeling the endogenous and exogenous sunlight inactivation of viruses (Mattle et al., 2015; Silverman et al., 2015); this paper builds upon the approach that was developed in Silverman et al.

The goals of this study were to evaluate the removal of indigenous FIB in a pilot-scale open-water wetland receiving nitrified, non-disinfected wastewater, and to develop a predictive model for FIB removal that accounts for endogenous and exogenous inactivation mechanisms. Inactivation rate constants were determined from lab experiments and an empirical correction factor was used to account for differences between lab and field conditions. The model was evaluated using one year of monitoring data from the pilot-scale open-water wetland. The improved understanding of mechanisms and the model can be used to optimize the design of unit process wetlands for FIB removal. The modeling approach can be applied to other sunlit waters, where sunlight inactivation also plays a key role in FIB disinfection.

3.2 Materials and Methods

The study consisted of six specific tasks. Tasks one through four consisted of experiments, which are summarized in Table 3.1 (the task numbers are indicated). The tasks were: (1) monitoring the removal of indigenous wastewater *E. coli* and enterococci in the open-water wetland for one year; (2) in-situ batch experiments to measure inactivation rates of indigenous FIB in the field under controlled conditions (e.g., simplified hydraulics and known initial concentration); (3) lab experiments to determine inactivation rates for endogenous and

exogenous mechanisms of lab-cultured *E. coli* and enterococcal isolates with simulated sunlight; (4) lab comparison of sunlight inactivation rates of lab-cultured and indigenous wastewater FIB collected from the wetland influent; (5) development of the model to predict sunlight inactivation rates of FIB in the wetland; and (6) comparison of modeling results with the monitoring data. A detailed description of each task is provided in the sections below.

Table 3.1. Summary of experiments conducted in Chapter 3.

Conditions	Experiments	Objectives
Pilot-scale open-water wetland (Task 1)	Monitoring concentrations of indigenous wastewater FIB for one year	- Characterize performance of pilot wetland - Determine removal rate constants of indigenous FIB (k_{obs}^{W}) in the pilot wetland
In-situ batch reactor (Task 2)	Dark reactors	- Measure dark removal rate constant of indigenous FIB (k_{dark}^{B})
	Light reactors	- Measure total removal rate constant of indigenous FIB (k_{obs}^{B})
Laboratory	Lab-cultured FIB in clear water (Task 3)	- Characterize importance of endogenous mechanisms - Determine endogenous inactivation rate constant (k_{endo}^{L})
	Lab-cultured FIB in wetland water (Task 3)	- Characterize importance of exogenous mechanism - Determine exogenous inactivation rate constants (k_{exo}^{L} and k_2)
	Lab-cultured FIB vs. Indigenous wastewater FIB in clear water (Task 4)	- Measure the difference in susceptibility to sunlight inactivation of FIB from these two sources

3.2.1 Experiments at the pilot-scale open-water wetland

Monitoring concentrations of indigenous FIB in the open-water wetland (Task 1). Concentrations of *E. coli* and enterococci in a pilot-scale open-water wetland in Discovery Bay, CA (37°54′N, 121°36′W) were monitored throughout the year. The 400 m^2 open-water cell was approximately 20 cm deep and received approximately 65 m^3 d^{-1} of nitrified, non-disinfected wastewater from the adjacent oxidation ditch at the Discovery Bay wastewater treatment plant. The wetland contained three baffles to promote plug-flow hydraulic conditions, and was lined with concrete and geotextile fabric to prevent the growth of emergent macrophytes. A 2 to 10-cm thick biomat containing a highly productive community of photosynthetic and associated microorganisms accumulated on the wetland bottom.

Grab samples were collected from one to seven times per month at different locations in the wetland (i.e., inlet, turns 1, 2, 3, and outlet, Figure 1.1) from January to December 2012. Samples collected in September, part of October, and November 2012 were considered as dark controls due to the growth of duckweed that covered the entire water surface of the wetland. Samples were collected in sterile bottles and stored on ice for less than 4 hours prior to analysis.

The concentrations (MPN/100 mL) of *E. coli* and enterococci were determined using Colilert and Enterolert defined substrate assays implemented in 97 well Quanti-Trays following vendor instructions (IDEXX, Westbook, MN).

pH, dissolved oxygen (DO), conductivity, and temperature measurements of the wetland water were recorded each sampling event using Manta multi-probes (Eureka Environmental) located at the inlet and outlet of the cell (Figure 3.1). Dissolved organic carbon (DOC) concentrations (TOC-VSH, Shimadzu) and UV-VIS absorbance spectra (280 – 700 nm; Lambda 35, Perkin-Elmer) were also measured using 1-cm quartz cuvettes (Figure 3.2). Solar irradiance was predicted using SMARTS on sunny days (Gueymard, 2005) (Figure 3.3), and measured using a spectroradiometer with a cosine detector (EPP2000-HR, CR2; StellarNet Inc.) on cloudy days. Solar irradiance at different depths in the water column (Figure 3.4) was estimated as described in previously in Chapter 2.

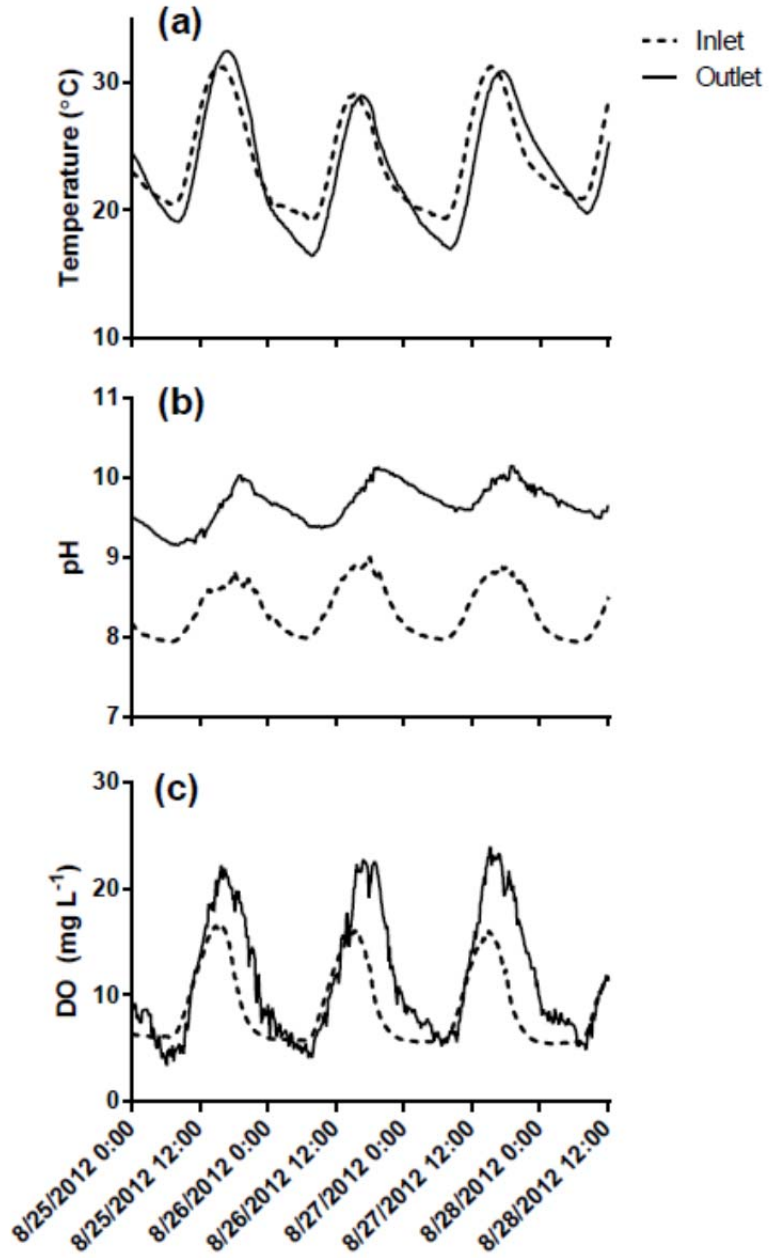

Figure 3.1. Recorded data of (a) temperature, (b) pH, and (c) dissolved oxygen (DO) over 84 hours at the inlet and outlet of the open-water wetland cell during clear skies.

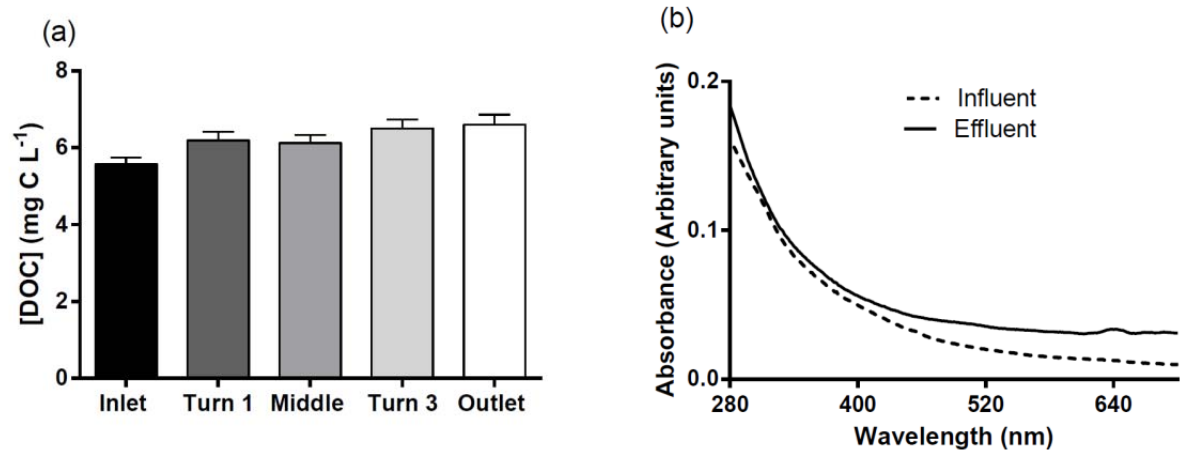

Figure 3.2. (a) Average DOC concentrations at different locations in the open-water wetland cell throughout the year (n=20, error bars indicate ± one standard error of replicate samples) and (b) UV-VIS absorbance of the wetland influent and effluent (n=7, only mean values are shown).

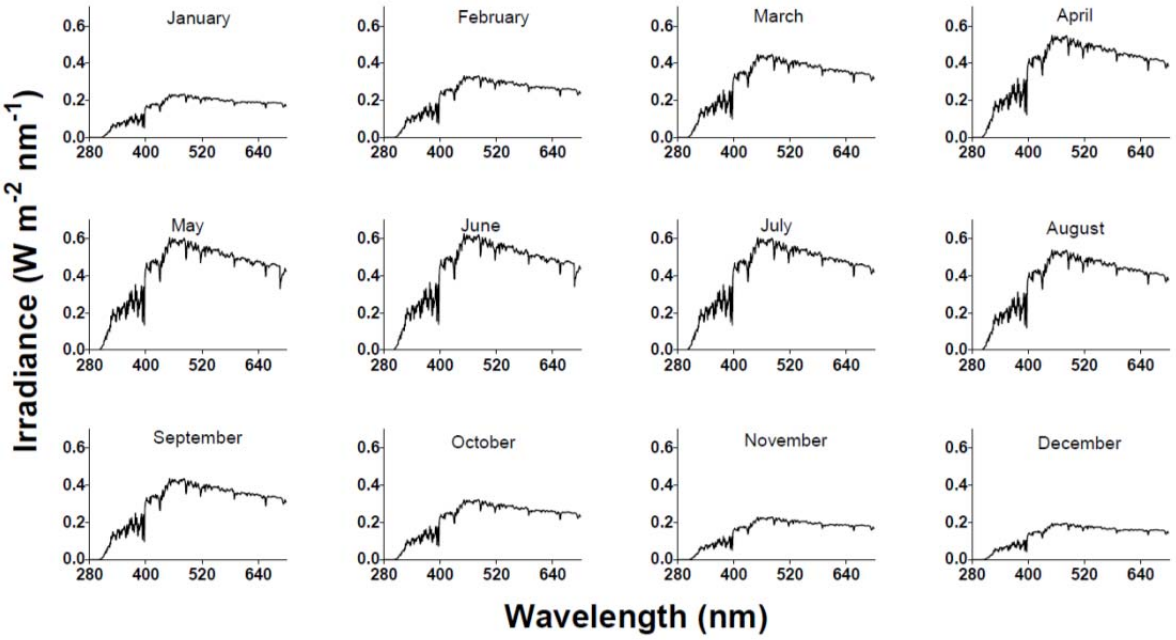

Figure 3.3. 24-hour averaged solar irradiance on the 21st day of each month throughout the year at Discovery Bay, CA. The irradiance data was modeled using SMARTS in sunny, clear sky conditions (Gueymard, 2005).

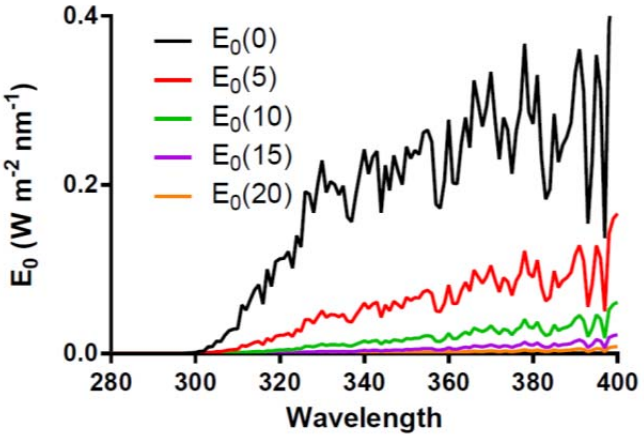

Figure 3.4. Estimated scalar solar irradiance (only UV portion is shown) at summer noon at different depths (0, 5, 10, 15, 20 cm) in the pilot-scale open-water wetland water column.

Experiments with in-situ batch reactors at the open-water wetland (Task 2). Acrylic tanks (open on top) containing biomat collected from the biomat layer at turn 2 in the open-water wetland and nitrified wastewater from the wetland influent were used for in-situ batch experiments. The wetland influent (rather than effluent) was used to ensure high enough initial concentrations of the indigenous indicator bacteria in the batch reactors. A biomat volume of 4.75 L was mixed with 19 L of nitrified wastewater, resulting in 20 cm total depth with 5 cm of sediment after the sediment settled down in ~10 mins. A separate experiment was conducted to verify that the inactivation rates in tanks were similar for 100% influent versus a 50:50 mixture of wetland influent and effluent (Figure 3.5), confirming that the wetland influent could be used to represent water in the whole wetland. Aluminum foil was used to cover the outside of the reactors for dark controls. One dark control was included in each experiment. A single biomat-free control that contained only nitrified wastewater was also included in one experiment. Reactors containing biomat and exposed to sunlight were duplicate in each experiment. Grab samples were collected at 8:00 and 17:00 (local time) on two consecutive days and analyzed for *E. coli* and enterococci concentrations using IDEXX. Experiments were conducted in August and October 2012, and June 2014.

The observed, first-order inactivation rate constants of indigenous wastewater bacteria in the in-situ batch reactors were calculated from linear regression of graphs of $\ln(C_t/C_0)$ versus time (k^B_{obs}, h^{-1}). The reported data are mean values of duplicate samples ± one standard error.

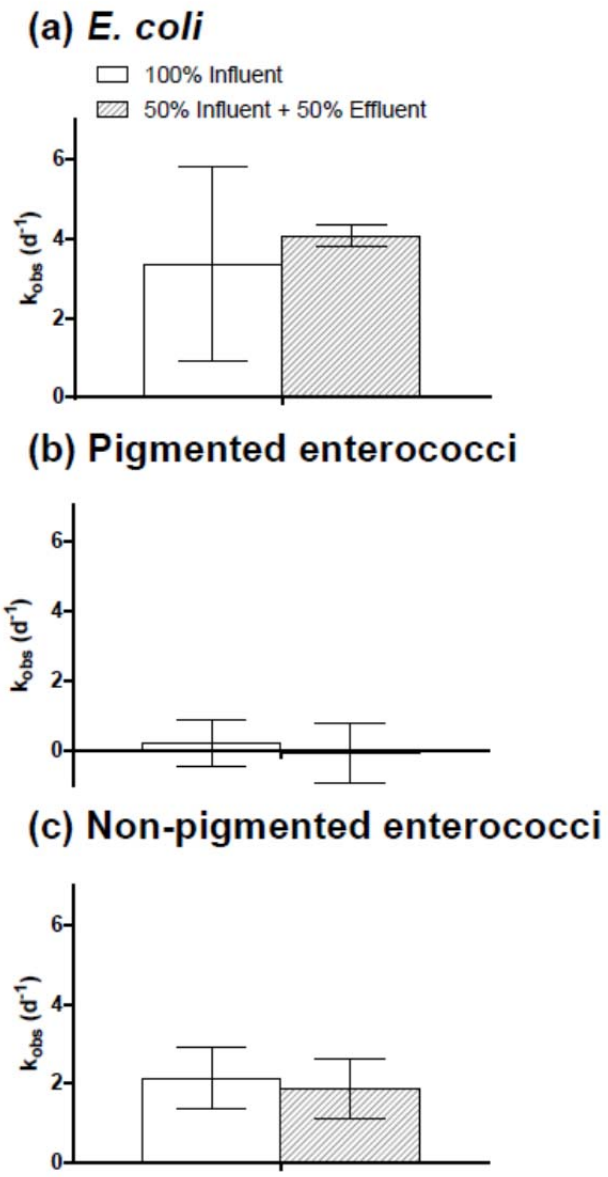

Figure 3.5. Measured inactivation rate constants of (a) *E. coli*, (b) pigmented enterococci, and (c) non-pigmented enterococci in in-situ batch reactors fed with 100% influent and 50% influent+50% effluent of the open-water wetland. Error bars indicate ± one standard error of the replicate samples. Experiments were conducted at Discovery Bay, CA in August and October 2012, and June 2014.

Isolation, pigmentation test, and speciation for indigenous wastewater enterococci (Tasks 1 and 2). The pigmentation test was conducted with samples collected from the wetland at three locations (inlet, turn 2, and outlet) on 3 days when the wetland was covered by duckweed, and 4 other days in October 2012 when the water was exposed to sunlight. For in-situ batch reactors, pigmentation tests were conducted for samples that the collected from dark controls and reactors exposing to sunlight on 4 days in October 2012. Indigenous enterococci from wetland water samples were isolated by streaking liquid culture from each positive well in the Enterolert

Quantitrays onto mEnterococcus agar plates. Single colonies that grew on the selective mEnterococcus agar were selected as candidate isolates and transferred onto Tryptic Soy Agar plates; typically one or two colonies were selected from each plate. After 24 h of incubation at 37°C, pigmentation tests were conducted for each isolate. The tip of a sterile cotton-tip swab was touched to the surface of a single colony grown on Tryptic Soy Agar and held under a lamp. Yellow colonies were characterized as pigmented (Facklam and Collins, 1989). A total of ~3,200 isolates were collected and tested for pigmentation. Results from the pigmentation tests for samples that exposed to sunlight in October were used to determine concentrations of pigmented and non-pigmented enterococci in the open-water wetland and in-situ reactors throughout the year. Eleven wetland water isolates (4 pigmented, 7 non-pigmented) were randomly chosen for 16S rRNA sequencing at the UC Berkeley DNA sequencing facility to be confirmed as enterococci. Details of 16S rRNA sequencing of these isolates are presented in Table 3.2. 10 out of 11 of the chosen candidate isolates were confirmed as enterococci and one was identified as *Lactococcus* spp. One pigmented and one non-pigmented enterococcal isolate were chosen for inactivation experiments under simulated sunlight (described below in Task 3).

Collecting indigenous FIB from nitrified wastewater from the wetland influent (Task 4). Four pre-sterilized positively charged NanoCeram VS2.5-5 cartridge filters (Argonide Corporation, Sanford, FL) were used to collect indigenous wastewater FIB from approximately 510 L (per filter) of the wetland influent. Sample collection steps were conducted following USEPA's instructions for concentrating waterborne viruses: Four pre-sterilized positively charged NanoCeram VS2.5-5 cartridge filters (Argonide Corporation, Sanford, FL) were used to collect indigenous FIB from approximately 510 L of nitrified wastewater (per filter) at the inlet of the open-water wetland. Sample collection steps were conducted followed USEPA's instructions for concentrating waterborne viruses using positive charge cartridge filters (Fout et al., 2001). The cartridge filters were stored on ice and processed for bacteria elution and concentration within 3 h after samples were taken. Beef extract (3% Beef Extract, 3% Tween 80, 0.3 M NaCl, pH 9.0) was added to the housing unit until the filter was completely immersed (~450 mL) for a hold time of 15 min. More beef extract (~550 mL) was then passed through the filter under positive pressure (N_2 gas) into a sterile beaker. Indigenous bacteria were collected from the eluate via the following steps:

- Step 1: The eluate of approximately 1 L was centrifuged at 8000×g for 5 min to collect for bacterial cells and settleable particles.
- Step 2: The pellet after centrifugation in step 1 was collected and resuspended in 10 mL of sterile phosphate-buffered saline (PBS, 5 mM NaH_2PO_4, 18 mM Na_2HPO_4, 145 mM NaCl, pH 7.5).
- Step 3: The PBS solution was centrifuged at 500×g for 5 min to separate settleable particles from the solution.
- Step 4: The supernatant after centrifugation in step 3 was collected and centrifuged at 8000×g for 5 min to collect for bacterial cells.
- Step 5: The pellet collected in step 4 was resuspended in 10 mL of PBS and used for inactivation experiments under simulated sunlight.

The initial concentrations of indigenous *E. coli* and enterococci in the wastewater were 3×10^4 MPN/100 mL and 10^3 MPN/100 mL, respectively. The concentrations of *E. coli and* enterococci after concentrating were 3×10^7 MPN/100 mL and 10^6 MPN/100 mL, respectively.

Table 3.2. 16S rRNA sequences of two chosen enterococcal isolates used in this study.

Non-pigmented isolate sequence – GenBank accession No. KJ434953
GCGGTTTCTTAAGTCTGATGTGAAAGCCCCCGGCTCAACCGGGGAGGGTCATTGGA AACTGGGAGACTTGAGTGCAGAAGAGGAGAGTGGAATTCCATGTGTAGCGGTGAA ATGCGTAGATATATGGAGGAACACCAGTGGCGAAGGCGGCTCTCTGGTCTGTAACT GACGCTGAGGCTCGAAAGCGTGGGGAGCAAACAGGATTAGATACCCTGGTAGTCC ACGCCGTAAACGATGAGTGCTAAGTGTTGGAGGGTTTCCGCCCTTCAGTGCTGCAG CAAACGCATTAAGCACTCCGCCTGGGGAGTACGACCGCAAGGTTGAAACTCAAAG GAATTGACGGGGGCCCGCACAAGCGGTGGAGCATGTGGTTTAATTCGAAGCAACG CGAAGAACCTTACCAGGTCTTGACATCCTTTGACCACTCTAGAGATAGAGCTTTCC CTTCGGGGACAAAGTGACAGGTGGTGCATGGTTGTCGTCAGCTCGTGTCGTGAGAT GTTGGGTTAAGTCCCGCAACGAGCGCAACCCTTATTGTTAGTTGCCATCATTTAGTT GGGCACTCTAGCGAGACTGCCGGTGACAAACCGGAGGAAGGTGGGGATGACGTCA AATCATCATGCCCCTTATGACCTGGGCTACACACGTGCTACAATGGGAAGTACAAC GAGTCGCTAGACCGCGAGGTCATGCAAATCTCTTAAAGCTTCTCTCAGTTCGGATT GCAGGCTGCAACTCGCCTGCATGAAGCCGGAAT
Pigmented isolate sequence – GenBank accession No. KJ434954
CACGCCGCGTGAGTGAAGAAGGTTTTCGGATCGTAAAACTCTGTTGTTAGAGAAGA ACAAGGATGAGAGTAAAATGTTCATCCCTTGACGGTATCTAACCAGAAAGCCACG GCTAACTACGTGCCAGCAGCCGCGGTAATACGTAGGTGGCAAGCGTTGTCCGGATT TATTGGGCGTAAAGCGAGCGCAGGCGGTTTCTTAAGTCTGATGTGAAAGCCCCCGG CTCAACCGGGGAGGGTCATTGGAAACTGGGAGACTTGAGTGCAGAAGAGGAGAGT GGAATTCCATGTGTAGCGGTGAAATGCGTAGATATATGGAGGAACACCAGTGGCG AAGGCGGCTCTCTGGTCTGTAACTGACGCTGAGGCTCGAAAGCGTGGGGAGCGAA CAGGATTAGATACCCTGGTAGTCCACGCCGTAAACGATGAGTGCTAAGTGTTGGAG GGTTTCCGCCCTTCAGTGCTGCAGCAAACGCATTAAGCACTCCGCCTGGGGAGTAC GACCGCAAGGTTGAAACTCAAAGGAATTGACGGGGGCCCGCACAAGCGGTGGAGC ATGTGGTTTAATTCGAAGCAACGCGAAGAACCTTACCAGGTCTTGACATCCTTTGA CCACTCTAGAGATAGAGCTTCCCCTTCGGGGGCAAAGTGACAGGTGGTGCATGGTT GTCGTCAGCTCGTGTCGTGAGATGTTGGGTTAAGTCCCGCAACGAGCGCAACCCTT ATTGTTAGTTGCCATCATTTAGTTGGGCACTCTAGCGAGACTGCCGGTGACAAACC GGAGGAAGGTGGGGGATGACGTCAAATCATCATGCCCCTTATGACCTGGGCTACAC ACGTGCTACAATGGGAAGTACAACGAGTTGCGAAGTCGCGAGGCTAAGCTAATCT CTTAAAGCTTCTCTCAGTTCGGATTGTAGGCTGCAACTCGCCTACATGAAGCCGGA ATCGCTAGTAN

3.2.2 Lab experiments (Task 3 and 4)

Growing and harvesting lab-cultured bacteria. The five lab-cultured bacteria used in this study were *Escherichia coli* NCM 4236, *Enterococcus faecalis* ATCC 19433, *Enterococcus casseliflavus* ATCC 25788, and pigmented and non-pigmented enterococcal isolates from the wetland (Table 3.3). Lab-cultured bacteria were stored as glycerol stocks at -80°C. Broth cultures were prepared fresh daily by inoculating the glycerol stocks in tryptic soy (BD, Difco 211825) and brain heart infusion (BD, Difco 237500) broths for *E. coli* and enterococci, respectively. Broth cultures were then incubated at 37°C for 24 h for the bacteria to reach stationary phase. Cells were pelleted by centrifuging at 6,800×g for 3 min, then washed and resuspended with

PBS. The initial concentrations of bacteria were ~10^7 colony forming units (CFU) mL^{-1} in sunlight inactivation experiments under simulated sunlight.

Table 3.3. Lab-cultured bacteria used in Chapter 3.

Bacteria	**Description/Source**
E. coli NCM 4236	Kanamycin-resistant K12 strain from Dr. Sidney Kustu's lab at UC Berkeley
Ent. faecalis ATCC 19433	Non-pigmented enterococci lab strain from ATCC
Ent. casseliflavus ATCC 25788	Pigmented enterococci lab strain from ATCC
Non-pigmented enterococcal isolate (*)	Non-pigmented *Enterococcus* spp. isolated from the wetland
Pigmented enterococcal isolate (*)	Pigmented *Enterococcus* spp. isolated from the wetland

Inactivation experiments under simulated sunlight. Bacteria were added to clear water (20 mM NaH_2PO_4, 10 mM NaCl, pH adjusted to 7.5) or wetland water (collected from the open-water wetland at Discovery Bay, pH adjusted to 7.5). Experiments were conducted in uncovered, 5-cm deep, black-painted, glass beakers, which were stirred and maintained at 20°C. The beakers were irradiated using an ozone-free 1000 W Xe arc lamp housed in a solar simulator (Oriel, model number 91194; Newport; Irvine, CA) fitted with a 1.5:G:A global air mass filter (Newport, part number 81388) and an atmospheric attenuation filter (Newport, part number 81017) to mimic the solar spectrum at summer noon at Discovery Bay. Some experiments were also conducted with a UVB-blocking filter (see Figure 3.6 for solar simulator spectra). Dark controls were maintained under the same conditions as light samples, but covered with aluminum foil. Subsamples were collected periodically for enumeration of *E. coli* or enterococci using spread plate method. Selective media mTEC agar (BD, Difco, 214884) and mEnterococcus agar (BD, Difco, 274620) were used for enumeration of *E. coli* and enterococci, respectively, to avoid interference of other microorganisms in wetland water. Experiments were conducted in duplicate reactors on the same day using the same bacterial seed culture.

The observed, first-order inactivation rate constants of bacteria in lab experiments were calculated from linear regression of graphs of $\ln(C_t/C_0)$ verses either time (k^L_{obs}, h^{-1}) or photon fluence ($k^L_{obs,photon}$, $m^2\ Ei^{-1}$). $k^L_{obs,photon}$ values were k^L_{obs}values after correcting for light screening. The observed inactivation rates of duplicate reactors were averaged and are reported as the mean values ± one standard error.

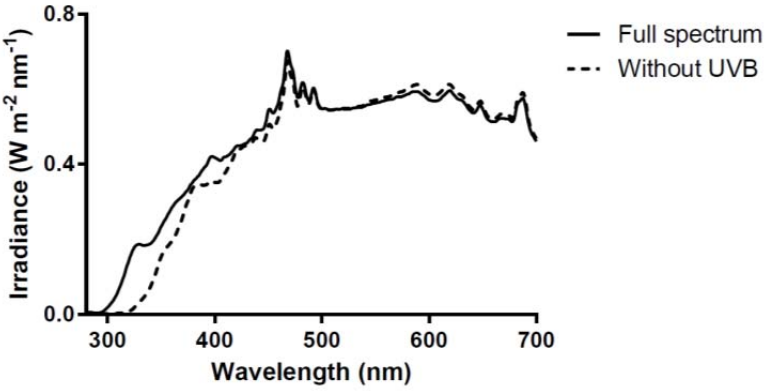

Figure 3.6. Solar simulator outputs in lab inactivation experiments with atmospheric attenuation filter and UVB-blocking filter.

3.2.3 Modelling inactivation of FIB in in-situ batch reactors and the open-water wetland (Task 5)

The modeled inactivation rate constants in the in-situ batch reactors and the open-water wetland (k^i_{tot}, i = B for in-situ batch reactors or W for open-water wetland) were estimated as the sum of the rate constants of all possible inactivation processes, including: sunlight inactivation (endogenous and exogenous mechanisms, k^i_{endo} and k^i_{exo}), and dark inactivation (k^i_{dark}):

$$k^i_{tot} = k^i_{endo} + k^i_{exo} + k^i_{dark} \quad (3.1)$$

k^W_{dark} values of the FIB were assumed to be equal to their k^B_{dark} values from dark controls in in-situ batch experiments. The water column was assumed to be equal to 20 cm throughout the whole wetland, and the water was well-mixed across this depth. As in previous research, k^i_{endo} and k^i_{exo} values of the FIB were multiplied by 15/20 to account for the shading effect of the 5-cm thick biomat layer on the bottom of the wetland (Jasper and Sedlak, 2013; Silverman et al., 2015).

The main steps for modeling the inactivation rate constants for indigenous FIB in the pilot-scale wetland, k^W_{endo} and k^W_{exo}, are summarized here with further description in sections below.

- Rate constants determined from lab experiments (k^L_{endo} and k^L_{exo}) were adjusted to the field conditions of the pilot-scale wetland (e.g., accounting for the sunlight spectrum, absorbance of the water column, and steady-state singlet oxygen concentration)
- A correction factor (r) was used to convert the rate constants for lab-cultured bacteria to rate constants for FIB in the wetland (k^W_{endo} and k^W_{exo}). The correction factor was determined from the in-situ batch experiments (k^B_{endo} and k^B_{exo}), as described below.

Calculating k^B_{endo}. Values of k^B_{endo} (d^{-1}) were estimated based on the inactivation rates of lab-cultured bacteria in clear water without photosensitizers (k^L_{endo}, h^{-1}) under full spectrum simulated sunlight. Due to the lack of information on photoaction spectra of the bacteria, it was

assumed that the inactivation rates scaled linearly with total UVA and UVB light (280 – 400nm) (Chapter 2), as these are the wavelengths responsible for the majority of endogenous inactivation of *E. coli* and enterococci (Davies-Colley et al., 1997; Kadir and Nelson, 2014; Sinton et al., 2002).

$$k_{endo}^{B} = 24 \times k_{endo}^{L} \times \frac{\sum_{\lambda=280}^{400} \langle E_0^{sun}(z,\lambda)\rangle_z}{\sum_{\lambda=280}^{400} \langle E_0^{sim}(z,\lambda)\rangle_z} \quad (3.2)$$

Values for k_{endo}^{L} (h^{-1}) are the inactivation rate constants determined from experiments of lab-cultured *E. coli*, and pigmented and non-pigmented enterococcal isolates in clear water with full-spectrum simulated sunlight. Equation 3.2 was multiplied by 24 h/d to convert units to d^{-1}. $\sum_{\lambda=280}^{400} \langle E_0^{sim}(z,\lambda)\rangle_z$ is the sum of depth-averaged scalar simulated light irradiance from 280 to 400 nm in the clear water column, and $\sum_{\lambda=280}^{400} \langle E_0^{sun}(z,\lambda)\rangle_z$ is the sum of 24 h-averaged, depth-averaged scalar solar irradiance in the wetland water column.

The average light transmitted over a well-mixed water column of depth z [$\langle E_0(z,\lambda)\rangle_z$] can be estimated as follows:

$$\langle E_0(z,\lambda)\rangle_z = E_d(0,\lambda)\left(\frac{1 - e^{-\psi \cdot a(\lambda) \cdot z}}{\psi \cdot a(\lambda) \cdot z}\right) \quad (3.3)$$

where $a(\lambda)$ is the naperian absorption coefficient (cm^{-1}), which is assumed to be equal to the vertical attenuation coefficient K_d assuming a negligible scattering effect .

ψ is a pathlength correction factor used to correct for light-path geometry; ψ was assumed to equal 1 in the lab (i.e., the solar simulator used in experiments created a collimated beam of light), and was calculated for the wetland using the following equation (Bodrato and Vione, n.d.):

$$\psi = \left(\sqrt{1 - (n^{-1}\sin\gamma)^2}\right)^{-1} \quad (3.4)$$

where γ is the solar zenith angle (Table 3.4) and n is the index of refraction (~1.34 for water) (Zepp and Cline, 1977).

Table 3.4. Values of solar zenith angle at Discovery Bay, CA at noon on the 21st of each month, and values of the correction factor ψ as determined by SMARTS.

Month	Solar zenith angle (γ)	Pathlength correction factor (ψ)
January	57.9	1.29
February	48.6	1.21
March	37.7	1.12
April	26.0	1.06
May	17.7	1.03
June	14.6	1.02
July	17.7	1.03
August	26.0	1.06
September	37.3	1.12

Month	Solar zenith angle (γ)	Pathlength correction factor (ψ)
October	48.7	1.21
November	57.9	1.29
December	61.3	1.32

Calculating k_{exo}^{B}. Exogenous inactivation rates were only calculated for enterococci due to the resistance of the lab strain *E. coli* to the exogenous mechanism (see Results). k_{exo}^{B} values of indigenous enterococci in in-situ batch reactors were calculated as a function of the steady-state concentration of $^1O_2$ because it was previously found to be an important reactive intermediate contributing to the inactivation of MS2 bacteriophage (Kohn and Nelson, 2007), and is likely involved in the exogenous inactivation of *Ent. faecalis* (Kadir and Nelson, 2014). The impact of •OH, which is mainly produced by photolysis of NO_3^- in the wetland ($[NO_3^-]_{influent}$ = 21 mgN L^{-1}) on the exogenous inactivation of the FIB was assumed to be negligible because there was no observed enhancement in sunlight inactivation of lab-cultured *E. coli* and *Ent. faecalis* in the presence of added NO_3^- (0, 20 and 100 mg N L^{-1}) (data not shown). It is likely that other reactive intermediates are involved in exogenous inactivation, but given the incomplete knowledge it was assumed that all exogenous processes scale with the steady-state concentration of $^1O_2$. Thus, inactivation by the exogenous mechanism was modeled as a pseudo, first-order reaction with the rate constant k_{exo}^{B} defined as follows:

$$k_{exo}^{B} = k_2 \times \left[{}^1O_2 \right]_{ss,bulk,mod} \tag{3.5}$$

where k_2 is an apparent second-order rate constant for the reaction between $^1O_2$ and enterococcal isolates, and $\left[{}^1O_2 \right]_{ss,bulk,mod}$ is the modeled steady-state concentration of singlet oxygen in wetland water in the field. The k_2 values were calculated from the measured $\left[{}^1O_2 \right]_{ss,bulk}$ and k_{obs}^{L} values in experiments in clear water and in wetland water under full spectrum simulated sunlight. Details of calculations of k_2 and $\left[{}^1O_2 \right]_{ss,bulk,mod}$ are presented as follows.

Calculating k_2. Under laboratory conditions, exogenous inactivation of enterococcal isolates in wetland water under full spectrum simulated sunlight were assumed to scale with the steady-state concentration of singlet oxygen in the wetland ($\left[{}^1O_2 \right]_{ss,bulk}$):

$$k_{exo}^{L} = k_2 \times \left[{}^1O_2 \right]_{ss,bulk} \tag{3.6}$$

where k_2 is the observed second-order rate constants between each bacterium and $^1O_2$; $k_{exo}^{L}$is the modeled exogenous inactivation rate of each bacterium in wetland water. To determine the values of k_2 for pigmented and non-pigmented enterococci, Equation 3.6 was solved for k_2, and k_{exo}^{L} and $\left[{}^1O_2 \right]_{ss,bulk}$values were determined from the lab experiments under full spectrum simulated sunlight. The value of k_{exo}^{L} was estimated as the difference between the total measured inactivation rate constant and the endogenous inactivation rate constant, after accounting for light attenuation (normalizing by photon fluence in wetland water and in clear water):

$$k^{L}_{exo,photon} = k^{L}_{obs,photon}(\text{in wetland water}) - k^{L}_{obs,photon}(\text{in clear water}) \quad (3.7)$$

Thus, k_2 (M^{-1} d^{-1}) can be estimated as:

$$k_2 = 24\frac{\sum_{\lambda=280}^{400}\langle E_0^{sim}(z,\lambda)\rangle_z \Delta\lambda}{\left[{}^1O_2\right]_{ss,bulk}}\left[\frac{k^{L}_{obs}(\text{in wetland water})}{\sum_{\lambda=280}^{400}\langle E_0^{sim}(z,\lambda)\rangle_z \Delta\lambda} - \frac{k^{L}_{obs}(\text{in clearwater})}{\sum_{\lambda=280}^{400}\langle E_0^{sim}(0,\lambda)\rangle_z \Delta\lambda}\right] \quad (3.8)$$

where $\left[{}^1O_2\right]_{ss,bulk}$ is the mean value of steady-state concentration of singlet oxygen produced in the wetland water under full spectrum simulated sunlight from measurements in lab. The measurements were conducted in triplicate with wetland water collected on different days, using furfulryl alcohol (FFA) (Haag et al., 1984) as a probe compound.

Calculating $\left[{}^1O_2\right]_{ss,bulk,mod}$. Due to the lack of equipment for direct measurement of singlet oxygen in the field, its steady-state concentration in in-situ batch reactors and in the wetland was predicted following the approach used by Jasper and Sedlak (Jasper and Sedlak, 2013), which is based on the research of Haag and Hoigne (1986):

$$\left[{}^1O_2\right]_{ss,bulk,mod} = 1\times10^{-14}\cdot[DOC]\cdot\left(\frac{1-e^{-\psi\cdot a(410)\cdot z}}{\psi\cdot a(410)\cdot z}\right)\cdot\frac{E_0(0,\lambda=410)}{E_0(0,\lambda=410)_{June-noon}} \quad (3.9)$$

[DOC] is the dissolved organic carbon concentration measured the in open-water cell – an average value of 8 mg C L^{-1} was used (Jasper and Sedlak, 2013). $\left[{}^1O_2\right]_{ss,bulk,mod}$ was adjusted for changes in light irradiance and corrected for light attenuation in the water column using data at 410 nm, given that this wavelength was previously found to best predict steady-state concentration of singlet oxygen (Haag and Hoigne, 1986). $E_0(0,\lambda=410)_{June-noon}$ was predicted by SMARTS to be 1.27 W m^{-2}.

Calculating the ratio of modeled and measured inactivation rates (r). To account for differences between lab and wetland conditions (e.g., susceptibility to sunlight inactivation of lab-cultured FIB vs. indigenous FIB, diurnal fluctuation of pH and DO), we calculated the ratio of modeled and measured inactivation rates in in-situ batch reactors in the field $\left(r = k^{B}_{tot}/k^{B}_{obs}\right)$ and used r as a correction factor for the prediction of inactivation rates in the pilot-scale wetland. k^{B}_{obs} values were measured from in-situ batch experiments, as described above. k^{B}_{tot} values are the modeled values, calculated as the sum of k^{B}_{endo}, k^{B}_{exo} , and k^{B}_{dark} using Equations 3.1, 3.2, and 3.5. Partition of pigmented and non-pigmented enterococci measured in the open-water wetland was used to calculate inactivation rates of indigenous pigmented and non-pigmented enterococci.

Calculating k^{W}_{endo} and k^{W}_{exo}. Sunlight inactivation rates of indigenous *E. coli* and enterococci in the wetland were calculated using Equations 3.2 and 3.5, and corrected for the difference between lab and wetland conditions using their respective r values:

$$k_{endo}^{W} = \frac{1}{r} \times 24 \times k_{endo}^{L} \times \frac{\sum_{\lambda=280}^{400} \langle E_0^{sun}(z,\lambda) \rangle_z}{\sum_{\lambda=280}^{400} \langle E_0^{sim}(z,\lambda) \rangle_z} \quad (3.10)$$

$$k_{exo}^{W} = \frac{1}{r} \times k_2 \times \left[{}^1O_2 \right]_{ss,bulk,mod} \quad (3.11)$$

3.2.4 Comparison of modeled and measured inactivation (Task 6)

The observed first-order inactivation rates of FIB in the pilot-scale open-water wetland (k_{obs}^{W}) were determined from the monitoring data using the same approach described in a previous study (Silverman et al., 2015). Briefly, k_{obs}^{W} values were calculated from monitoring data using the Wehner-Wilhelm equation, which describes a system with non-ideal flow and first-order kinetics (Wehner and Wilhelm, 1956).

$$\left[\frac{C_x}{C_0}\right]^{W} = \frac{4a \exp\left(\frac{1}{2d}\right)}{(1+a)^2 \exp\left(\frac{a}{2d}\right) - (1-a)^2 \exp\left(-\frac{a}{2d}\right)} \quad (3.12)$$

where $a = \sqrt{1 + 4k_{obs}^{W} \cdot \theta_x \cdot d}$; C_x and C_0 are the bacteria concentrations at each sampling location (x) and at the inlet, respectively, d is the dispersion number, and θ_x is the mean hydraulic retention time for each sampling location. C_x and C_0 values are the monitoring data measured on a particular day. Values of d and total θ_x were determined to be 0.08 and 1.12 d from a tracer test (Silverman et al., 2015). It was assumed that θ_x values at sampling locations turns 1, 2, and 3 correspond to 1/3, 1/2, and 2/3 of total θ_x, respectively. Values of k_{obs}^{W} were solved from Equation 4 using Solver (Microsoft Excel) by minimizing the root-mean-square error between C_x/C_0 values calculated from Equation 6 and observed C_x/C_0 values of FIB throughout the year. The observed C_x/C_0 values of pigmented and non-pigmented enterococci were estimated based on measured concentrations of total enterococci and pigmentation test results.

The modeled values, k_{mod}^{W}, were calculated as the sum of k_{endo}^{W}, k_{exo}^{W}, and k_{dark}^{B} using Equations 3.1, 3.10, and 3.11, and then compared with the observed values, k_{obs}^{W}.

3.2.5 Statistical tests

GraphPad Prism 6.0.1 (GraphPad Software, La Jolla, CA) was used to perform all statistical tests. Comparison of inactivation rate constants was performed using two-way ANOVA or paired t-tests, depending on the number of variables examined.

3.3 Results

3.3.1 Removal of the FIB in the open-water wetland

The removal of *E. coli* from the inlet to the outlet in the open-water wetland $\left[-\log\left(\frac{C_{out}}{C_0}\right)\right]$ generally increased with in solar intensity, from 0.6 log in December to about 3 logs in June and July (Figure 3.7a). The lowest *E. coli* removal (~0.5 log) occurred when the water surface was completely covered by duckweed (i.e., the water had minimal exposure to sunlight), suggesting that sunlight inactivation was the main contributor to the removal of *E. coli* in the wetland. From April to July, the removal of *E. coli* from the inlet to turn 1(~2 logs) was significantly higher than from turn 1 to the outlet (<1 log). The exposure to sunlight during the first turn might be enough to inactivate most of *E. coli* strains that are susceptible to sunlight inactivation, resulting in the high removal observed from the inlet to turn 1.

Similar to *E. coli,* the removal of enterococci was lowest (~0.6 log) when duckweed covered the wetland, and increased when water was exposed to sunlight with the highest removal of 2.1 logs in April 2012 (Figure 3.7b). Pigmentation tests revealed that the composition of enterococci in the wetland water included both pigmented and non-pigmented species (Figure 3.8). The concentration of non-pigmented enterococci decreased significantly throughout the wetland, whereas there was no significant change in pigmented enterococci concentration, suggesting that the lower removal of enterococci compared to *E. coli* was due to the resistance of pigmented cells to sunlight inactivation.

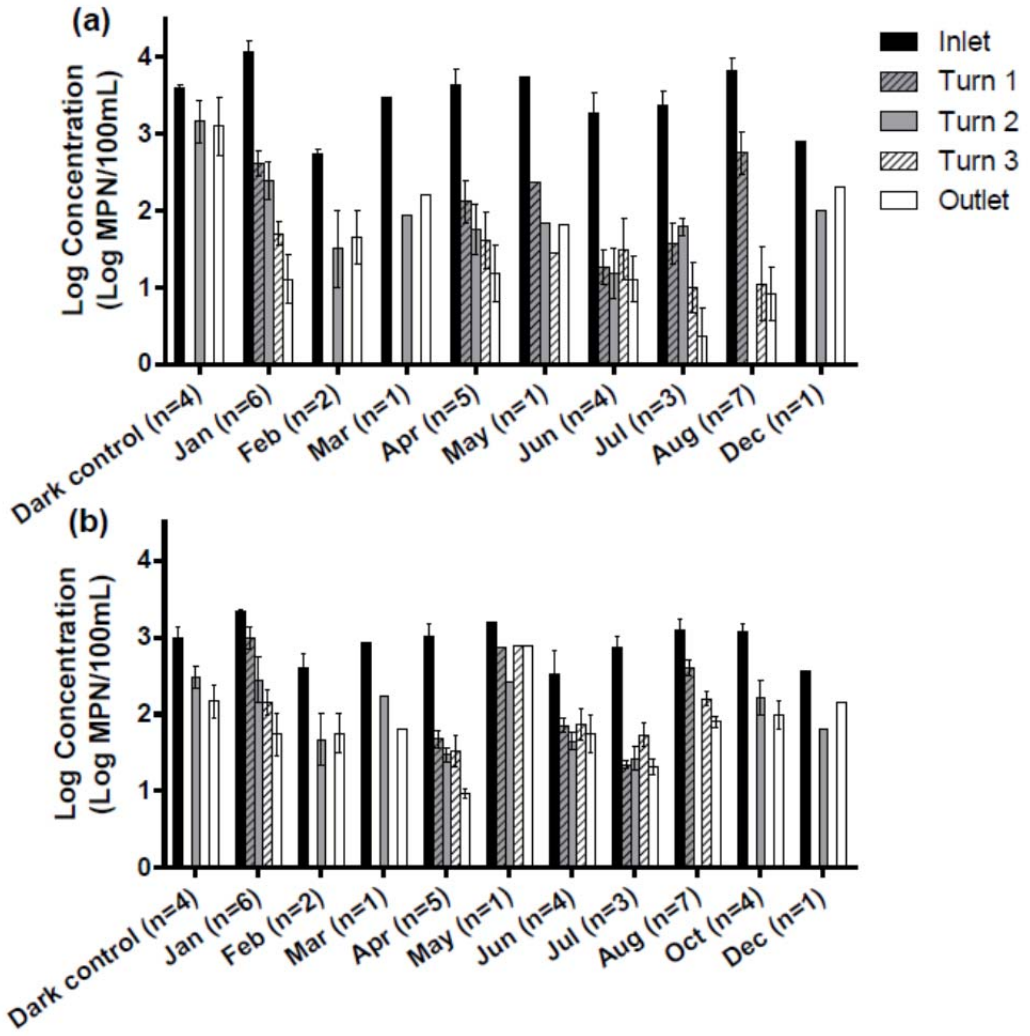

Figure 3.7. Concentrations of (a) *E. coli* and (b) enterococci at different locations in the wetland cell in different months throughout the year. Error bars indicate ± one standard error of duplicate measurements during each month. The numbers in parentheses represent the number of sampling days. Dark controls refer to samples collected in September, part of October and November, when the wetland was completely covered with duckweed. Representative monthly 24-hour averaged solar irradiance for each month is shown in Figure 3.3.

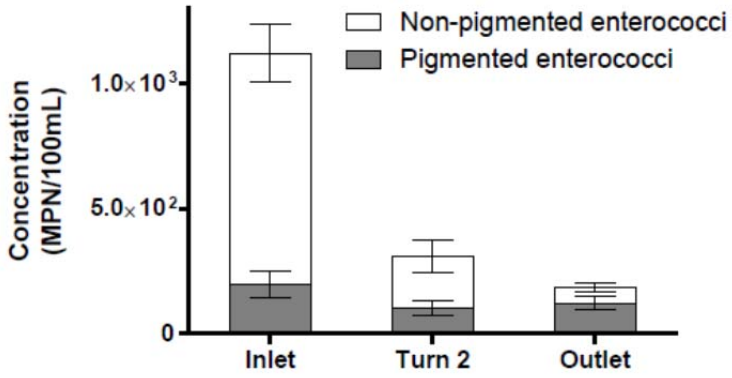

Figure 3.8. Concentrations of pigmented and non-pigmented enterococci determined from pigmentation test results of samples collected from the inlet, turn 2, and outlet of the open-water wetland on 4 days in October 2012 when water exposed to sunlight. Error bars indicate ± one standard error of replicate samples.

3.3.2 Inactivation of lab-cultured bacteria under simulated sunlight

Lab experiments were conducted with clear water and wetland water under both full spectrum and UVB-blocked simulated sunlight to determine the kinetic parameters for endogenous and exogenous inactivation of lab-cultured bacteria. Under both light conditions, the inactivation of *E. coli* was lower in wetland water than in clear water before correcting for light screening (Figure 3.9a), but was similar to clear water after correcting for light screening (Figure 3.9b), indicating that exogenous mechanisms did not play an important role in the inactivation of *E. coli* in wetland water. The inactivation rates of *E. coli* in both clear water and wetland effluent water under full spectrum simulated sunlight were significantly higher than under UVB-blocked simulated sunlight (ANOVA, $p < 0.0001$), indicating the important role of UVB in endogenous inactivation.

The inactivation rates of all four lab-cultured enterococci were faster in wetland water as compared to clear water (Figure 3.9a). The difference was even greater after correcting for light screening (Figure 3.9b), indicating that the lab-cultured enterococci were susceptible to exogenous inactivation in wetland water. The inactivation rates of two non-pigmented enterococci (*Ent. faecalis* and non-pigmented isolate) were higher than two pigmented enterococci (*Ent. casseliflavus* and pigmented isolate) under all conditions, indicating that the pigmented enterococci were more resistant to sunlight inactivation than the non-pigmented enterococci.

The k_{endo}^{L} values (mean ± one standard error) for *E. coli,* pigmented and non-pigmented enterococcal isolates were determined to be $3.97 \pm 0.35\ h^{-1}$, $1.04 \pm 0.07\ h^{-1}$, and $1.72 \pm 0.16\ h^{-1}$, respectively. The k_2 values for pigmented and non-pigmented enterococcal isolates were estimated to be $2.3\times10^{14}\ M^{-1}\ d^{-1}$ and $4\times10^{14}\ M^{-1}\ d^{-1}$, respectively. Inputs for the estimation of k_2 values include k_{obs}^{L} values of the pigmented and non-pigmented enterococcal isolates in wetland water [$1.04 \pm 0.07\ h^{-1}$ and $2.35 \pm 0.27\ h^{-1}$], their k_{obs}^{L} values in clear water ($= k_{endo}^{L}$ values listed

above), and the average steady-state singlet oxygen concentration in wetland water of 9.23×10^{-14} ± 9.56×10^{-15} M measured in experiments under full spectrum simulated sunlight (Table 3.5).

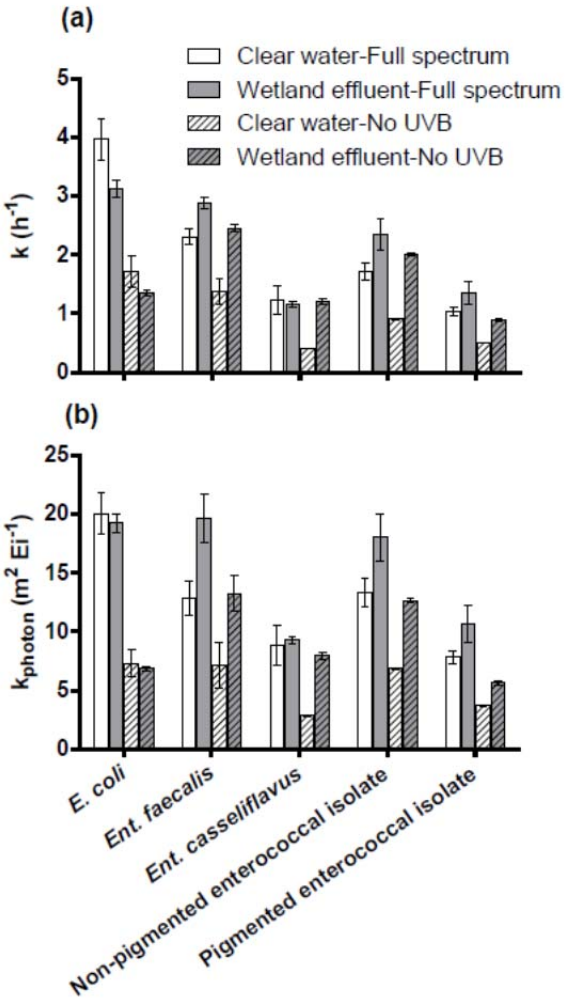

Figure 3.9. Inactivation rate constants of lab-cultured *E. coli, Ent. faecalis, Ent. casseliflavus*, and field isolated non-pigmented and pigmented enterococci in clear water and wetland water under full spectrum and UVB-blocked simulated sunlight as (a) a function of time (k^{L}_{obs}, before correcting for light screening) or (b) a function of photon fluence ($k^{L}_{obs,photon}$, after correcting for light screening). Error bars indicate ± one standard error of duplicate experiments.

Table 3.5. Data from lab experiments used to calculate k_2 values for lab-cultured pigmented and non-pigmented enterococcal isolates.

	Pigmented enterococcal isolate	**Non-pigmented enterococcal isolate**
$\sum_{\lambda=280}^{400} \langle E_0^{sim}(z,\lambda)\rangle_z \Delta\lambda$	11.8 W m^{-2}	
$\sum_{\lambda=280}^{400} \langle E_0^{sim}(0,\lambda)\rangle_z \Delta\lambda$	25.3 W m^{-2}	
$[{}^1O_2]_{ss,bulk}$	$9.23\times10^{-14} \pm 9.56\times10^{-15}$ M	
k_{obs}^L(in wetland water)	1.04 ± 0.07 h^{-1}	2.35 ± 0.27 h^{-1}
k_{obs}^L(in clear water)	1.35 ± 0.20 h^{-1}	1.72 ± 0.16 h^{-1}

3.3.3 Sunlight inactivation of lab-cultured FIB versus indigenous wastewater FIB

Lab results. To test whether the susceptibility of lab-cultured FIB to sunlight inactivation was different than indigenous wastewater FIB, an experiment was conducted to measure inactivation rates of FIB from the two sources in clear water under full spectrum simulated sunlight (Figure 3.10). Both k_{obs}^L and $k_{photon,obs}^L$ values showed that FIB cultured under lab conditions were more susceptible to endogenous inactivation than the indigenous wastewater FIB (t-test, $p < 0.05$).

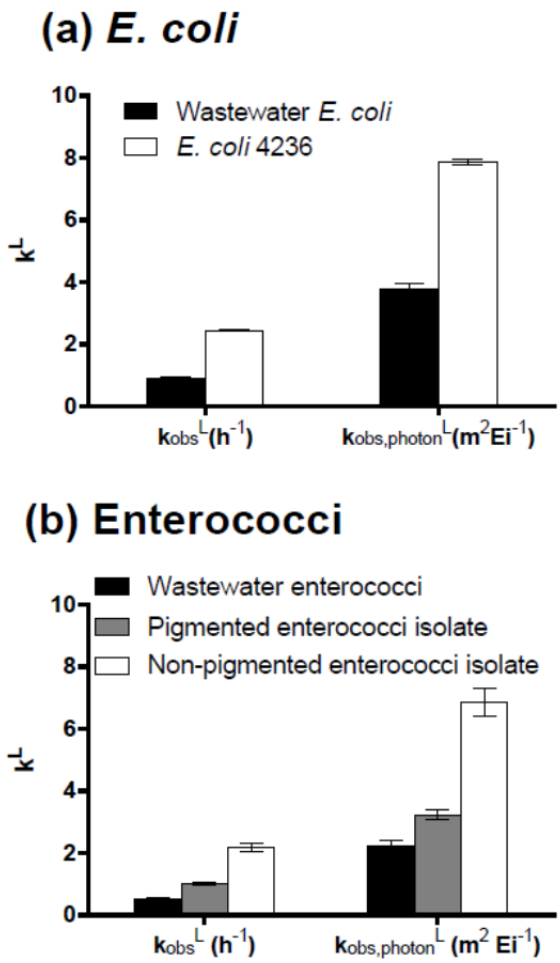

Figure 3.10. Inactivation rate constants as functions of time (k^{L}_{obs}, before correcting for light screening) and as functions of photon fluence ($k^{L}_{obs,photon}$, after correcting for light screening) of indigenous wastewater FIB in comparison with lab-cultured FIB for (a) *E. coli* and (b) pigmented and non-pigmented enterococcal isolates in clear water under full spectrum simulated sunlight. Error bars indicate ± one standard error of duplicate experiments.

In-situ batch reactors. The inactivation rates of the FIB in batch reactors (k^{B}_{tot}) under field conditions were modeled using Equations 3.1, 3.2, and 3.5, and compared with the measured values (k^{B}_{obs}). The k^{B}_{tot} values of all three indicators were generally higher than the k^{B}_{obs} values (Figure 3.11). Inactivation rates of pigmented and non-pigmented enterococci in the open-water wetland were calculated separately based on partition of indigenous pigmented and non-pigmented enterococci measured (Table 3.6). Details of k^{B}_{obs} and k^{B}_{tot} values of all three indicators are provided in Table 3.7. The ratio of modeled and measured inactivation rates in in-situ batch reactors $\left(r = {k^{B}_{tot}}/{k^{B}_{obs}} \right)$ of *E. coli*, and pigmented and non-pigmented enterococci are 1.77, 12.81, and 3.06, respectively. To adjust for the differences between lab and field

conditions (e.g., diurnal fluctuations in solar irradiance, pH and DO), we used the r values as a correction factor.

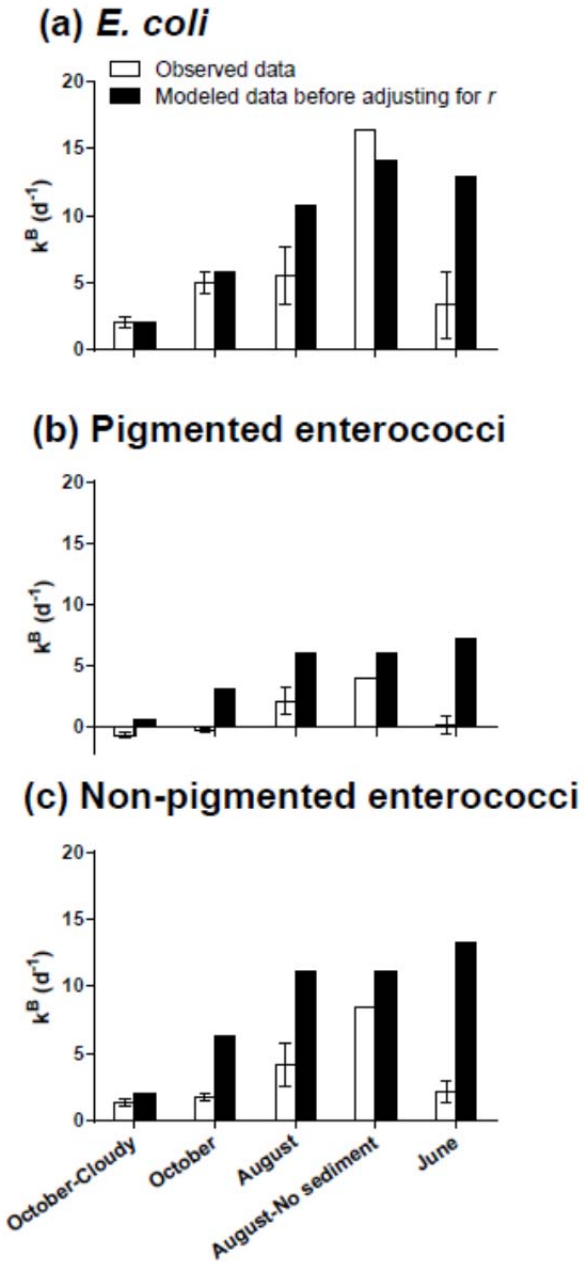

Figure 3.11. Comparison between observed (k^B_{obs}) and modeled inactivation rate constants (k^B_{tot}, before adjusting with the correction factor r) of (a) *E. coli*, (b) pigmented enterococci, and (c) non-pigmented enterococci in in-situ batch reactors. Error bars on the experimental data indicate ± one standard error of duplicate experiments. No error bar was shown for experiment with single sample. Experiments were conducted at Discovery Bay, CA in August and October 2012, and June 2014.

Table 3.6. Relative abundance (%) of pigmented and non-pigmented enterococci in the open-water wetland at different locations and in in-situ batch reactors at different time points. Pigmentation tests results of water samples collected from the wetland and in-situ batch reactors under both light and dark controls were used to estimate the partition of pigmented and non-pigmented enterococci.

Wetland under sunlight			**Wetland in dark (covered by duckweed)**		
Location	*Pigmented enterococci*	*Non-pigmented enterococci*	*Location*	*Pigmented enterococci*	*Non-pigmented enterococci*
Inlet	5.6	94.4	Inlet	6.5	93.5
Middle	27.7	72.3	Middle	23.2	76.8
Outlet	65.4	34.6	Outlet	34.3	65.7
Batch reactors under sunlight			**Batch reactors in dark (covered by foil)**		
Time (h)	*Pigmented enterococci*	*Non-pigmented enterococci*	*Time (h)*	*Pigmented enterococci*	*Non-pigmented enterococci*
0	12.2	87.8	0	12.4	87.6
8	44.7	55.3	8	13.0	87.0
24	61.1	38.9	24	22.0	78.0
32	71.8	28.2	32	33.2	66.8

Table 3.7. Measured [k_{obs}^{B}, (d^{-1})] and modeled inactivation rate constants [k_{tot}^{B}, (d^{-1}), before adjusting with the correction factor r] of *E. coli*, pigmented enterococci, and non-pigmented enterococci in in-situ batch reactors. Error bars on the experimental data indicate ± one standard error of duplicate experiments. No error bar was shown for experiment with single sample.

Month	***E. coli***		**Non-pigmented enterococci**		**Pigmented enterococci**	
	k_{obs}^{B}	k_{tot}^{B}	k_{obs}^{B}	k_{tot}^{B}	k_{obs}^{B}	k_{tot}^{B}
October-Cloudy	2.03±0.37	2.08	1.34±0.23	2.00	-0.61±0.20	0.63
October	5.03±0.83	5.85	1.75±0.27	6.33	-0.20±0.18	3.15
August	5.56±2.20	10.79	4.20±1.64	11.20	2.18±1.15	5.99
August-No sediment	16.42	14.10	8.42	11.14	3.97	6.01
June	3.36±2.46	12.94	2.13±0.78	13.28	0.21±0.69	7.20
$\left(r = {k_{tot}^{B}}/{k_{obs}^{B}}\right)$	1.77		3.06		12.81	

3.3.4 Modeling inactivation of the FIB in open-water wetland (k_{tot}^{W} vs. k_{obs}^{W})

The best-fit inactivation rate constants, k_{obs}^{W}, were calculated from the monitoring data using Equation 3.12 (Figures 3.12-3.14). In Figure 3.15, these observed values are compared with the modeled inactivation rates of *E. coli*, and pigmented and non-pigmented enterococci in the wetland (k_{tot}^{W}, determined from Equations 3.1, 3.13, and 3.14; the values of k_{endo}^{W} and k_{exo}^{W}

are listed in Table 3.8) for each month. The monitoring data are highly variable and unexpectedly high in January, which was likely due to experimental errors (Figure 3.15). Nevertheless, the k_{tot}^{W} values are the same order of magnitude as the k_{obs}^{W} values, and generally follow the same trends (Figure 3.15). The model over-predicts k_{obs}^{W} values of pigmented enterococci for most months, and for non-pigmented enterococci from May to August by factors of 1.2 to 2.6 indicating the model may not capture some factor(s) that inhibit sunlight inactivation. The model suggests that endogenous mechanisms were the main contributor to *E. coli* inactivation (65% –87% of the total inactivation), while exogenous contributed slightly more than endogenous mechanisms to inactivation of pigmented and non-pigmented enterococci.

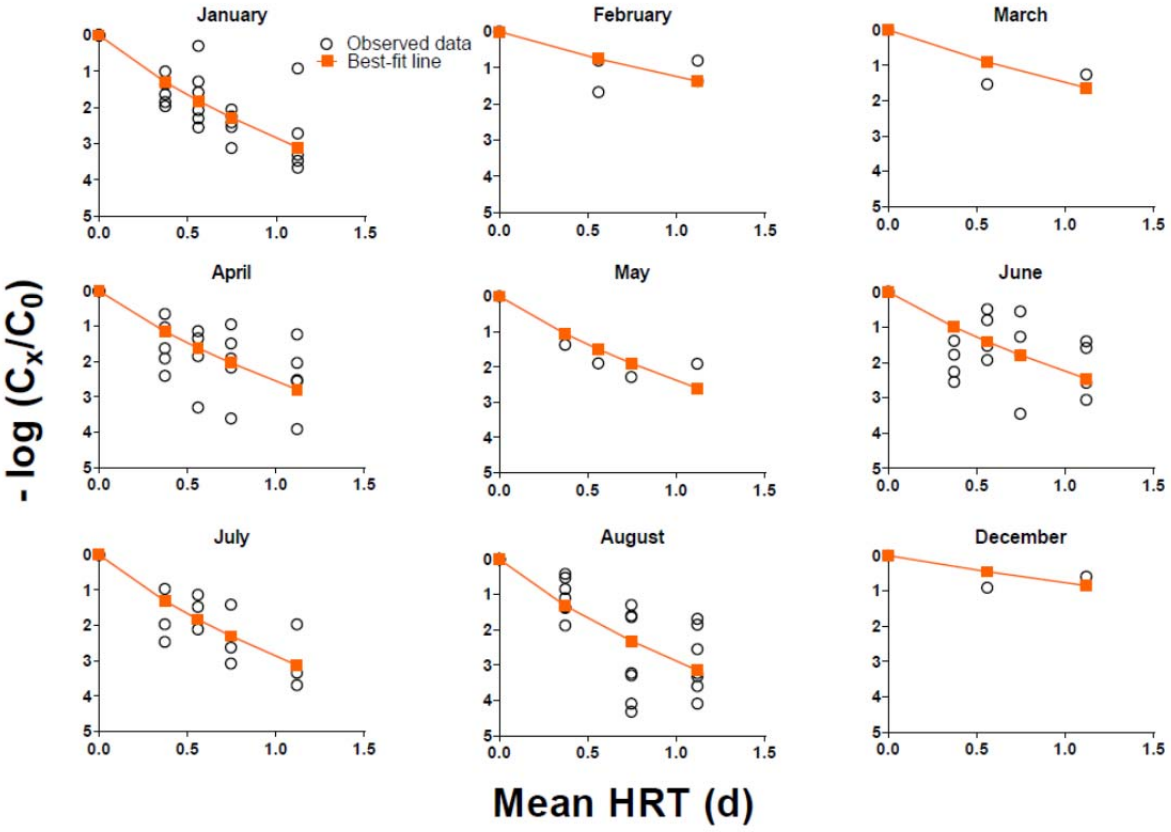

Figure 3.12. Log removal values based on monitoring data and the best-fit line for *E. coli* in different months at Discovery Bay open-water wetland. The best-fit lines are based on the k_{obs}^{W} values from solving the Wehner-Wilhelm equation (Equation 3.15).

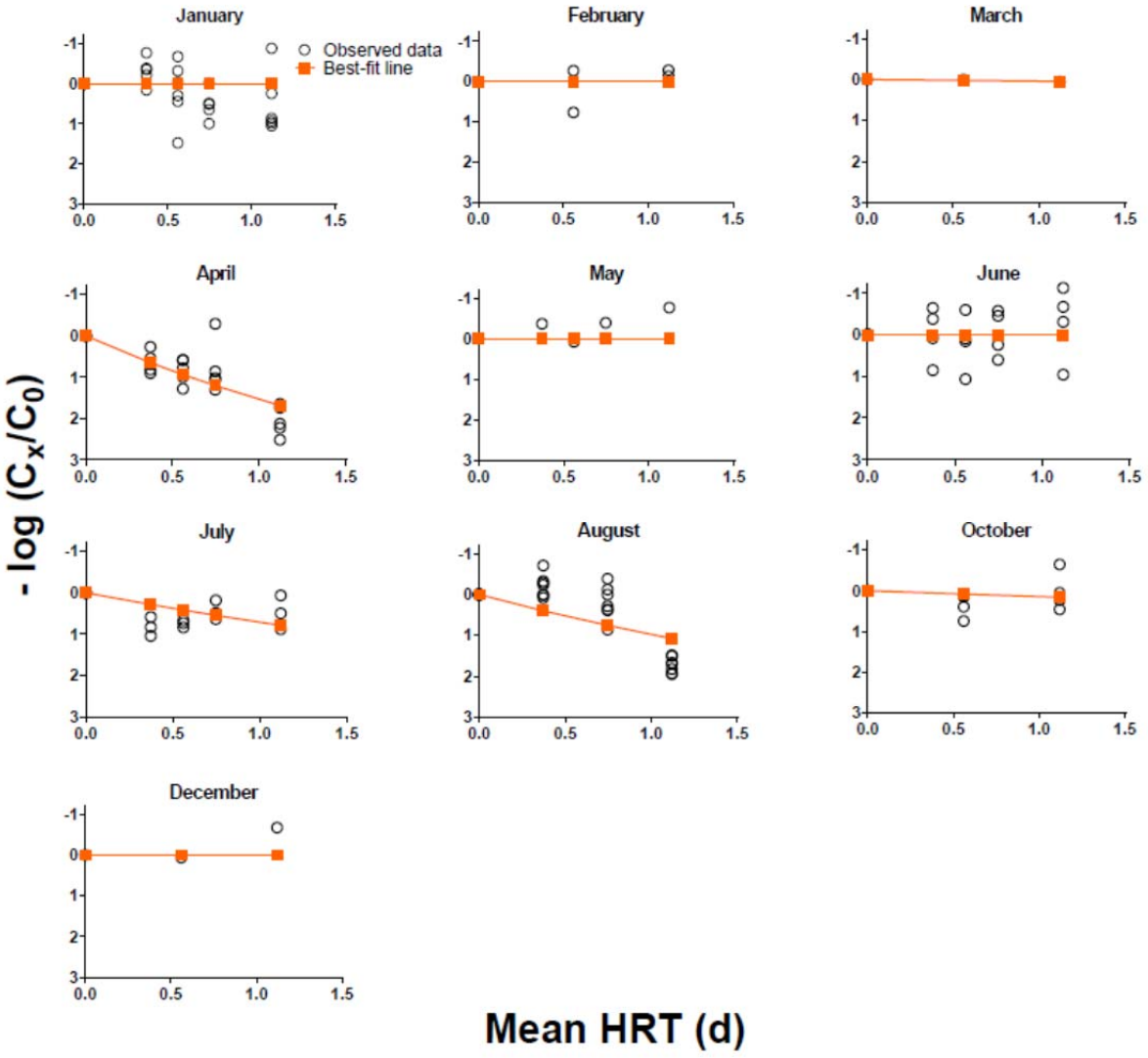

Figure 3.13. Log removal values based on monitoring data and the best-fit line for pigmented enterococci in different months at Discovery Bay open-water wetland. The best-fit lines are based on the k_{obs}^{W} values from solving Equation 3.15.

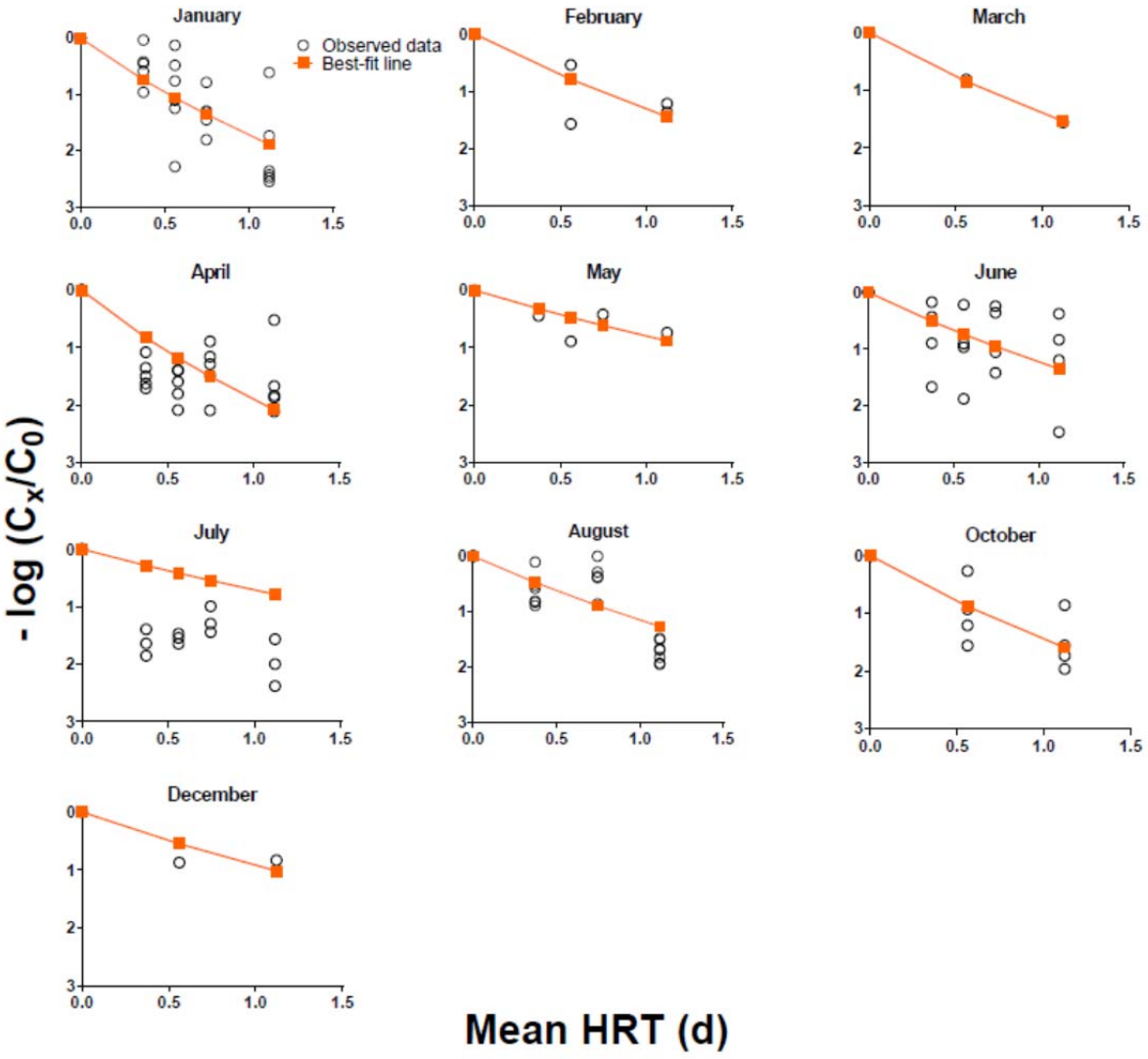

Figure 3.14. Log removal values based on monitoring data and the best-fit line for non-pigmented enterococci in different months at Discovery Bay open-water wetland. The best-fit lines are based on the k_{obs}^{W} values from solving Equation 3.15.

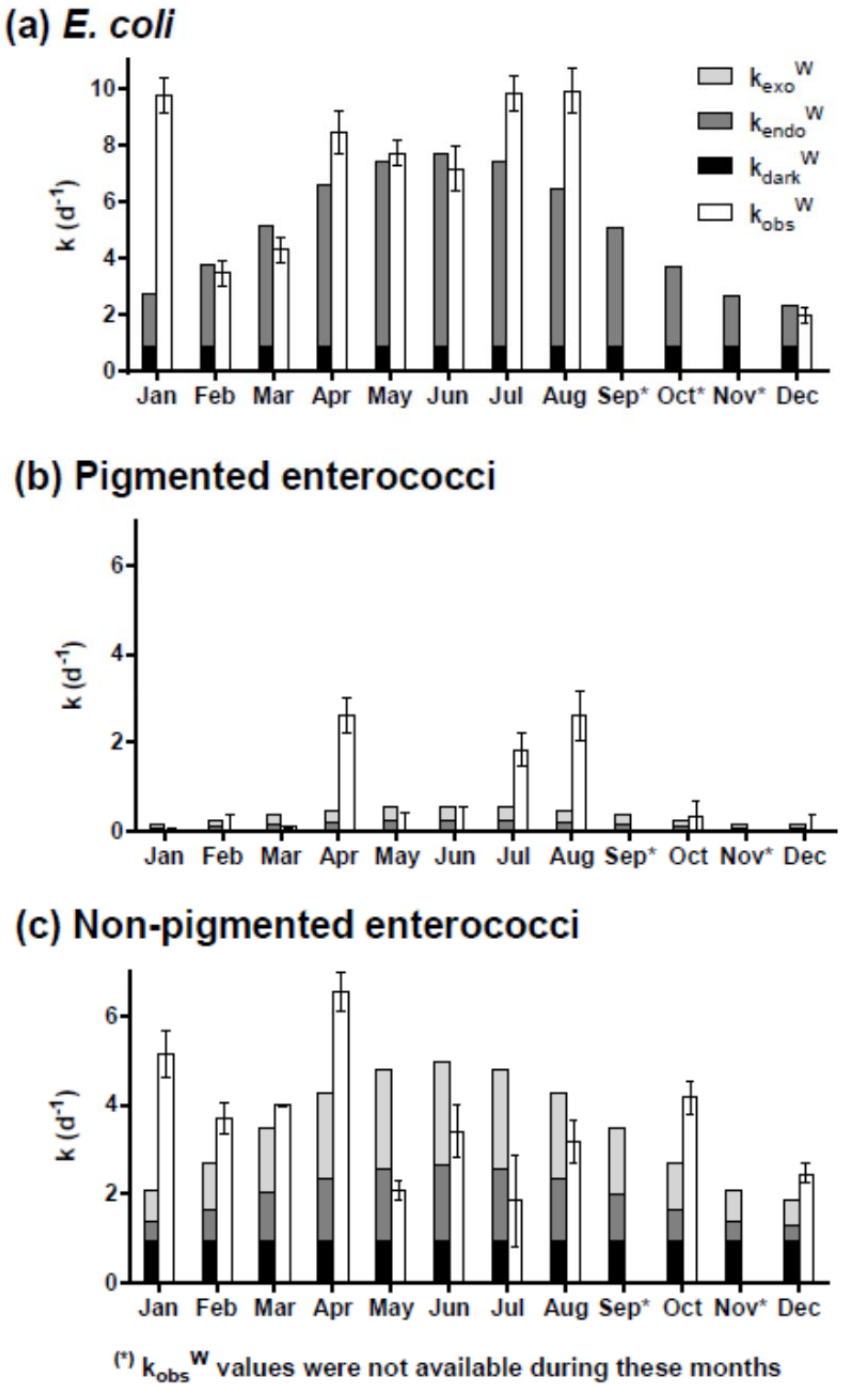

Figure 3.15. Comparison between observed (k_{obs}^{W}) and modeled inactivation rate constants (k_{tot}^{W}, after adjusting with the correction factor r) of (a) *E. coli*, (b) pigmented enterococci, and (c) non-pigmented enterococci in the open-water wetland in different months of the year. k_{obs}^{W} values were not available in September, October and November for *E. coli*, and September and November for enterococci. Error bars on k_{obs}^{W} are root-mean-square errors.

Table 3.8. Modeled inactivation rate constants [k^W_{endo}, k^W_{exo}, and k^W_{dark}, (d^{-1})] of indigenous wastewater E. coli, pigmented and non-pigmented enterococci in the open-water wetland in different months. Note that inactivation rate values reported in this table were divided by r (1.44 for E. coli, 3.49 for non-pigmented enterococci and 14.53 for pigmented enterococci) to correct for the difference between lab-grown and wastewater bacteria in responding to sunlight inactivation.

Month	***E. coli***			**Pigmented enterococci**			**Non-pigmented enterococci**		
	k^W_{endo}	k^W_{exo}	k^W_{dark}	k^W_{endo}	k^W_{exo}	k^W_{dark}	k^W_{endo}	k^W_{exo}	k^W_{dark}
Jan	1.85	0	0.86	0.07	0.09	0.01	0.46	0.68	0.93
Feb	2.90	0	0.86	0.11	0.14	0.01	0.73	1.02	0.93
Mar	4.31	0	0.86	0.16	0.20	0.01	1.08	1.46	0.93
Apr	5.72	0	0.86	0.21	0.26	0.01	1.43	1.91	0.93
May	6.55	0	0.86	0.24	0.30	0.01	1.64	2.21	0.93
Jun	6.83	0	0.86	0.25	0.31	0.01	1.71	2.32	0.93
Jul	6.55	0	0.86	0.24	0.30	0.01	1.64	2.22	0.93
Aug	5.61	0	0.86	0.20	0.26	0.01	1.40	1.95	0.93
Sep	4.22	0	0.86	0.15	0.21	0.01	1.05	1.51	0.93
Oct	2.82	0	0.86	0.10	0.14	0.01	0.70	1.06	0.93
Nov	1.82	0	0.86	0.07	0.09	0.01	0.45	0.69	0.93
Dec	1.50	0	0.86	0.05	0.08	0.01	0.37	0.56	0.93

3.4 Discussion

3.4.1 Contribution of endogenous and exogenous mechanisms to sunlight inactivation of lab-cultured bacteria under simulated sunlight

The susceptibility of all four lab-cultured enterococci (*Ent. faecalis, Ent. casseliflavus,* pigmented and non-pigmented enterococcal isolates), but not *E. coli*, to exogenous mechanisms is consistent with previous studies on sunlight inactivation of these bacteria in waste stabilization pond water (Davies-Colley et al., 1999; Kadir and Nelson, 2014). This study adds to the existing literature by demonstrating that both pigmented and non-pigmented enterococci strains are susceptible to exogenous inactivation, but that the pigmented strains are more resistant to exogenous inactivation than non-pigmented strains, which has been previously reported only for endogenous inactivation (Maraccini et al., 2011). The resistance of pigmented enterococci to both endogenous and exogenous sunlight inactivation is likely due to the presence of carotenoids, which are able to quench ROS, in the bacterial membrane of the yellow pigmented bacteria (Pellieux et al., 2000).

The greater resistance of *E. coli* to exogenous mechanisms as compared to enterococci may be due to differences between the cellular membranes of Gram-negative bacteria (including *E. coli*) and Gram-positive bacteria (including enterococci). Gram-negative bacteria have an extra outer membrane (Valduga et al., 1993) that limits the uptake of exogenous photosensitizers into bacterial cells, reducing the ability of short-lived reactive intermediates (i.e., lifetimes of ns-µs) to damage Gram-negative cells (Nitzan and Pechatnikov, 2011). In addition, the cell walls of

Gram-negative bacteria contain water and other reactive intermediate quenchers which provide protection from exogenous reactive intermediates (Dahl et al., 1987).

3.4.2 Lab-cultured bacteria as indicators for indigenous bacteria and pathogens in open-water wetlands receiving wastewater

The greater susceptibility of lab-cultured FIB than indigenous wastewater FIB to sunlight inactivation is likely due in part to the differences in the growth conditions of the lab-cultured bacteria versus indigenous wastewater bacteria (Fisher et al., 2012). Specifically, the lab-cultured bacteria were grown on rich media under aerobic conditions, which could increase the biosynthesis of endogenous photosensitizers (Pedersen et al., 1978) and increase susceptibility of the bacteria to sunlight inactivation (Berney et al., 2006a). In contrast, the indigenous wastewater bacteria likely grew in anaerobic and iron-scarce conditions with lower specific growth rates (Fisher et al., 2012).

The difference between indigenous wastewater bacteria and lab-cultured bacteria also highlighted the challenges with using lab-cultured indicators to study inactivation of indigenous indicator microorganisms and human bacterial pathogens in wastewater. While research with lab-cultured indicator organisms provides valuable insight into the inactivation mechanisms, their inactivation rates in lab conditions cannot be directly used to estimate the inactivation rates of indigenous indicator organisms in the field. From this understanding and the field data, we propose using the correction factor r as an adjustment for the discrepancy between inactivation rates of lab-cultured and indigenous organisms. Further research is necessary to determine what differences may exist between the inactivation rates between lab FIB, field FIB, and actual human bacterial pathogens. A better understanding of inactivation mechanisms of human bacterial pathogens is also needed to provide insight into what factors influence the sunlight inactivation susceptibility of different species or serovars. For example, a limited number of studies on human pathogens has documented a difference in susceptibility to sunlight inactivation of lab-cultured *E. coli* and bacterial pathogens including *Salmonella, Shigella, Vibrio cholerae,* and *Campylobacter* (Berney et al., 2006b; Sinton et al., 2007). Even within the same species, there were differences in the sunlight inactivation rates of different *Salmonella* serovars (Boehm et al., 2012).

3.4.3 Comparison with High Rate Algal Ponds

Inactivation rates of *E. coli* derived from wetland field data are approximately three times higher than those reported for high rate algal ponds (HRAPs) with similar solar irradiation, depth, pH, temperature, and DO (2.9 d^{-1} in winter and 7.0 d^{-1} in summer in this study as compared to 0.5 d^{-1} in winter and 1.9 d^{-1} in summer in HRAPs) (Craggs et al., 2004). The lower inactivation rates of *E. coli* in the HRAPs were likely because less UV light was able to penetrate the HRAP water column, which contains suspended algae, as compared to the open-water wetland ($a^{W}_{340nm} = 12\ m^{-1} < a^{HRAP}_{340nm} = 150\ m^{-1}$, where a is absorption coefficient, and 340 nm was chosen as a representative wavelength in the UV range) (Craggs et al., 2004). Thus, open-water wetlands, which allow greater penetration of sunlight in the water column, appear to increase the inactivation rates of the FIB relative to other types of ponds. Although estimated scalar solar irradiance at different depths in the wetland water column showed that UV light may not be able to travel more than 20-cm depth (Figure 3.4), deeper open-water cells may provide

more effective treatment because longer hydraulic retention time can potentially compensate for light screening effects. Prior studies predicted that open-water wetlands with depths from 20 cm to 50 cm provide practical land area requirements and effective treatment for trace organic contaminants via photolysis (Jasper and Sedlak, 2013) and viruses via sunlight inactivation (Silverman et al., 2015). However, deeper water may encourage the dominance of suspended algae instead of the biomat that dominated the photosynthetic community in the pilot, open-water wetland.

3.4.4 Modeling the inactivation of the FIB in the open-water wetland

The inactivation rates derived from field data for pigmented and non-pigmented enterococci were highly variable, and they were difficult to predict with the model. A major source of uncertainty is likely the difficulty in separately quantifying pigmented and non-pigmented fractions of bacteria. The model confirmed the important contribution of exogenous mechanisms to inactivation of both pigmented and non-pigmented enterococci in the wetland. 16s rRNA sequencing of wetland isolates suggested species other than *Enterococcus* may be quantified using Enterolert, further complicating interpretation of the field-data derived inactivation rates. Future research to study factors influencing exogenous mechanisms, such as properties of photosensitizers in wetland water (i.e., their association with indicator bacteria and pathogens, spectroscopic characteristics, and production of reactive intermediates) is necessary. A better understanding of exogenous mechanisms can provide insight into how to optimize the design and operation of open-water wetlands to enhance sunlight inactivation.

A factor that likely contributed to the high variability in the inactivation rates of the monitoring data for all three FIB is that influent and effluent concentrations typically vary over time, due to changes in wastewater characteristics and treatment performance of upstream processes, and deposition of animal feces in the wetland (the culture-based enumeration methods cannot distinguish between human and animal sources of FIB). It is common for FIB concentrations to vary over several orders of magnitude over short time and spatial scales (Boehm et al., 2002). It is also likely that discrepancies between the model and the field-derived inactivation rates were caused by the simplified approach used to characterize the wetland hydraulics, because tracer data may not be sensitive enough to show the effects of short-circuiting on bacterial removal efficiency. Preferential flow paths, such as leaks through the wetland baffles, can cause water parcels to have different residence times in the wetland (Lightbody et al., 2008). If just 1% of the wetland water short-circuited through the wetland, an amount could not be observed with the Rhodamine tracer test used by Jasper et al. (2014a), the actual bacterial removal would be limited to 1 log as compared to the modeled removal of 3 logs. These results emphasize the importance of good hydraulic design and minimizing short-circuiting in natural treatment systems used for disinfection (Jasper et al., 2013).

3.4.5 Estimation of wetland area necessary for inactivation of the FIB

Typical concentrations of FIB in non-disinfected secondary effluents range from 10^2 to 10^5 MPN/100 mL (Bitton, 2010), such that a 3-log reduction would lower the concentrations below 100 MPN/100 mL, which is below the requirement for *E. coli* concentration of the National Pollution Discharge Elimination System (NPDES) permit for discharges from wastewater treatment plants (i.e., no greater than 126 CFU/100 mL based on five samples taken over a 30-day period, nor any instantaneous reading exceed 406 CFU/100 mL) (US EPA, 2004).

Thus, for the purpose of assessing the land required for FIB treatment, the area needed to achieve 3-log removal of bacterial indicators from 1 MGD of wastewater effluent (A^1_{3log}) was calculated based on an approach developed by Jasper and Sedlak (2013).

Predicted A^1_{3log}values for *E. coli* and non-pigmented enterococci [5.5 ha and 7.0 ha per million gallons of wastewater effluent per day (MGD), respectively] are within the range of existing wetland system areas [i.e., 3 ha MGD^{-1} for Prado Wetlands (Orange County, California) and 22 ha MGD^{-1} Easterly Wetlands (Orlando, Florida)], indicating that open-water wetland cells of a practical size could provide efficient treatment for pathogens that share similar characteristics with these indicators throughout the year (Figure 3.16). The high modeled values of A^1_{3log} for pigmented enterococci are due to their resistance to sunlight inactivation; thus, total enterococci may be an overly conservative indicator for non-pigmented bacterial pathogens when removal is dominated by sunlight inactivation.

It should be noted that the actual A^1_{3log}values might be higher than modeled values due to cloudy weather or the challenge of minimizing hydraulic short-circuiting in full-scale wetlands. Nonetheless, our modeled results show that open-water wetlands can play an important role in the multi-barrier approach to control the transmission of FIB and possibly waterborne pathogens.

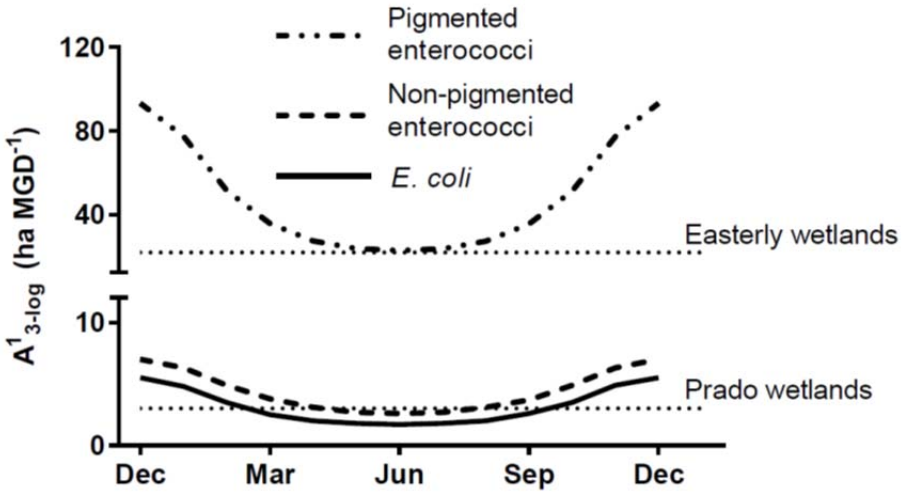

Figure 3.16. Area predicted from model to provide 3-log removal (99.9 %) of E. coli, pigmented enterococci, and non-pigmented enterococci from 1 MGD of wastewater effluent in open-water treatment wetlands (A^1_{3log}) during different seasons. Characteristics of the wetlands: [DOC] = 8 mg C L-1; depth = 20 cm; daily averaged solar intensity under sunny, cloudless condition at 37°54′ N. Dashed lines show the area per MGD of existing full-scale wetland systems. Prado Wetlands (Orange County, California) receives water from Santa Ana River, yielding a footprint of about 3 ha MGD-1 (Orange County Water District, 2008), and Easterly Wetlands (Orlando, Florida), with a footprint of about 22 ha MGD-1 (Florida Department of Environmental Protection, 2011).

CHAPTER 4. Natural photosensitizers in constructed unit process wetlands: Spectroscopic characterization, production of reactive species and effect on inactivation of indicator organisms

Reproduced with permission from Mi T. Nguyen[1]; Jannis Wenk[2]; and Kara L. Nelson[3]. Natural photosensitizers in constructed unit process wetlands: Spectroscopic characterization, production of reactive species and effect on inactivation of indicator organisms. In preparation for submission to *Environmental Science and Technology.*

[1]Primary author and researcher

[2]Author and researcher of the isolation and characterization of wetland isolates sections

[3]Editor and advisor

4.1 Introduction

Sunlight inactivation of indicator organisms and pathogens is usually insignificant in constructed wetlands due to the shading of emergent macrophytes. An open-water cell has been shown to achieve significant removal of indicator bacteria and viruses via sunlight inactivation (Chapter 3, Silverman et al., 2015), as well as to remove recalcitrant organic compounds and nitrate (Jasper and Sedlak, 2013; Jasper et al., 2014a, 2014b). Such open-water cell(s), if integrated into a series of unit process wetlands, have the potential to improve the overall treatment achieved by the wetland system (Jasper et al., 2013). However, a range of factors affect the preferred order for the different wetland cells. One consideration is the concentration and characteristics of the chromophoric dissolved organic matter (CDOM), which contains natural photosensitizers involved in the formation of reactive intermediates (Richard and Canonica, 2005) that lead to indirect photolysis of organic compounds and exogenous inactivation of susceptible indicator organisms and pathogens. CDOM also attenuates light (Zepp and Cline, 1977), which decreases direct photolysis and endogenous inactivation, and scavenges or quenches reactive species (Canonica and Laubscher, 2008; Cory et al., 2008; Vione et al., 2006), which may decrease indirect and exogenous removal mechanisms.

The observed role of dissolved organic matter (DOM) in sunlight inactivation and photochemical processes depends on the type and source of DOM, which define the photochemical characteristics of the DOM (Boreen et al., 2008; Guerard et al., 2009; Paul et al., 2004). Natural organic matter (NOM) found in aquatic systems consists mainly of products from the degradation of plants and microbial processes (Blough and Zepp, 1995). Wastewater effluent organic matter (EfOM) is a complex and heterogenous mixture of organic matter from drinking water, microbial products from biological treatment processes at wastewater treatment plants, and trace organic contaminants (Shon et al., 2006). It has been shown that EfOM undergoes transformations in treatment wetlands, governed by processes including biodegradation, bio-uptake, sorption, volatilization, and photolysis (Barber et al., 2001). Nontheless, there is still limited characterization of DOM from different types of constructed wetlands (Barber et al., 2001; Lee et al., 2014), and limited knowledge about how different types of DOM impact the exogenous inactivation of microorganisms (Silverman et al., 2013). This information is needed to guide the design, sequencing, and operation of unit process wetlands for which pathogen removal is a treatment goal.

The goals of this study were to investigate the characteristics of DOM in unit process wetlands, and to relate these results to the exogenous sunlight inactivation of pathogen indicator organisms. DOM in the influent and effluents of three different types of pilot-scale unit process wetlands (bulrush, cattail, and open-water) was isolated and characterized for spectroscopic properties and reactive intermediates formation. The sunlight inactivation rates of one bacterial indicator, *Ent. faecalis,* and one virus indicator, MS2, in solutions of wetland DOM isolates were determined from lab experiments. These two indicators were chosen because previous research has demonstrated their susceptibility to exogenous inactivation by sunlight (Kadir and Nelson, 2014; Kohn and Nelson, 2007). The role of wetland DOM in exogenous inactivation of the indicators is discussed considering the inactivation rate constants, DOM characteristics, and association between the DOMs and microorganisms. Two standard DOM isolates (Suwannee River Fulvic Acid and Pony Lake Fulvic Acid) were also analyzed to provide a comparison with the wetland DOM isolates.

4.2 Materials and Methods

This study consisted of four tasks: (1) isolation of DOMs from the influent and effluents of different cells of a pilot-scale unit process wetlands (bulrush, cattail, and open-water); (2) spectroscopic characterization of wetland water samples, DOM isolates, and standard DOM isolates; (3) quantification of light-induced formation of reactive species and inactivation of pathogen indicators (*Ent. faecalis* and MS2); and (4) determination of the association between the DOMs and *Ent. faecalis* cells.

4.2.1 Chemicals, preparation of solutions and analytical methods.

All chemicals were from commercial sources and used without further purification: Benzene (anhydrous 99.8%, Sigma-Aldrich), furfuryl alcohol (FFA, 99%, Acros Organics) 2,4,6-trimethylphenol (TMP, 99%, Acros Organics), phenol (Fluka, ≥99.5%). Standard humic substances Pony Lake Fulvic Acid (PLFA, reference number 1R109F) and Suwannee River Fulvic Acid standard II (SRFA, 2S101F) were obtained from the International Humic Substances Society (IHSS). Chemicals and agents related to *Ent. faecalis* and MS2 preparation and enumeration are specified in the *Inactivation of pathogen indicators* section. All aqueous solutions including stock solutions, phosphate buffered saline (PBS: 4 mM NaH_2PO_4, 16 mM Na_2HPO_4, and 10 mM NaCl; pH adjusted to 7.5), and clear water for inactivation experiments with bacteria (20 mM NaH_2PO_4, 10 mM NaCl; pH adjusted to 7.5) were prepared from ultrapure water (resistivity >18 MΩcm) obtained from a Milli-Q (Millipore) water purification system. Microbial broths were prepared from deionized water. Reactive species probe compound measurements were performed using a high-performance liquid chromatography (HPLC) system (Gynkotek) with a reverse-phase C18 column (Cosmosil C18-5-MS-II, 100×3 mm Nacalay Tesque, Kyoto, Japan) equipped with a guard column (Nacalay Tesque) and a 2-μm pre-filter (Agilent Technologies). Concentration of total organic carbon (TOC) for whole water samples, standard humic substances and DOM isolates was determined using a Shimadzu V-CPH TOC analyzer (Kyoto, Japan). Dissolved ion concentrations were measured using either IC (DX-120 Ion chromatograph, Dionex) or ICP/MS (7700 Series, Agilent Technologies). Electronic absorption spectra were collected with a UV-2600 UV-Vis Spectrophotometer (Shimadzu) using quartz-glass cuvettes (Hellma, Germany).

4.2.2 Field site and sampling.

Whole water samples for experiments and DOM isolation were collected from a pilot-scale unit process wetland (Discovery Bay, CA, 37°54′N, 121°36′W). The wetland system consists of four free-surface, horizontal flow wetlands (each 400 m^2), including an open-water cell (approximately 0.2 m depth) that lacks emergent macrophytes and three vegetated cells (approximately 0.5 m depth) [two bulrush (*Scirpus* spp.) cells and a cattail (*Typha* spp.) cell]. Three wetlands including the open-water, cattail, and one of the bulrush cells were investigated in this study. During the sampling period from June 2013 to December 2013, each cell received approximately 4.4×10^{-4} m^3 s^{-1} of non-disinfected, nitrified wastewater from an adjacent oxidation ditch wastewater treatment plant as influent. Hydraulic retention times ranged from approximately 1 day in the open-water cell to 3 days in the vegetated cells; all wetlands contained baffles to promote plug-flow conditions. Water samples were collected at the inlet (from a free-falling pipe, before mixing with the wetland water) and outlet of the open-water cell, and at the outlet of the bulrush and cattail cells in clean 20-L plastic containers or 1-L glass

bottles at the same time in December 2013. Sampling containers were transferred to the lab, filtered through 1-µm glass fiber filters and stored in the dark at 4°C until further use. The water quality parameters for the water samples are provided in Table 4.1.

4.2.3 Concentration and isolation of DOM from unit process wetlands (Task 1).

Isolation of DOM by solid-phase extraction. Wetland DOM was isolated from water samples using a solid-phase extraction (SPE) method (Dittmar et al., 2008). Wetland water sample pre-filtered through 1-µm filters was acidified to pH 2 using concentrated HCl (10 M). Cartridges (Bond Elut PPL, No. 12255002, Agilent Technologies) used in this SPE method were rinsed with 10 mL methanol and 10 mL ultrapure water. Two liters of water sample were passed through each cartridge at a flow rate of 30 – 40 mL min^{-1} using a vacuum pump. Samples of the discharge were taken after passage of 0.1 L, 1 L and 2 L of water through the cartridges. After the extraction, any remaining salts were removed from cartridges by passing 10 mL of HCl 0.01M. The cartridges were dried for 5 min using the air stream of the vacuum. DOM sorbed in the cartridges was eluted with 10 mL methanol. The volume of the extracts was decreased by evaporating the methanol in a water bath at 30°C under a gentle stream of nitrogen. The remaining concentrate was diluted with at least 95% volume of ultrapure water, freeze dried and stored until further use. All glassware involved in DOM isolation and DOC measurements was baked at 500°C for 5h.

4.2.4 Spectroscopic characterization of wetland waters, DOM isolates and standard DOM solutions (Task 2).

Spectroscopic characterization is useful to obtain qualitative information on some DOM properties, such as aromaticity and molecular size (Helms et al., 2008). Spectral parameters used in this study included specific absorption coefficient [$a_S(\lambda)$], specific UV absorbance at 254 nm ($SUVA_{254}$), and spectral slope (S), which were selected and calculated based on established approaches for spectroscopic investigation of aquatic DOMs (Helms et al., 2008; Twardowski et al., 2004; Weishaar et al., 2003). Specific absorption coefficient $a_S(\lambda)$ (L mgC^{-1} m^{-1}) can be calculated as follow:

$$a_S(\lambda) = \frac{\alpha(\lambda)}{l \cdot [DOC]} \quad (4.1)$$

Where $\alpha(\lambda)$ was measured using a UV-VIS spectrophotometer, with l is the pathlength (l=0.01 m), and [DOC] is the dissolved organic carbon concentration of the sample. $SUVA_{254}$ values are defined as $a_S(254)$. Spectral slopes S (nm^{-1}) were calculated by non-linear least square fits of absorption data for the wavelength range 300 to 700 nm with a single exponential decay function (reference wavelength 350 nm). The total absorption $a_S(250 – 450)$ was obtained by integrating $a_S(\lambda)$ data over the wavelength range 250 to 450 nm. Data fits and integrations were performed using Origin 8.5 data analysis software (Origin Lab).

Table 4.1. Characteristics of wetland water samples, DOM isolates and solid phase extraction discharges.

Sample	pH	TOC (mgC L^{-1})	Cl^- (mg L^{-1})	NO_3^- (mg N L^{-1})	PO_4^{3-} (mg P L^{-1})	SO_4^{2-} (mg L^{-1})	Mg^{2+} (mg L^{-1})	Ca^{2+} (mg L^{-1})	Fe^{3+} (mg L^{-1})	Na^+ (mg L^{-1})
Wetland water samples										
Wetland influent (nitrified municipal wastewater)	8.5	4.7	362	6.2	1.5	157	4.1	0.64	10×10^{-3}	39
Open-water wetland effluent	8.7	5.2	388	1.6	3.1	159	4.1	0.67	11×10^{-3}	39
Cattail wetland effluent	8.3	5.3	392	2.0	2.0	156	4.4	0.74	30×10^{-3}	40
Bulrush wetland effluent	8.3	5.2	388	2.3	2.3	151	4.3	0.72	12×10^{-3}	40
SPE discharge										
Wetland influent SPE discharge	-[a]	2.4[b]	-[d]	6.2	1.5	157	n.d.	n.d.	n.d.	n.d.
Open-water wetland effluent SPE discharge	-[a]	2.5[b]	-[d]	1.6	3.1	159	n.d.	n.d.	n.d.	n.d.
Cattail wetland effluent SPE discharge	-[a]	2.6[b]	-[d]	2.0	2.0	156	n.d.	n.d.	n.d.	n.d.
Bulrush wetland effluent SPE discharge	-[a]	2.3[b]	-[d]	2.3	2.3	151	n.d.	n.d.	n.d.	n.d.
DOM isolates										
Wetland influent DOM	-	5[c]	n.d.[*]	n.d.	n.d.	n.d.	14×10^{-4}	3×10^{-4}	1×10^{-4}	2.4
Open-water wetland effluent DOM	-	5[c]	n.d.	n.d.	n.d.	n.d.	19×10^{-4}	4×10^{-4}	2×10^{-4}	3.3
Cattail wetland effluent DOM	-	5[c]	n.d.	n.d.	n.d.	n.d.	10×10^{-4}	1×10^{-4}	1×10^{-4}	2.8
Bulrush wetland effluent DOM	-	5[c]	n.d.	n.d.	n.d.	n.d.	5×10^{-4}	2×10^{-4}	1×10^{-4}	4.6
SRFA	-	5[c]	n.d.	n.d.	n.d.	n.d.	350×10^{-4}	53×10^{-4}	3×10^{-4}	0.4
PLFA	-	5[c]	n.d.	n.d.	n.d.	n.d.	22×10^{-4}	4×10^{-4}	3×10^{-4}	0.3

[*]n.d.: not determined. [a] prior to extraction pH lowered to 2 and subsequently raised to initial values. [b] average values. [c] re-dissolved at 5 mgC L^{-1}.
[d] addition of hydrochloric acid led to high chloride concentrations in the discharge.

Irradiation experiments were conducted in uncovered, 2.5-cm deep, black-painted, glass beakers, which were stirred and maintained at 20°C. Solutions in the beakers were wetland water samples, or DOM-free PBS/clear water, or PBS/clear water that was supplemented with the desired amount of DOM stock-solution (up to 15 mgC L^{-1} final concentration). Photochemical probe compounds (with or without addition of methanol as quencher of •OH) or pathogen indicators were also added to the solutions. The beakers were irradiated using an ozone-free 1000 W Xe arc lamp housed in a solar simulator (Oriel, model number 91194; Newport; Irvine, CA) fitted with a 1.5:G:A global air mass filter (Newport, part number 81388) and a UVB-blocking filter (Newport, part number 81050) to reduce the effects of endogenous inactivation caused by UVB light. Dark controls were maintained under the same conditions as light samples, but covered with aluminum foil.

4.2.6 Formation of reactive species and calculation of quantum yields.

Formation of reactive intermediates was measured using the established probe compounds furfuryl alcohol (FFA, 50μM) (6 h irradiation) for singlet oxygen $^1O_2$ (Haag et al., 1984), 2,4,6-trimethylphenol (TMP,10 μM) (6 h irradiation) for triplet state DOM ($^3DOM^*$) (Canonica et al., 1995), and phenol formation from benzene (3 mM) (10h irradiation) for hydroxyl radical ($^{\bullet}OH$) (Dong and Rosario-Ortiz, 2012). For each probe compound, 1-mL samples were withdrawn at equidistant time intervals and immediately analyzed for their concentrations using HPLC. Beakers containing benzene were covered with quartz-glass lids and sealed on the edges using parafilm to reduce the evaporation of benzene. Pseudo-first order depletion rate constants of probe compounds k_{FFA} and k_{TMP} were determined by linear regression of $\ln([FFA]_t/[FFA]_0)$ and $\ln([TMP]_t/[TMP]_0)$, respectively. k_{phenol} was determined by linear regression of its formation from benzene versus time. Rates for photochemical probe compounds and pathogen indicator inactivation were corrected for light screening using the rate of light-absorption of the samples (R_A):

$$R_A = \sum_{\lambda=280nm}^{700} \frac{E_p(\lambda) \cdot \varepsilon_{DOM}(\lambda) \cdot (1 - 10^{-(\varepsilon_{DOM}(\lambda) \cdot [DOC] \cdot z)})}{\varepsilon_{DOM}(\lambda) \cdot [DOC] \cdot z} \quad (4.2)$$

where $E_p(\lambda)$ is the measured photon fluence rate (Einstein m^{-2} s^{-1}) of the simulated sunlight, $\varepsilon_{DOM}(\lambda)$ is the specific molar absorption coefficient (L mgC^{-1} m^{-1}) of each DOM isolate or water sample and z is the depth of solution in the reactors (0.025m).

Singlet oxygen ($^1O_2$). Bulk-phase steady-state concentrations of singlet oxygen $[^1O_2]_{ss,bulk}$ were calculated by dividing the observed rates of FFA depletion by the second-order reaction rate of FFA with $^1O_2$ ($k = 1.2\times10^8$ M^{-1} s^{-1}) (Haag et al., 1984). To account for •OH-induced FFA depletion, measurements were conducted with and without addition of 0.1 M of the •OH-quencher methanol. Singlet oxygen quantum yields $\Phi_{^1O_2}$ were calculated according to:

$$\Phi_{^1O_2} = \frac{[^1O_2]_{ss,bulk} \cdot k_{d^1O_2}}{R_A} \quad (4.3)$$

where $k_{d\,^1O_2}$ is the pseudo first-order deactivation rate constant for $^1O_2$ in water ($k_{d\,^1O_2}=2.5\times10^5 s^{-1}$) (Wilkinson and Brummer, 1981).

Triplet state DOM ($^3DOM^*$). Quantum yield coefficients of TMP as a probe for $^3DOM^*$ f_{TMP} (M^{-1}) were calculated as follows (Sharpless et al., 2014):

$$f_{TMP} = \frac{k_{TMP}}{R_A} \tag{4.4}$$

Hydroxyl radical (•OH). Formation rates of •OH ($R_{•OH}$) and apparent quantum yields for •OH formation $\phi_{•OH_{app}}$ were determined by the method of a previous study (Dong and Rosario-Ortiz, 2012).

4.2.7 Inactivation of pathogen indicators.

Enterococcus faecalis (ATCC 19433). *Ent. faecalis* was grown in brain heart infusion broth (BD) for 24 hours at 37°C to reach stationary phase. Cells were pelleted by centrifuging at 6,800×g for 3 min, washed and re-suspended into sterile PBS. Then, cells were spiked into DOM-free clear water or clear water with addition of DOM to obtain a final concentration of ~10^7 colony forming units (CFU) mL^{-1} and irradiated for 8h. Subsamples were collected every hour for enumeration of *Ent. faecalis* using the spread plate method on selective media mEnterococcus agar (BD). Experiments with DOM solutions were conducted in duplicate. Controls with DOM-free clear water were included in every experiment resulting in 20 replicates.

MS2 (ATCC 15597-B1). MS2 was propagated by broth enrichment using *E. coli* F_{amp} host (ATCC 700891). Crude MS2 stocks were extracted using chloroform (1:3 vol/vol) to remove broth constituents and precipitated overnight in polyethylene glycol solution (8% PEG 6000, wt/vol; 0.3 M NaCl) at 4 °C, and centrifuged at 23,000×g for 30 min. The resulting virus pellets were re-suspended in PBS, chloroform extracted (1:3 vol/vol), and filtered through 0.22 μm filters. Purified MS2 stocks were stored at -80 °C. MS2 was assayed using the double agar layer method with modified Luria Bertani (LB) top and bottom agar consisting the following ingredients: Bacto Agar [0.75% (top) or 1.5% (bottom) wt/vol; BD], 10 g L^{-1} Bacto Tryptone (BD), 0.137 M NaCl, 1 g L^{-1} yeast extract (EMD Chemicals), 0.0055 M dextrose (EMD Chemicals), 0.002 M $CaCl_2$ (Fisher)]. For virus counting, MS2 containing solutions were diluted in 1:10 dilution series using PBS until appropriate virus concentrations were reached. Subsequently, 100 μL aliquots were added to molten top agar that was supplemented with *E. coli* host (exponential growth phase). Molten top agar was mixed and poured onto bottom agar plates. After solidification, double agar layer plates were incubated at 37°C for 18–24 h and plaque forming units (PFU) were counted. Irradiation experiments with MS2 were conducted in duplicate, including six replicates for PBS, over 10 h (2 h sampling interval) at a concentration of ~10^4 PFU mL^{-1}.

Inactivation data analysis. Inactivation rates of *Ent. faecalis* and MS2 were determined from the slope of the linear regression of $\ln(C_t/C_0)$ versus either time (k_{obs}, h^{-1}) or incident photon fluence rate E_p (k_{photon}, m^2 Ei^{-1}). k_{obs} values of *Ent. faecalis* and MS2 under UVB-blocked simulated sunlight were subtracted to their k_{obs} values in DOM-free clear water/PBS in the dark

before reported in the Results and Discussion section. k_{photon} was used to correct for light screening in the water column. Photon fluence rate E_p refers to the number of photons available for absorption by the indicators and photosensitizers, and is used to correct for the effect of light screening on endogenous inactivation of the indicators in the water column. For *Ent. faecalis*, the values for E_p were measured over the UV wavelengths from 280 nm to 400 nm, which were shown to be most important for endogenous inactivation of *Ent. faecalis* (Davies-Colley et al., 1997; Kadir, 2010; Sinton et al., 2002). For MS2, the values for E_p were calculated from 280 to 320 nm, because UVB was observed to be most important for MS endogenous inactivation (Love et al., 2010; Silverman et al., 2013). Statistical tests including linear regressions to calculate pathogen indicator inactivation rates were performed using GraphPad Prism 6.0.1 (GraphPad Software, La Jolla, CA). Two-way ANOVA analysis was conducted to compare inactivation rate constants of *Ent. faecalis* and MS2 in different DOM solutions.

4.2.8 Association between Ent. faecalis and DOM (Task 4).

The adsorption of DOM onto *Ent. faecalis* cells was determined followed a previously published protocol (Fein et al., 1999; Frost et al., 2003; Maurice et al., 2004). Briefly, bacterial stock were added to 20 mL standard or DOM isolate solutions (25 mgC L^{-1}) made with clear water to reach final concentration of 10^{10} CFU mL^{-1}. Controls were prepared using DOM-free clear water. Suspensions were stirred and maintained at room temperature in the dark for 4 h to reach adsorption steady-state conditions (Maurice et al., 2004). Samples were taken before adding bacteria and after 4 h. *Ent. faecalis* cells were removed from the samples using 0.45 µm nylon filters (Fisher Scientific) and the light absorption of the filtrate at 450 nm was measured (Fein et al., 1999). To determine concentration of DOM in each solution, light-absorption calibration curves ([DOC] = 0 – 30 mg C L^{-1}) were also collected for each DOM isolate. Mass of adsorbed DOM onto *Ent. faecalis* cells was estimated by calculating the difference in mass of DOM in the filtrate at t = 0 and 4 h.

4.3 Results

4.3.1 Isolation and spectroscopic characterization of wetland DOM.

Spectroscopic characterization was used to determine the optical properties of the whole water samples and the DOM isolates collected from the influent and effluents of three unit process wetlands. Spectroscopic characterization was also conducted for the non-recoverable DOM fractions to evaluate the performance of the SPE procedure. In this study, non-recoverable DOM is defined as the fraction of the DOM from a given water sample that did not adsorb to the SPE cartridge and was present in the SPE discharge.

The specific absorption coefficient spectra for the whole water samples of the wetland influent, three effluents and the two standard DOMs (SRFA and PLFA) are shown in Figure 4.1a. The effluents of both vegetated wetland cells exhibited higher specific absorption than the influent of the wetland system, while the open-water effluent had the lowest overall absorption. A comparison to SRFA and PLFA, which are recognized as fulvic acid end-members of terrestrially/higher-plant derived (allochthonous) and aquatic/microbial derived (autochthonous) aquatic DOM (D'Andrilli et al., 2013), respectively, suggests that DOM in the vegetated cells became more terrestrial-like, while DOM in the open water cell became more microbial-like.

The TOC concentration increased in all three wetland cells (compared to the influent water; Table 4.1), indicating that new organic matter was produced within the wetlands. The specific absorption coefficient spectra for the DOM isolates and the two standard DOMs are shown in Figure 4.1b; the isolates were more similar to each other than the whole water samples.

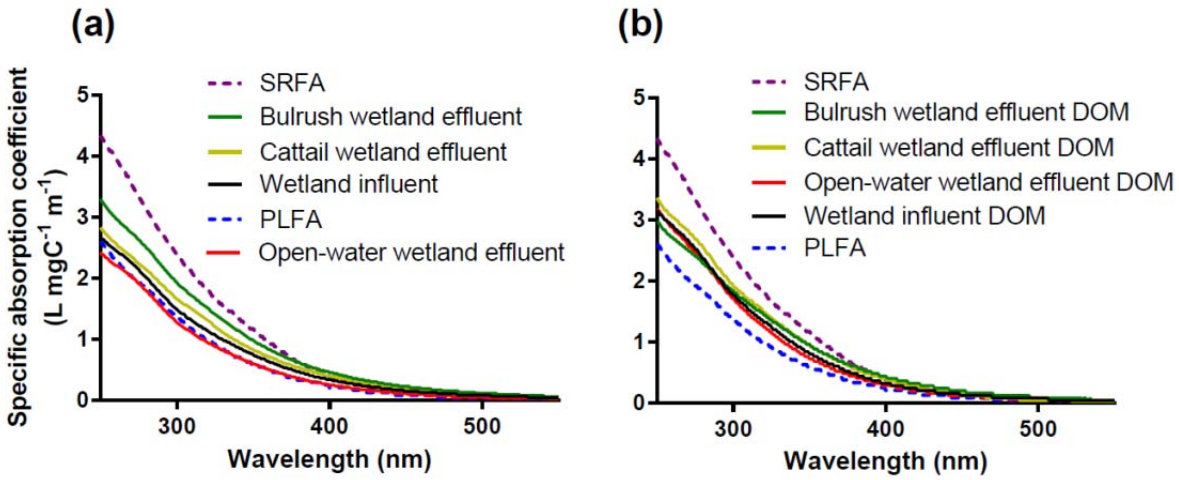

Figure 4.1. Specific absorption coefficient spectra $a_S(\lambda)$ (L mgC^{-1} m^{-1}) of (a) whole water samples and (b) DOM isolates in comparison with standard DOMs (SRFA and PLFA).

The whole water samples and DOM isolates from the two vegetated wetlands had slightly higher $SUVA_{254}$ and spectral slopes as compared to the influent, whereas the opposite trend was observed for the open-water wetland effluent (Figure 4.2). These differences in optical properties indicate that DOM in the vegetated wetland effluents was characterized by higher aromaticity and molecular size compared to the wetland influent (Helms et al., 2008). Conversely, the aromaticity and molecular size of DOM in the open-water wetland effluent were lower than the wetland influent. Compared to the standard DOMs, the wetland DOM isolates appeared to have higher aromaticity and molecular size than PLFA, but less than SRFA.

The difference in spectroscopic properties of the wetland influent and effluents was relatively small. However, the observed trends indicate that the influent organic matter underwent transformation and that new organic matter was introduced in the wetlands, characteristic of either plant-derived or microbially-derived DOM. Analysis of optical parameters showed that SPE method was able to extract the majority of light-absorbing DOM in the wetland waters and thus potentially the majority of reactive species precursor moieties within the DOM, while a small fraction of DOM was non-recoverable and remained in the SPE discharges during the extraction process.

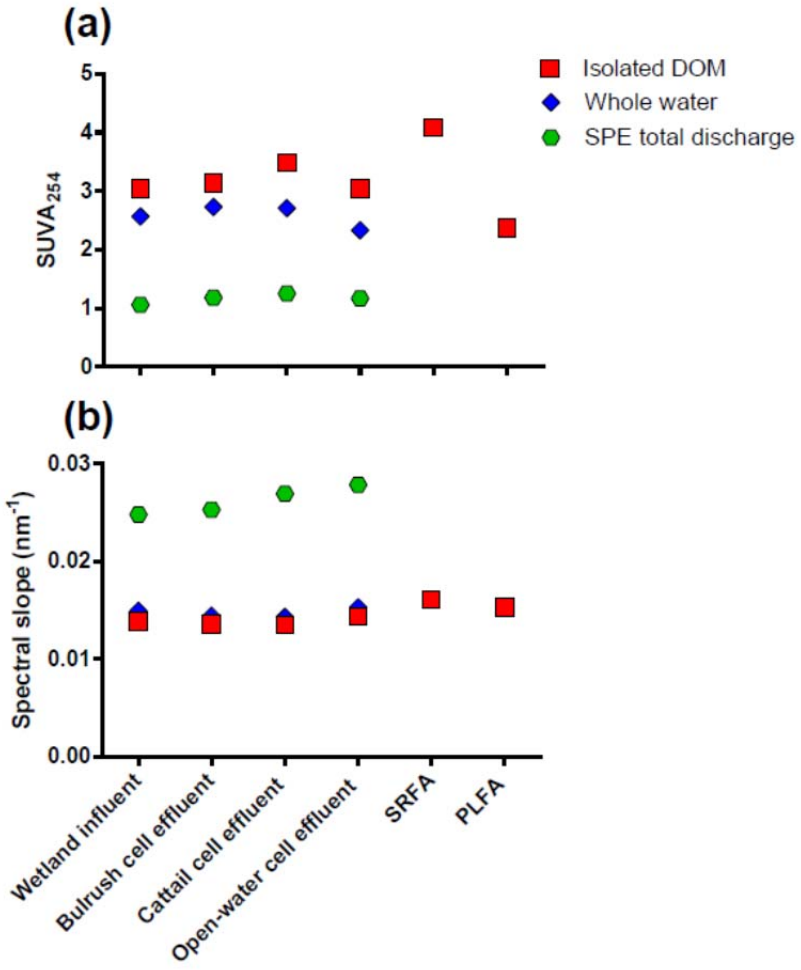

Figure 4.2. (a) $SUVA_{254}$ and (b) spectral slopes S of whole water samples, wetland DOM isolates, and total SPE discharges in comparison to standard DOMs (SRFA and PLFA).

To further evaluate the performance of the SPE method, the specific absorption coefficient spectra of the whole water sample, DOM isolates, and SPE discharges was measured. The results for the cattail cell are shown as an example (Figure 4.3; results for other samples were similar). Spectra V_1, V_2 and V_3 were collected from the SPE discharges after 0.1 L, 0.5 L and 2.0 L of water samples had passed through the SPE cartridges, respectively. Although there was a small increase in the specific absorption of the SPE discharges during the extraction (spectra V_3 as compared to V_1 and V_2), most of the DOM was adsorbed on the cartridge material (47% – 59%), with adsorption decreasing slightly during the extraction (Table 4.2). These values were within the range of the SPE extraction efficiencies reported in previous studies, for example DOM recovery from marine environments was reported to be 43% – 62% (Dittmar et al., 2008), and recovery from wastewater effluent around 57% (Gonsior et al., 2011). Each SPE cartridge was loaded with approximately 0.8 – 0.9 mM C, which did not exceed the recommended maximum load of 2 mM C per cartridge (Dittmar et al., 2008). Both spectra and optical properties (i.e., $SUVA_{254}$ and S) (Figures 4.2 and 4.3) indicate there was an enrichment of light-

absorbing components with higher aromaticity and molecular weight in the DOM isolates (Helms et al., 2008), whereas the opposite trend was observed in the non-recoverable DOM fractions that remained in the discharges.

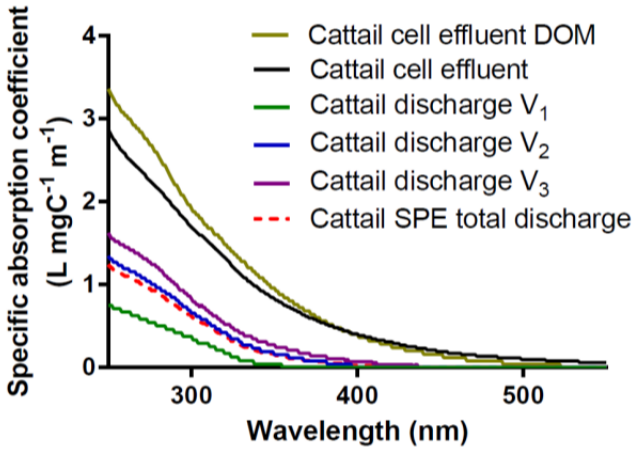

Figure 4.3. Specific absorption coefficient spectra of cattail wetland effluent as an example for wetland water samples subject to SPE. V_1,V_2 and V_3 show the spectra of the discharge after 0.1 L, 0.5 L and 2 L wetland water were passed over each SPE-column, respectively. Total SPE discharge shows the spectrum of the combined discharge (continuous collection). Samples were readjusted to initial pH, before measurement of absorption spectra.

Table 4.2. Concentration of TOC (mgC L^{-1}) in initial samples and SPE discharge after different volumes (0.1 L, 0.5 L, and 2.0 L) of wetland water passed through each column; percentage of TOC adsorbed to SPE columns (%).

[DOC] (mgC L^{-1})	**Initial sample**	**V_1 (0.1 L)**	**V_2 (0.5 L)**	**V_3 (2.0 L)**	**Adsorption on cartridges (%)**
Wetland influent	4.7	2.3	2.4	2.5	46.8 – 51.1
Open-water cell effluent	5.2	2.3	2.3	2.7	48.1 – 53.8
Cattail cell effluent	5.2	2.4	2.6	2.9	44.2 – 53.8
Bulrush cell effluent	5.3	2.2	2.3	2.4	54.7 – 58.5

4.3.2 Photochemical reactive species formation in wetland waters and wetland DOM isolates.

Photochemical properties of the whole water samples, DOM isolates, and total SPE discharges were determined by measuring the formation of reactive species, including $^1O_2$, $^3DOM^*$ and $^\bullet OH$. In Figure 4.4, the bulk-phase steady-state concentration of singlet oxygen, $[^1O_2]_{ss,bulk}$, and the TMP-depletion rate constants, k_{TMP}, are shown for the cattail cell whole water sample, the SPE discharge, and different concentrations of the DOM isolate (Similar results were found for the other samples, data not shown). For the same DOC concentration, the

$[^1O_2]_{ss,bulk}$ was similar in the whole water and for the DOM isolate. Consistent with this result, there was no FFA depletion observed in the SPE discharges ($[^1O_2]_{ss,bulk} \approx 0$), indicating that the SPE method was efficient in the extraction of $^1O_2$ sensitizing moieties. However, the value of k_{TMP} was higher in the DOM isolate than in the whole water. Also, the observed k_{TMP} values in the SPE discharges were significantly greater than 0, suggesting that the non-recoverable DOM in the total SPE discharge contained triplet precursors whose excited states are reactive with TMP but do not lead to the production of $^1O_2$.

The $[^1O_2]_{ss,bulk}$ values of both the wetland DOM isolates and standard DOMs are shown in Figure 4.5. For the same DOC concentration, the $[^1O_2]_{ss,bulk}$ was highest in the open-water wetland DOM isolate, followed by the cattail wetland DOM isolate, SRFA, influent DOM isolate, bulrush wetland DOM isolate, and PLFA. As expected, the $[^1O_2]_{ss,bulk}$ increased linearly with increasing DOM concentration (Figure 4.5); the values of k_{TMP} also increased as the concentration of the DOM isolate increased (Figure 4.4).

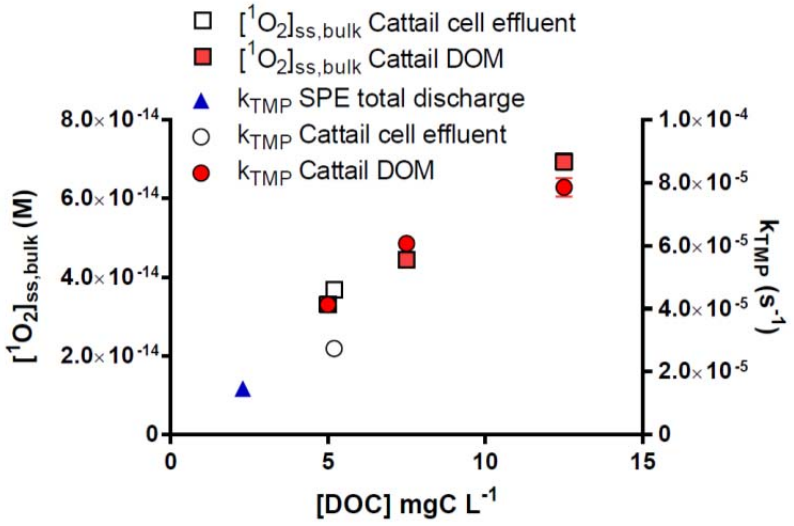

Figure 4.4. Steady-state concentration of singlet oxygen in the bulk phase ($[^1O_2]_{ss,bulk}$) and TMP depletion rate constants (k_{TMP}) of cattail wetland effluent samples as an example for wetland water samples during SPE. Error bars indicate ± one standard error of duplicate samples; some are too small to be seen.

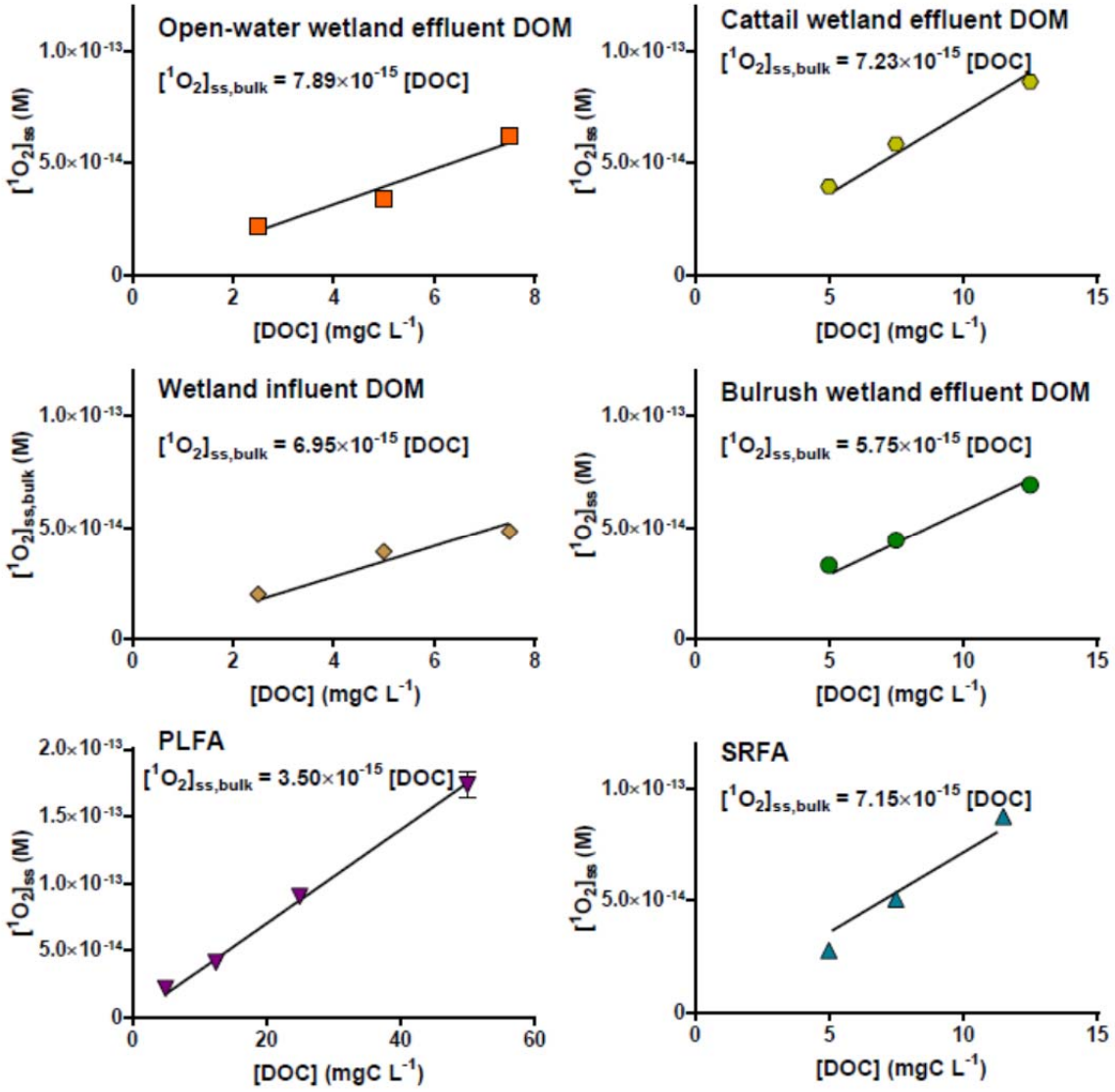

Figure 4.5. Linear regression relationship between steady-state concentration of singlet oxygen in the bulk phase ($[^1O_2]_{ss,bulk}$) and DOC concentration. Error bars indicate ± one standard error of duplicate samples; some are too small to be seen.

The $^1O_2$ quantum yields ($\Phi_{^1O_2}$) and TMP quantum yield coefficients (f_{TMP}) in the whole water samples were generally lower than in their corresponding DOM isolates (Figure 4.6), indicating that the enriched components of the DOM isolates that increased $SUVA_{254}$ values are photochemically active, and contributed to the formation of $^1O_2$ and $^3DOM^*$. Comparing the different water types, both $\Phi_{^1O_2}$ and f_{TMP} were lower in the vegetated wetland effluents compared to the wetland influent and open-water wetland effluent, indicating that the higher $SUVA_{254}$ values for the vegetated cells were attributed to light-screening components of the DOM. The slight increase in quantum yields that was observed in the open-water wetland

compared to the influent is probably due to the decrease of light-screening components and the enrichment of reactive species precursor moieties during passage through the wetland. The differences were more pronounced for $\phi_{^1O_2}$ than for f_{TMP}. Similar values for $\phi_{^1O_2}$ and f_{TMP} were reported in previous studies for the standard DOMs (Mostafa and Rosario-Ortiz, 2013; Sharpless et al., 2014).

Figure 4.6 also shows that there was no significant difference in $\phi_{^1O_2}$ values in presence of $^{\bullet}OH$ scavenger methanol, indicating that the production of $^{\bullet}OH$ radical in the whole water samples and DOM isolates was not significant in our experimental setup. Experiments with benzene also confirmed that there was no significant formation of $^{\bullet}OH$ radical in our experimental setup ($[^{\bullet}OH]_{ss} \approx 0$).

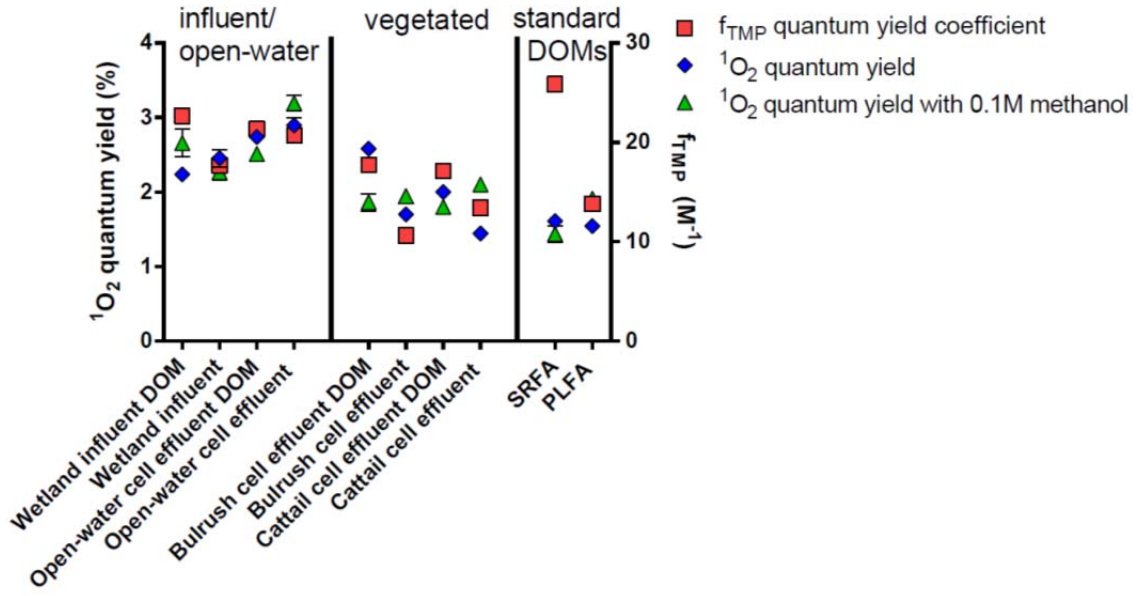

Figure 4.6. Singlet oxygen quantum yields ($\phi_{^1O_2}$) and TMP quantum yield coefficients fTMP (M-1) of wetland water samples, DOM isolates and standard DOMs. Error bars indicate ± one standard error of duplicate samples, but are mostly too small to be seen.

4.3.3 Role of DOMs in sunlight inactivation of MS2.

Experiments with MS2 in wetland DOM isolate solutions at various concentrations were conducted under UVB-blocked simulated sunlight to investigate the role of wetland derived DOMs in MS2 exogenous inactivation. There was a strong correlation between inactivation rates of MS2 [both observed inactivation rate (k_{obs}) and rate after corrected for light screening (k_{photon})] and DOM concentration in wetland DOM isolates and standard DOMs (Figure 4.7). These results indicate that the photosensitizing effect of the DOM was greater than its role in attenuating light. Consistent with previous research, negligible inactivation of MS2 was observed in DOM-free PBS under UVB-blocked simulated sunlight (Fisher et al., 2011; Love et al., 2010). The k_{obs} and k_{photon} values increased with increasing concentration of the DOMs, indicating that both wetland DOMs and standard DOMs acted as photosensitizers.

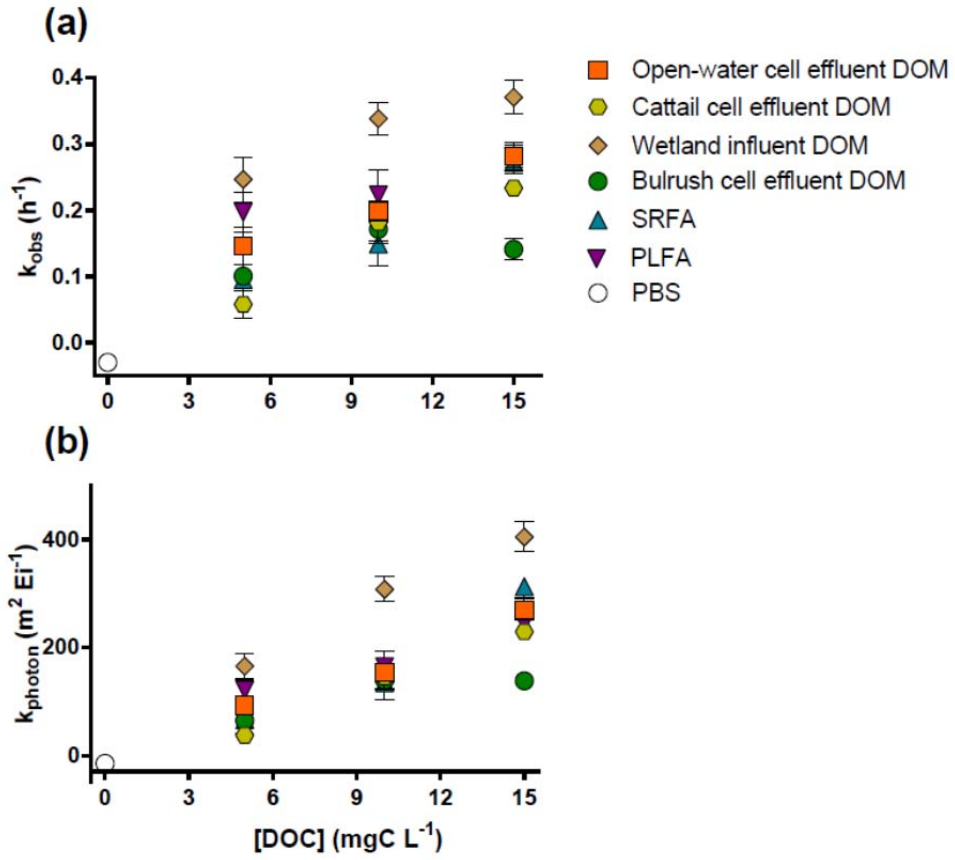

Figure 4.7. Inactivation rates of MS2 in DOM isolates as a function of [DOC] under UVB-blocked simulated sunlight (a) before and (b) after correction for light screening. Error bars indicate ± one standard error of replicate experiments; some are too small to be seen.

The production of reactive species (e.g., $^1O_2$, $^3DOM^*$, $^\bullet OH$) in water samples from different sources (e.g., waste stabilization ponds, coastal areas, rivers) has been shown to be a key factor influencing exogenous inactivation of MS2 (Kohn and Nelson, 2007; Rosado-Lausell et al., 2013; Silverman et al., 2013). In this study, the inactivation rates of MS2 in most tested DOM isolate solutions (except Bulrush cell effluent DOM) were observed to have strong linear correlation with $[^1O_2]_{ss,bulk}$ (Figure 4.8, Table 4.3), which is strong evidence that $^1O_2$ was the most important reactive species causing exogenous inactivation of MS2. Nonetheless, from the observed correlation it is not possible to separate inactivation by $^3DOM^*$ and $^1O_2$, since $^3DOM^*$ is a precursor to $^1O_2$, and $^3DOM^*$ and $^1O_2$ formation rates were also correlated (e.g., Figure 4.4). Interestingly, the inactivation rate of MS2 was slightly higher in the SPE discharges, which had low formation rate of $^3DOM^*$ but no detectable formation of $^1O_2$ (Figure 4.4), than in PBS (Figure 4.9), implicating the involvement of $^3DOM^*$. Any contribution of $^\bullet OH$ to MS2 sunlight inactivation was negligible, as its formation in all tested waters was not detectible in our experimental setup.

The wetland DOM isolate and standard DOM solutions affected the MS2 inactivation rates differently (Figures 4.7 and 4.8). For the same DOC and $[^1O_2]_{ss,bulk}$ concentrations, the k_{obs} was highest in the influent DOM isolate and PLFA, followed by the open-water, bulrush, cattail wetland effluent DOM isolates, and SRFA. A possible explanation is that there might be greater association between MS2 and the influent DOM isolate and PLFA, compared to the other DOM isolates. As mentioned above (section 4.3.1), the influent DOM isolate and PLFA have the lowest molecular size compared to other DOM isolates, which could lead these two DOM isolates to have better access to MS2 pores and RNA (Silverman et al., 2015). If this is the case, the RNA would be exposed to higher concentrations of $^1O_2$ and $^3DOM^*$. Differences in association between MS2 and the various DOM isolates might also explain why there was no linear correlation between MS2 k_{obs} and $SUVA_{254}$ values in this study, as reported in a previous study (Rosado-Lausell et al., 2013).

We found that the inactivation rate of MS2 was significantly higher in whole water samples compared to their respective DOM isolates (Figures 4.7 and 4.9). A similar observation was reported in a previous study showing that there was a difference between the whole waters and DOM isolated using SPE method in photolysis of organic chemicals (Bodhipaksha and MacKay, 2014). To determine whether the difference was due to the incomplete recovery of DOM by the SPE method, we compared inactivation rates of MS2 in solutions of DOM isolates that were added back to the SPE discharge (at the same DOC concentration)(Figure 4.9). k_{obs} and k_{photon} values in the wetland influent and open-water effluent were significantly higher than in the SPE discharges plus DOM isolate solutions, indicating that the discrepancy was not due to the non-recoverable DOM. One possibility is that some of the DOM sorbed on the SPE cartridge was not eluted. Another possibility is that other constituents of the wetland waters, which contribute to MS2 inactivation, were removed by the SPE method. For example, the SPE method removes all ions (Dittmar et al., 2008); concentrations of divalent cations (e.g., Mg^{2+} and Ca^{2+}) in wetland DOM isolate solutions were negligible and approximately 2,000 times lower than in whole wetland waters (Table 4.1). Such high divalent cation concentrations in wetland waters might increase virus-photosensitizer association, and sunlight inactivation, through cation bridging (Kohn et al., 2007). Silverman et al. also observed that the MS2 apparent second-order rate constant with $^1O_2$ (k_2) in the open-water wetland effluent was significantly larger than k_2 observed in other environmental waters (Kohn and Nelson, 2007; Silverman et al., 2015, 2013a). One of the explanations given by the authors for such high k_2 value in the open-water wetland effluent was relatively high divalent cation concentration measured in the wetland water (Silverman et al., 2015).

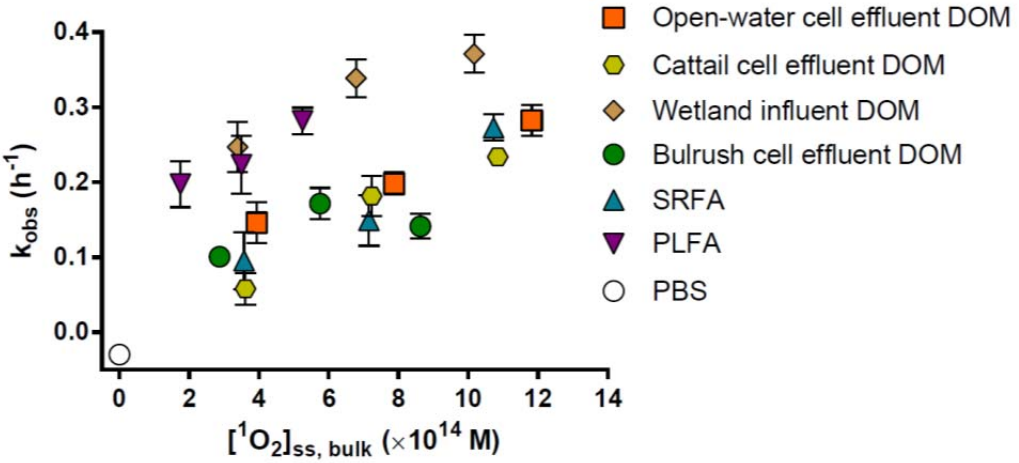

Figure 4.8. The observed inactivation rates of MS2 as a function of steady-state concentration of singlet oxygen in the bulk phase $[^1O_2]_{ss,bulk}$. Error bars indicate ± one standard error of inactivation rates of the indicators; some are too small to be seen. Values of $[^1O_2]_{ss,bulk}$ for different [DOC] were calculated from linear regressions of [DOC] and measured $[^1O_2]_{ss,bulk}$ (Figure 4.5).

Table 4.3. Linear regression of MS2 observed inactivation rates k_{obs} and steady-state concentration of singlet oxygen in the bulk phase $[^1O_2]_{ss,bulk}$ produced in the DOM isolates (Data of k_{obs} and $[^1O_2]_{ss,bulk}$ is presented in Figure 4.8).

DOM	**Slope ± Standard Error**	**R^2**
Wetland influent DOM	0.018 ± 0.005	0.93
Open-water cell effluent DOM	0.017 ± 0.002	0.98
Cattail cell effluent DOM	0.024 ± 0.006	0.95
Bulrush cell effluent DOM	0.007 ± 0.010	0.32
SRFA	0.025 ± 0.006	0.95
PLFA	0.024 ± 0.005	0.95

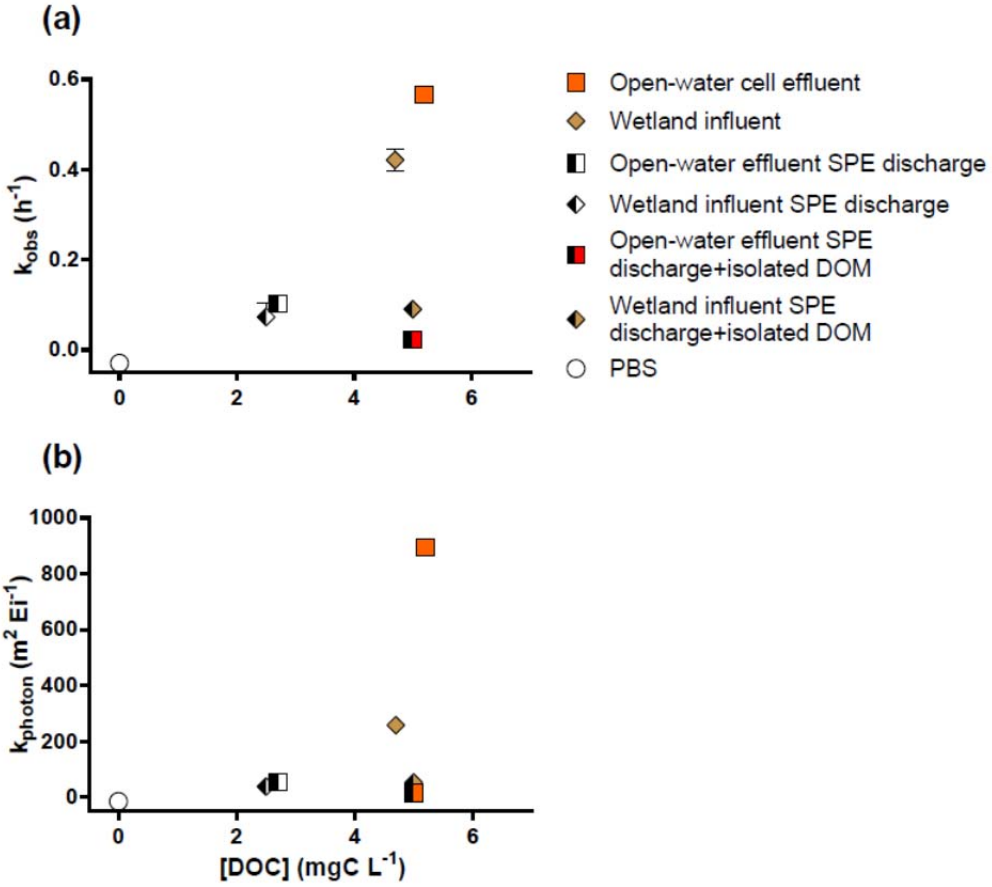

Figure 4.9. Inactivation rates of MS2 in wetland waters, total SPE discharges, and total SPE discharges with addition of DOM isolates (a) before and (b) after correction for light screening. Error bars indicate ± one standard error; some are too small to be seen.

4.3.4 Role of DOM in sunlight inactivation of Ent. faecalis.

Similar to MS2, the role of DOM in sunlight inactivation of *Ent. faecalis* was investigated by comparing inactivation rates in solutions of wetland DOM isolates to DOM-free water. k_{obs} and k_{photon} values of *Ent. faecalis* generally increased with increasing concentration of wetland DOM isolates and PLFA (Figure 4.10, linear regression slopes between k_{photon} and [DOC] wetland DOM isolates and PLFA significantly greater than 0, $p < 0.0001$), indicating that the photosensitizing effect of the wetland DOM isolates and PLFA was greater than the light screening effect for *Ent. faecalis*. The open-water and cattail cell effluent DOMs were more effective than the wetland influent and bulrush wetland effluent DOMs (F-test, $p < 0.0001$). This trend is different than that observed for MS2, for which the influent DOM isolate had a higher inactivation rate than the three wetland effluent DOMs. The effect of SRFA was also different for *Ent. faecalis* and MS2; for *Ent. faecalis* k_{obs} decreased in the presence of these standard DOMs, indicating that SRFA light screening was significant. Because the k_{photon} values (which account for light screening) were constant for all DOM concentrations, it appears that SPFA was not an effective photosensitizer for *Ent. faecalis*.

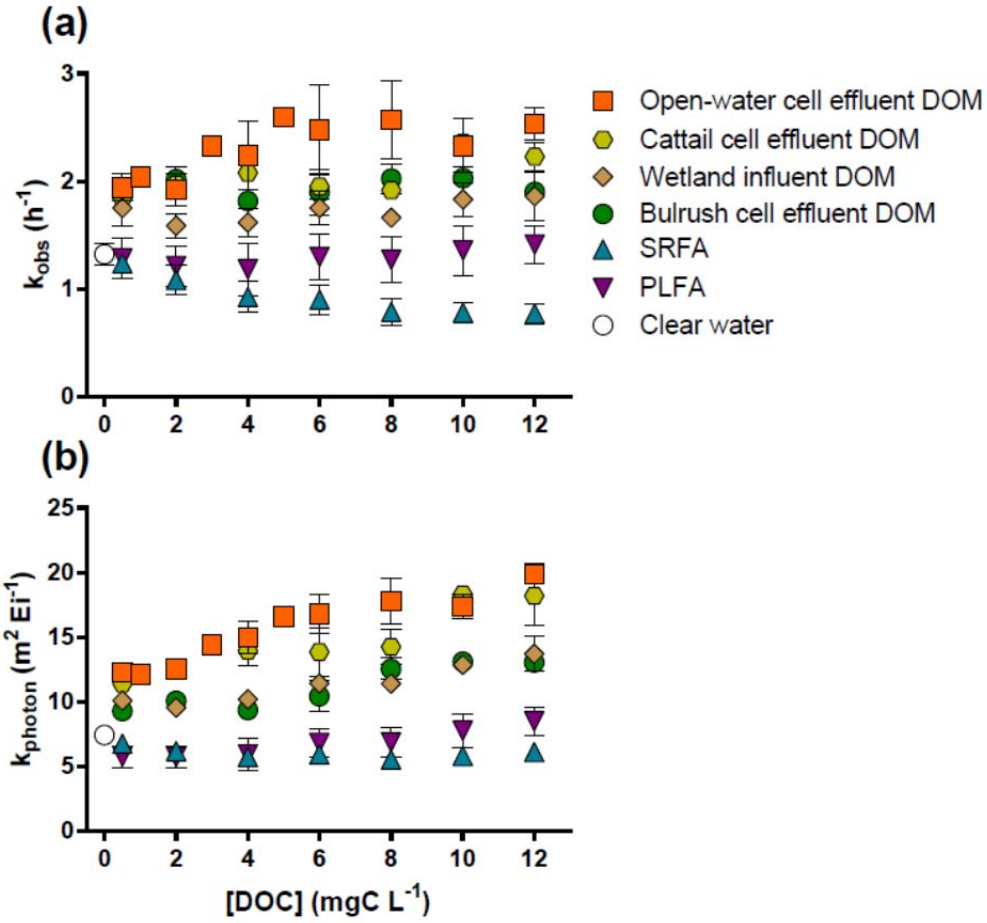

Figure 4.10. Inactivation rates of *Ent. faecalis* in solutions of DOM isolates as a function of [DOC] under UVB-blocked simulated sunlight (a) before and (b) after correction for light screening. DOMs in wetland waters were isolated using the SPE method. Error bars indicate ± one standard error of duplicate samples.

There was a positive correlation between k_{obs} and $[^1O_2]_{ss,bulk}$ for the wetland DOM isolate solutions and PLFA, whereas, there was a negative correlation for SRFA (Figure 4.11, Table 4.4). Thus, other factors appear to influence the inactivation rate. One possibility is that other reactive species are involved. However, the role of $^{\bullet}OH$ in *Ent. faecalis* in wetland DOM isolates was likely negligible as its formation rate was below the detection limit under these experimental conditions. A contribution by $^3DOM^*$ is unlikely to explain the difference, as $^3DOM^*$ and $^1O_2$ are also correlated. Also, $^3DOM^*$ production in the solutions of SPE discharges did not significantly increase inactivation rates of *Ent. faecalis* (Figure 4.12), suggesting that the contribution of $^3DOM^*$ was less important than $^1O_2$.

There was no significant difference in inactivation rates of *Ent. faecalis* in the whole wetland waters as compared to in their corresponding solutions of DOM isolates at similar DOC concentrations (Figures 4.10 and 4.12), suggesting the recoverable DOM isolated from the SPE method was the main contributor to *Ent. faecalis* inactivation.

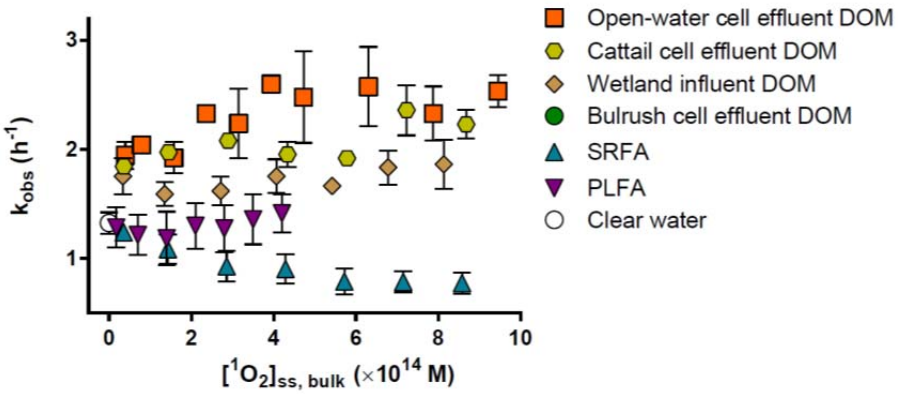

Figure 4.11. The observed inactivation rates of *Ent. faecalis* as a function of steady-state concentration of singlet oxygen in the bulk phase $[^1O_2]_{ss,bulk}$. Error bars indicate ± one standard error of inactivation rates of the indicators. Values of $[^1O_2]_{ss,bulk}$ at different [DOC] in the DOM solutions shown in this figure was calculated from linear regression lines of [DOC] and measured $[^1O_2]_{ss,bulk}$ (Figure 4.5).

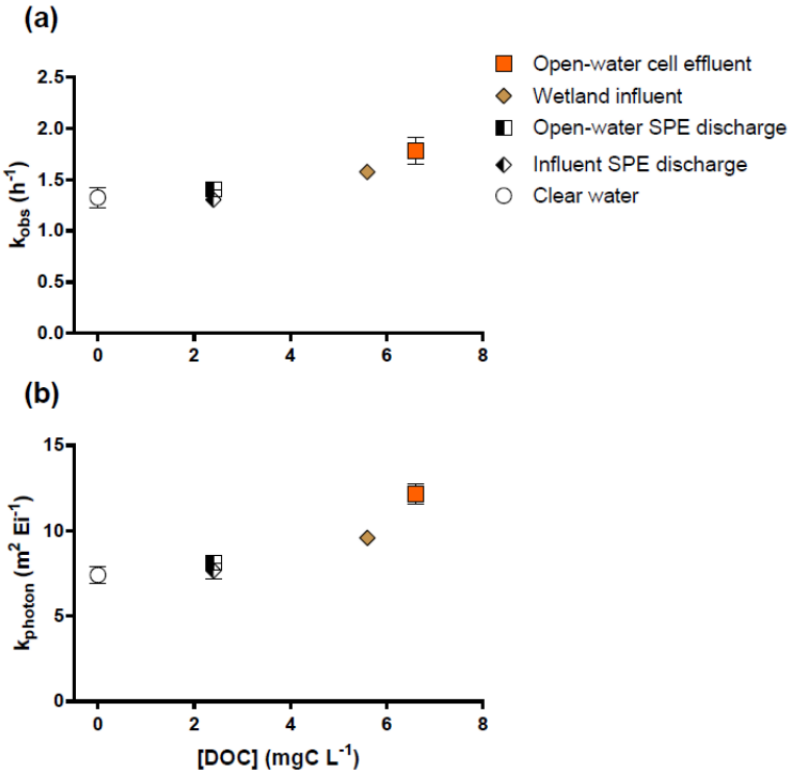

Figure 4.12. Inactivation rates of *Ent. faecalis* in whole wetland waters and total SPE discharges (a) before and (b) after correction for light screening. Error bars indicate ± one standard error of duplicate samples.

Another factor that could explain the difference in k_{obs} between the wetland DOM isolates and the standard DOM isolates is the degree of association between the sensitizers and cells. To explore this possibility, we measured the association between DOM isolates and *Ent. faecalis* bacterial cells. (Unfortunately we could not perform the same measurements for MS2, as the method was not sensitive enough.) Indeed, the mass of adsorbed DOM varied significantly among the isolates (Figure 4.13a). The adsorbed DOM mass was highest for the isolates from the two vegetated wetlands and the open-water cell, followed by the wetland influent, SRFA, and PLFA. Assuming 1 g wet weight of *Ent. faecalis* cells is similar to *E. coli* and approximates 10^{12} CFU (Pilarek et al., 2011), we found that the mass of adsorbed DOM onto *Ent. faecalis* cells in this study ranged from 0.3 to 0.9 mgC/g *Ent. faecalis*, similar to the mass of adsorbed fulvic acids isolated from a coastal-plain stream onto *Bacillus subtilis* cells in a previous study (0.55 mgC/g *B. subtilis*) (Maurice et al., 2004).

To determine whether this association between *Ent. faecalis* and the DOM isolates could explain the observed trends in k_{obs}, we plotted the value of the slope from the k_{photon} vs. [DOC] (Table 4.4) as a function of the mass of adsorbed DOM. A linear relationship was observed (R^2 = 0.77, Figure 4.13b). This finding strongly suggests that the association between DOMs and bacterial cells was an important factor in sunlight inactivation of *Ent. faecalis*. The wetland isolates were more effective photosensitizers of *Ent. faecalis* than SRFA and PLFA because a higher mass of DOM was directly attached to the cells, such that the reactive species were produced in close proximity to the biomolecules that are targets for damage. These results complement previous research showing that sensitizer association is also important for the exogenous inactivation of MS2 (Kohn et al., 2007). Similar results for bacteria have also been shown for synthetic photosensitizers used for photodynamic therapy (Dahl et al., 1989b; George et al., 2009).

Previous studies showed that hydrophobic interactions control the adsorption of DOMs onto Gram-positive bacteria: DOMs with higher molecular weight were more hydrophobic and adsorbed more onto bacterial cells (Fein et al., 1999; Maurice et al., 2004). Similarly, we found that the DOM isolates from the two vegetated wetland cells had higher hydrophobicity (assuming that hydrophobicity and aromaticity are directly correlated) and molecular weight, and greater adsorption to *Ent. faecalis* bacterial cells, compared to the wetland influent (Figures 4.2 and 4.13), which was associated with higher k_{obs}. However, this explanation does not explain the behavior of the open-water DOM isolate nor SRFA. The open-water cell DOM had lower molecular weight and hydrophobicity than the wetland influent DOM, but greater association with *Ent. faecalis* cells. The association between SRFA and *Ent. faecalis* cells was lower than all four wetland DOM isolates, but SRFA had higher hydrophobicity and molecular size than the DOM isolates. It appears that the association between this particular DOM and *Ent. faecalis* cells may be influenced by other interactions (e.g., electrostatic or steric interactions), rather than hydrophobic interaction. Another possible factor influencing the association is active involvement of *Ent. faecalis* cells in uptaking the wetland DOM isolates from the solutions via protein transporters, which were suggested as one of the pathways mediating the uptake of photosensitizers into *Ent. faecalis* cells (George et al., 2009).

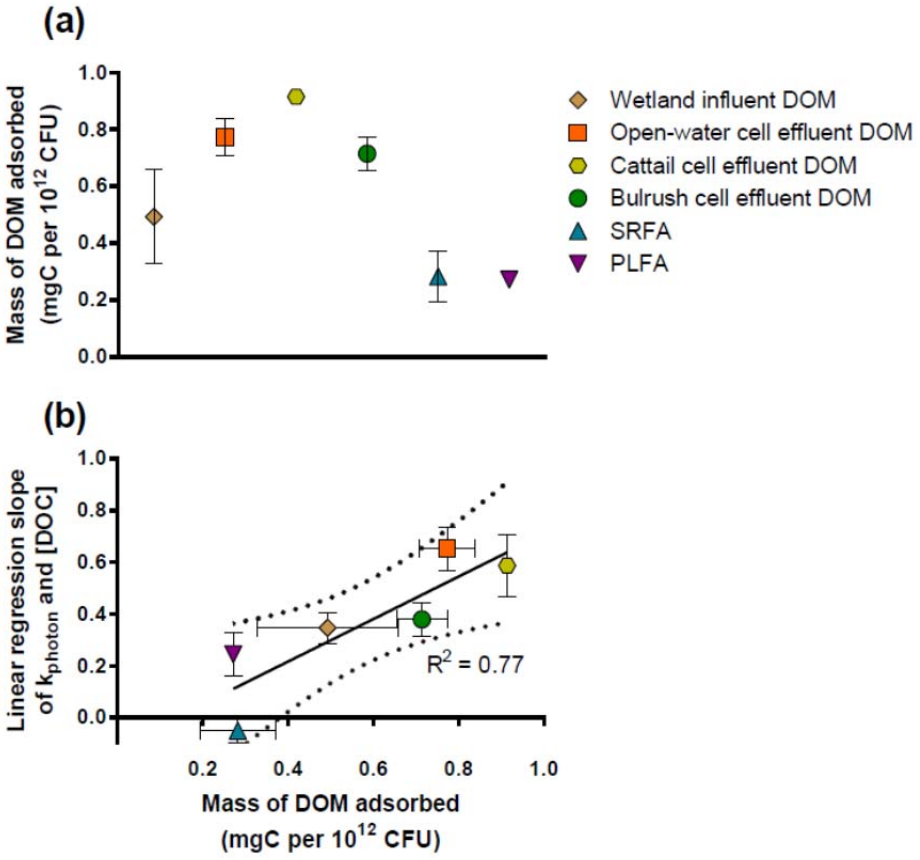

Figure 4.13. (a) Normalized mass of DOM adsorbed onto *Ent. faecalis* cells ([DOC] = 25 mgC L^{-1}; 2×10^{10} CFU mL^{-1}) and (b) Linear regression slopes between k_{photon} and [DOC] of the DOM isolates versus normalized mass of DOM absorbed to *Ent. faecalis*. Error bars indicate ± one standard error of duplicate experiments. Solid line in (b) is the linear regression line, dotted lines are the 95% confidence intervals of the linear regression.

Table 4.4. Linear regression slope from the k_{photon} vs. [DOC] (Figure 4.10b) as a function of the mass of adsorbed DOM (Figure 4.13a).

DOM	**Mass of adsorbed DOM ± Standard Error (mg C per 10^{12} CFU)**	**Slope from k_{photon} vs. [DOC] ± Standard Error**
Wetland influent DOM	0.493 ± 0.166	0.347 ± 0.059 (R^2 = 0.74)
Open-water cell effluent DOM	0.774 ± 0.065	0.652 ± 0.084 (R^2 = 0.80)
Cattail cell effluent DOM	0.914 ± 0.000	0.587 ± 0.118 (R^2 = 0.67)
Bulrush cell effluent DOM	0.714 ± 0.060	0.379 ± 0.063 (R^2 = 0.75)
SRFA	0.283 ± 0.089	-0.051 ± 0.045 (R^2 = 0.09)
PLFA	0.272 ± 0.000	0.244 ± 0.083 (R^2 = 0.42)

4.3.5 Implications for unit process wetlands design.

Results from experiments with two fecal indicators *Ent. faecalis* and MS2 in water samples collected from different cells in the pilot-scale unit process wetlands and their isolated DOMs suggest that DOMs in wetland waters play a key role in exogenous inactivation of both indicators. The effects of DOM on inactivation were different for the two indicators: while inactivation of MS2 was higher in solutions of the influent isolate than in the wetland effluent isolates, *Ent. faecalis* inactivation was higher in solutions of the open-water and cattail isolates compared to the influent and bulrush isolates. In considering the implications of these results for the design of unit process wetlands, we must keep in mind that the DOM in the open water cell is a mixture of whater it is fed with, and the DOM produced and transformed within the cell. Also, this study only evaluated the exogenous inactivation mechanism, whereas the contribution by endogenous inactivation is expected to be greater for some organisms (Chapter 3, Silverman et al., 2015). Nonetheless, several recommendations can be made based on the results. First, there is not compelling evidence that it is beneficial to feed an open-water wetland with effluent from a vegetated cell compared to feeding it directly with secondary wastewater. Second, if a vegetated cell is to be placed before the open-water cell, a cattail wetland appears to be a better choice, given that the bulrush wetland isolate was a poor photosensitizer for *Ent. faecalis* and also had high specific absorbance. The choice of which unit process wetlands to include, and in what sequence, depends on the overall treatment goals. With respect to indicator organisms, it is important to remember that there is a risk of adding more organisms and possibly pathogens from birds and other animals that use the wetlands as habitat. If vegetated wetlands provide habitat for more animals, the operation of open-water wetlands alone may have the best performance with respect to indicator organism and pathogen removal.

CHAPTER 5. Effects of association between photosensitizers and indicator bacteria on exogenous inactivation by simulated sunlight.

Reproduced with permission from Mi T. Nguyen[1] and Kara L. Nelson[2]. Effects of association between photosensitizers and indicator bacteria on exogenous inactivation by simulated sunlight. In preparation for submission to *Applied and Environmental Microbiology.*

[1]Primary author and researcher

[2] Editor and advisor

5.1 Introduction

Exogenous inactivation is one of the key mechanisms contributing to sunlight inactivation of microorganisms in sunlit water bodies. Natural photosensitizers absorb light to form reactive intermediates [e.g., excited triplet state dissolved organic matter ($^3DOM^*$), singlet oxygen ($^1O_2$), hydroxyl radical (•OH)] (Cooper et al., 1989), which can react with components of microorganisms and cause inactivation (Davies-Colley et al., 1999; Jagger, 1985; Mattle et al., 2015; Silverman et al., 2013). Although numerous species may participate, singlet oxygen has been found to play a key role in the exogenous inactivation of MS2 (Kohn and Nelson, 2007; Mattle et al., 2015), and evidence has also been found that it participates in the exogenous inactivation of *Ent. faecalis* (Kadir, 2010). Because $^1O_2$ is short-lived, its concentration is highest at the site of production - natural organic matter (NOM) (Latch and McNeill, 2006). For MS2 coliphage, a surrogate for human enteric viruses, the inactivation rate under simulated sunlight increased with greater association with NOM (Kohn et al., 2007). In photodynamic therapy – which is analogous to exogenous inactivation by sunlight – the association with synthetic photosensitizers was shown to be an essential requirement for inactivation of indicator and pathogenic bacteria (Dahl et al., 1989a; Demidova and Hamblin, 2005). However, knowledge about the effects of the association with NOM on exogenous inactivation of bacteria in sunlit water bodies is still limited.

Previous studies on sunlight inactivation and photodynamic therapy of bacteria showed that gram-negative bacteria are more resistant to inactivation than gram-positive bacteria in the presence of photosensitizers under natural or simulated sunlight (Davies-Colley et al., 1999; Kadir, 2010; Malik et al., 1992; Valduga et al., 1993). The resistance of gram-negative bacteria to photodynamic therapy is due to the existence of a lipopolysaccharide outer membrane, which serves as an effective permeability barrier to potential harmful substances, including photosensitizers (Denyer and Maillard, 2002). In comparison, most gram-positive bacteria lack a barrier comparable to the outer membrane of gram-negative bacteria, and only contain a thick, porous layer of peptidoglycan as the outermost component of the cell wall (Madigan et al., 2010). Thus, the association between synthetic photosensitizers and gram-positive bacterial cells is generally greater than with gram-negative bacterial cells, resulting in more inactivation for gram-positive bacteria in photodynamic therapy (Dahl et al., 1989a; Hamblin et al., 2002). The goal of this study was to determine whether the difference in susceptibility to exogenous inactivation between two types of bacteria is due to lower association with NOM for gram-negative bacteria, or because the outer membrane effectively protects gram-negative bacteria from damage even if photosensitizers are associated with the cell.

This study evaluated the association of one gram-positive and one gram-negative bacterial indicator species with natural and synthetic photosensitizers, and determined the effects of association on sunlight inactivation of the bacteria. Experiments were conducted with *Ent. faecalis* (gram-positive) and *E. coli* (gram-negative) in solutions of Rose Bengal (RB) and DOM isolated from secondary wastewater effluent (EfOM). Rose Bengal, a synthetic anionic photosensitizer, was used as a model for natural DOM. Polymer beads coated with RB (RB-Beads) were used in an attempt to generate singlet oxygen in the absence of bacteria-sensitizer association. A better understanding of the effects of bacterial association with RB and natural DOM on exogenous inactivation provides greater insight into the mechanism, and can be used to

improve estimates of sunlight inactivation of bacteria in different environments, as well as to inform strategies to enhance sunlight-mediated inactivation.

5.2 Materials and Methods

This study consisted of five specific tasks: (1) quantifying the association between photosensitizers and bacterial cells (*Ent. faecalis* and *E. coli*) in the absence and presence of Mg^{2+}; (2) measuring inactivation rates of indicator bacteria in photosensitizer solutions in the absence and presence of Mg^{2+}; (3) synthesizing RB-Beads as an exogenous source of reactive species (i.e., $^1O_2$); (4) measuring inactivation rates of the bacterial indicators in the presence of RB-Beads; and (5) quantifying the association between the indicators and RB-Beads. In task 4, the inactivation rate of MS2 coliphage in the presence of RB-Beads was also measured to provide a comparison for the bacterial indicators.

5.2.1 Chemicals and analytical instruments

All chemicals were from commercial sources and used without further purification: chloromethylated polystyrene: 1% divinylbenzene copolymer beads (Acros Organics), N,N-dimethylformamide (99%, Acros Organics), Rose Bengal sodium salt (90%, Acros Organics), benzene (99%, Fisher Scientific), methanol (99%, Fisher Scientific), ethanol (99%, Acros Organics), ethyl acetate (99%, Acros Organics), methylene chloride (99%, Fisher Scientific), furfuryl alcohol (FFA, 99%, Acros Organics). All aqueous solutions including broth media, phosphate buffered saline (PBS: 4 mM NaH_2PO_4, 16 mM Na_2HPO_4, and 10 mM NaCl; pH adjusted to 7.5), and clear water for inactivation experiments with bacteria (20mM NaH_2PO_4, 10 mM NaCl; pH adjusted to 7.5) were prepared from deionized water.

Singlet oxygen probe compound measurement was performed using a high-performance liquid chromatography (HPLC) system (Gynkotek) with a reverse-phase C18 column (Cosmosil C18-5-MS-II, 100×3 mm Nacalay Tesque, Kyoto, Japan) equipped with a guard column (Nacalay Tesque) and a 2-μm pre-filter (Agilent Technologies). Concentration of total organic carbon (TOC) for whole water samples, standard humic substances and DOM isolates was determined using a Shimadzu V-CPH TOC analyzer (Kyoto, Japan). Electronic absorption spectra were collected with a UV-2600 UV-Vis spectrophotometer (Shimadzu) using quartz-glass cuvettes (Hellma, Germany).

5.2.2 Synthesis of RB-immobilized beads (RB-Beads)

The procedure for synthesizing RB-Beads followed previous studies (Bezman et al., 1978; Schaap et al., 1975). Briefly, a mixture of 60 ml of N,N-dimethylformamide, 1.6 g of RB and 2.0 g chloromethylated polystyrene 1% divinylbenzene copolymer beads was magnetically stirred at 60°C for 20 h. RB was covalently bonded to chloromethylate groups of the white polystyrene beads to form dark red RB-Beads (Schaap et al., 1975). RB-Beads were separated from the solution using membrane filtration. To remove any residue of unattached RB and N,N-dimethylformamide, collected RB-Beads were washed thoroughly with 200-ml portions of solvents in the following order: ethyl acetate, ethanol, ethanol-water (1:1, vol/vol), water, methanol-water (1:1, vol/vol), and methanol. The cleaning procedure for RB-Beads was continued by extracting the collected RB-Beads in a mixture of methylene chloride and methanol (1:1, vol/vol) in a Soxhlet extractor for at least 20 h until no visible color appeared in the

solution. RB-Beads were then dried in a vacuum oven at 60°C for 12 h. The amount of immobilized RB was determined to be 8% by weight (of the total RB-Bead weight) by measuring the difference in weight of the beads before and after the procedure.

5.2.3 Isolation of EfOM

The EfOM used in this study was isolated from nitrified municipal wastewater (effluent of an oxidation ditch at Discovery Bay wastewater treatment plant). A solid-phase extraction (SPE) method was used to isolate the EfOM (Dittmar et al., 2008). Briefly, wetland water samples pre-filtered through 1-μm filters were acidified to pH 2 using concentrated HCl (10 M). Cartridges (Bond Elut PPL, No. 12255002, Agilent Technologies) used in this SPE method were rinsed with 10 mL methanol and 10 mL ultrapure water. Then, two liters of water sample were passed through each cartridge at a flow rate of 30 – 40 mL min^{-1} using a vacuum pump. After the extraction, any remaining salts were removed from cartridges by passing through 10 mL of HCl 0.01 M. The cartridges were dried for 5 min using the air stream of the vacuum. DOM sorbed on the cartridges was eluted with 10 mL methanol. The volume of the extracts was decreased by evaporating the methanol in a water bath at 30°C under a gentle stream of nitrogen. The remaining concentrate was diluted with at least 95% volume of ultrapure water, and freeze dried in at least 48 hours. Powder of the EfOM was stored at room temperature until further use.

5.2.4 Indicators for sunlight inactivation experiments

Bacterial indicators. *Escherichia coli* (NCM 4236) and *Enterococcus faecalis* (ATCC 19433) were stored as glycerol stocks at -80°C. Broth cultures were prepared fresh daily by inoculating the glycerol stocks in Tryptic Soy broth (BD) with addition of Kanamycin (0.025 g L^{-1}) for *E. coli* and Brain Heart Infusion broth (BD) for *Ent. faecalis*. Broth cultures were then incubated at 37°C for 24 h for the bacteria to reach stationary phase. Cells were pelleted by centrifuging at 6,800×g for 3 min, then washed and resuspended with PBS. Concentrations of bacteria were determined by plating samples from inactivation experiments on Modified Luria Bertani (LB) agar [10 g L^{-1} Tryptone (BD), 1 g L^{-1} Yeast extract (BD), 8 g L^{-1} NaCl (Fisher Scientific), 0.0055 M dextrose (EMD Chemicals), 0.002 M $CaCl_2$ (Fisher Scientific), 15 g L^{-1} Agar (BD)] with addition of 0.025 g L^{-1} Kanamycin for *E. coli* and mEnterococcus agar (BD) for *Ent. faecalis.* Modified LB agar plates and mEnterococcus agar plates were incubated at 37 °C for 24 h and 48 h, respectively, after which colony forming units (CFU) were counted.

Virus indicator. MS2 (ATCC 15597-B1) was propagated by broth enrichment using Tryptic Soy broth, *E. coli* F_{amp} (ATCC 700891) host and Ampicillin-Streptomycin antibiotics (0.015 g L^{-1}, each). To purify crude virus stocks, MS2 stock was first chloroform extracted to remove cell debris. Chloroform was added to the incubated broth at a 1:3 (vol/vol) concentration, the solution was vortexed for 2 min, then centrifuged at 2000×g for 10 min. To remove broth constituents, the supernatant was polyethylene glycol (PEG) precipitated overnight at 4°C (9% PEG, 0.3 M NaCl), centrifuged at 20,000×g for 15 min to produce virus pellets that were resuspended in PBS, chloroform extracted as above and filtered through a 0.22 μm filter. Virus stocks were stored at -80°C. MS2 were enumerated using the double agar layer (DAL) plaque assay with 100 μL sample inocula, modified LB top (0.75% agar, wt/vol, BD) and bottom (1.5% agar, wt/vol, BD) agars, and Ampicillin-Streptomycin antibiotics. DAL plates were incubated at 37 °C for 18–24 h, after which plaque forming units (PFU) were counted.

5.2.5 Irradiation experiments

Experiments were conducted using a 1000W collimated beam Oriel Solar Simulator (Spectra Physics, serial no. 91194) equipped with a Xe lamp and a UVB-blocking filter (Spectra Physics, serial no. 81050) to remove the UVB portion of the spectrum. Bulb irradiance was measured at the beginning of each experiment using a spectroradiometer (EPP2000C-SR-100 with CR2 cosine receptor, Stellarnet).

For experiments with photosensitizer solutions, reactors were 150-mL glass beakers painted black on the outside to minimize the effect of light reflection. Reactors were filled with 100 mL photosensitizer solutions [clear water with addition of RB (final concentration of 2.5 mgC L^{-1}) or EfOM (final concentration of 25 mgC L^{-1})], divalent cation [Mg^{2+} (0 or 20 mM)], and bacterial stocks (*Ent. faecalis* or *E. coli*) to reach final concentration of ~10^7 CFU mL^{-1}. To measure the steady-state concentration of singlet oxygen in the bulk phase, furfuryl alcohol (FFA, 50μM) was added instead of bacterial stocks. Reactors were well mixed, with temperature maintained at 20°C, and exposed to simulated sunlight for 8 hours. Subsamples were collected every hour and immediately analyzed. Dark controls were maintained in the same way, but were covered with aluminum foil. Experiments were conducted in duplicate from same bacterial seed culture.

For experiments with RB-Beads, quartz tubes were used for the mixing of RB-Beads in clear water because the polymer beads are highly hydrophobic and were difficult to wet and suspend with aqueous media in glass beakers. Quartz tubes (10.5 mm inner diameter, 12.75 mm outer diameter, 100 mm length; Technical Glass Products, Inc.; Painesville Township, OH) were filled with 8.4 mL of clear water, inoculated with bacterial or viral stocks to reach concentrations of ~10^7 CFU mL^{-1} for *E. coli* and *Ent. faecalis* or ~6×10^7 PFU mL^{-1} for MS2, with addition of various amounts of RB-Beads or uncoated beads (Beads) and closed with polyethylene chloride caps (Polyethylene Press snap cap; Fisher Scientific) with minimal headspace. Experiments with bacteria were conducted in duplicate using the same bacterial seed cultures. MS2 experiments were conducted in triplicate using the same MS2 stock. The amount of RB-Beads was 0, 2.3, 5.6, or 11.3 mg per tube, which is approximately equal to 0, 20, 50, and 100 μM of immobilized RB, respectively. The amount of uncoated beads in control samples was 0, 2.3 or 11.3 mg per tube. Quartz tubes that allowed light transmission at all relevant wavelengths were rotated vertically under UVB-blocked simulated sunlight using a tube rotator (Thermo Scientific) to ensure that RB-Beads were well-mixed in the solutions. To measure the concentration of singlet oxygen, FFA (50μM) was added instead of bacterial stocks. During all experiments, duplicate samples were collected at each time point: two tubes were collected sacrificially, and sub-samples from the collected tubes analyzed for concentrations of indicator organisms or FFA. RB-Beads were removed from samples using 1-μm glass fiber filters before measuring for [FFA] by HPLC, but were not removed before plating to enumerate concentrations of the indicators. Dark controls were maintained under the same conditions as light samples, but wrapped in aluminum foil.

The possibility that RB detached from RB-Beads was evaluated by quantifying dissolved RB using UV-VIS spectrophotometer (detection limit for dissolved RB: 10^{-10} M). Quartz tubes containing clear water with 0, 2.3, 5.6, or 11.3 mg of RB-Beads per tube were rotated for 8 hours in darkness to prevent possible dye photobleaching. RB-Beads were removed by filtration

through 0.8-μm cellulose acetate filters (Thermo Scientific). The absorbance of filtered water samples was measured at 550 nm.

5.2.6 Measuring bulk-phase steady-state concentration of singlet oxygen

The steady-state concentration of singlet oxygen in the bulk phase, $[^1O_2]_{ss,bulk}$, was determined by measuring the concentration of the probe compound FFA (50μM) (6h irradiation) using HPLC (Haag et al., 1984). The pseudo-first order depletion rate constant of the probe compound, k_{FFA}, was determined by linear regression of $\ln([FFA]/[FFA]_0)$. $[^1O_2]_{ss,bulk}$ values were calculated by dividing the observed rates of FFA depletion by the second-order reaction rate of FFA with $^1O_2$ ($k = 1.2\times10^8$ M^{-1} s^{-1}) (Haag et al., 1984).

5.2.7 Measuring association between the indicator organisms and RB-Beads

Membrane filtration was used to measure the association between the indicators and RB-Beads. Quartz tubes with suspensions of clear water, the indicator organism (*Ent. faecalis, E. coli,* or MS2), and RB-Beads were prepared similarly to sunlight inactivation experiments. The indicator organism (from stock solution) was added to clear water with the addition of RB-Beads (0 or 11.3 mg per tube) to reach a final concentration of ~10^7 CFU mL^{-1} for *Ent. faecalis* and *E. coli* or ~6×10^7 PFU mL^{-1} for MS2. Quartz tubes were rotated vertically using a tube rotator (Thermo Scientific) in the dark. Subsamples were taken at the beginning of the experiments and after 4 h to measure the number of the indicators that was attached to RB-Beads. 1-mL subsamples were filtered through 40-μm Nylon-Net Steriflip Vacuum Filter (EMD Milipore). Because the membrane pore size is bigger than the sizes of the indicators (i.e., ~1 μm for bacterial cells, and ~0.03 μm for MS2 particles) but smaller than RB-Beads (~74 – 149 μm), the indicators found on the membrane were considered to be associated with the membrane and RB-Beads. To determine the number of each indicator not associated with beads, the filtrate was assayed for the concentration of MS2 using DAL method, or plated on modified LB agar or mEnterococcus agar to determine concentration of *Ent. faecalis* and *E. coli*, respectively. To determine the number of the indicators associated with RB-Beads, the membranes were eluted by adding 1 mL of 3% Beef Extract (pH 9; 30 g L^{-1} Beef Extract, 30 mL L^{-1} Tween 80, 0.3 M NaCl) to a tube containing the membrane and swirling for 6 min. The eluent from the filters was assayed for the concentration of each indicator as mentioned above for the filtrate. After elution, the filters were also plated face down on appropriate media. Plates were incubated at 37 ºC for 18–48 h and enumerated as CFUs or PFUs. The number of the indicators associated with RB-Beads was calculated by adding counts from the filter eluent and membrane plates.

5.2.8 Association of bacterial cells to photosensitizers

The adsorption of photosensitizers onto bacterial cells was determined using a method described in detail in several previous studies (Fein et al., 1999; Frost et al., 2003; Maurice et al., 2004). Bacterial seeds were added to 20 mL of photosensitizer solutions [RB (2.5 mgC L^{-1}) or EfOM (25 mgC L^{-1}), and divalent cation [Mg^{2+} (0 or 20 mM)] to reach final concentration of ~10^{10} CFU mL^{-1}. Controls were prepared using clear water without the addition of photosensitizers. Suspensions were gently stirred and maintained at room temperature in the dark for 4 h for adsorption to reach steady-state (Maurice et al., 2004). Subsamples were taken before adding bacteria and after 4 h. Bacterial cells were removed from sample solutions using syringe filtration with 0.8-μm cellulose acetate filters (Thermo Scientific) for RB samples and 0.45-μm

nylon filters (Fisher Scientific) for EfOM samples. The choice of filters was made based on the selectivity of filter materials to photosensitizer solutions. Absorption spectra of filtered and unfiltered solutions of sensitizers showed that RB and the EfOM did not sorb onto cellulose acetate and nylon filters, respectively (data not shown). To avoid any possible effects caused by the difference in pore size of two types of filters, the control samples prepared in photosensitizer-free water were filtered through 0.8-µm cellulose acetate filters in experiments with RB, and through 0.45-µm nylon filters in experiments with the EfOM. The filtrates were measured at 550 nm for RB samples and 450 nm for EfOM samples using a UV-VIS spectrophotometer (Fein et al., 1999). To determine the exact photosensitizer concentration in solution, light-absorption calibration curves were also generated for each photosensitizer (0 – 3 mgC L^{-1} for RB solutions, and 0 – 30 mgC L^{-1} for wetland influent DOM). The mass of adsorbed photosensitizer onto *Ent. faecalis* and *E. coli* cells was estimated by calculating the difference in mass of RB or EfOM in the filtrate at t = 0 and 4 h and normalized by the number of bacterial cells in the solutions.

5.2.9 Data analysis

Inactivation rates of *E. faecalis, E. coli* and MS2 were determined from the slope of linear regression of $\ln(C_t/C_0)$ versus time (k_{obs}, h^{-1}). Statistical tests including linear regressions, t-tests, and Pearson correlation tests were performed using GraphPad Prism 6.0.1 (GraphPad Software, La Jolla, CA).

5.3 Results and Discussion

5.3.1 Association between dissolved photosensitizers and bacterial cells

The mass of adsorbed RB and EfOM onto bacterial cells was higher for *Ent. faecalis* than *E. coli* (Figure 5.1), although the difference was only statistically significant for the RB solutions (t-test, $p < 0.05$). Photosensitizers can associate with bacterial cells by binding on the surface of the cell or penetrating and accumulating inside of cell membranes (Dahl et al., 1989b). Thus, the difference in association with photosensitizers between the two bacteria is likely due to their different membrane structures. *Ent. faecalis* cells have a porous peptidoglycan layer as the outside layer, which can uptake macromolecules with molecular weight up to 57 kDa (Lambert, 2002). *E. coli* cells have an additional outer membrane layer as an effective barrier, that only allows the uptake of small molecules (less than 0.7 kDa) through porin channels (Denyer and Maillard, 2002). More accessible binding sites for photosensitizers either on the surface and in the *Ent. faecalis* cell membrane resulted in greater association of RB and EfOM onto *Ent. faecalis* cells as compared to *E. coli* cells. The mass of adsorbed RB on both bacteria was similar to the mass of adsorbed EfOM even though the concentration of dissolved RB was ten times lower than the EfOM ([RB] = 2.5 mgC L^{-1} and [DOC] = 25 mgC L^{-1}), indicating that the association of RB to the bacterial cells was greater than the EfOM. RB molecules with their lower molecular weight [1 kDa as compared to up to 100 kDa for the EfOM (Leenheer and Croué, 2003)] and high hydrophobicity enables RB to overcome the outer cell wall lipopolysaccharide barrier and accumulate in the outer membrane of gram-negative bacteria (Dahl et al., 1989b). The mass of adsorbed EfOM to *Ent. faecalis* cells in this study was similar to the mass of adsorbed fulvic acids to *Bacillus subtilis* cells (also a gram-positive bacterium) in a previous study [0.37 mgC/g *Ent. feacalis* in this study as compared to 0.55 mgC/g *B. subtilis* in

Maurice et al. (Maurice et al., 2004), assuming 1 g wet weight of *Ent. faecalis* cells is similar to *E. coli* and approximates 10^{12} CFU (Pilarek et al., 2011)].

In the presence of the divalent cation Mg^{2+}, there was an increase in adsorption of both photosensitizers onto *Ent. faecalis* cells (Figure 5.1), although the increase is statistically significant only for RB solutions (t-test, $p < 0.05$). For *E. coli*, only the adsorption of RB was observed to be enhanced in the presence of Mg^{2+}. The *Ent. faecalis* result agrees with a previous study, which showed that the addition of Ca^{2+} and Mg^{2+} significantly increased the uptake of RB onto *Ent. faecalis* cells (George et al., 2009). Although the membrane structure of *Ent. faecalis* and *E. coli* are different, both bacterial cells have net negative charge at neutral pH due to the presence of teichoic acids and lipopolysaccharide in their cell walls, respectively (Lambert, 2002; Madigan et al., 2010). Given that both photosensitizers (RB and the EfOM) also have net negative charge at neutral pH, the presence of Mg^{2+} can neutralize the net negative charge of the bacterial cell walls and reduce the repulsion of the photosensitizers (George et al., 2009). Alternatively, Mg^{2+} can complex the negatively charged functional groups on the surface of the photosensitizers and the bacterial cell walls (Hancock, 1997; Rose et al., 1997). These effects of Mg^{2+} can explain the enhancement of the association between *Ent. faecalis* and both photosensitizers, as well as for *E. coli* and RB. However, there was no effect of Mg^{2+} observed in the association between the EfOM and the *E. coli* cells. One hypothesis is that the change in structure of EfOM molecules by charge neutralization in the presence of Mg^{2+} (Clark and Lucas, 1998) may affect its association with *E. coli* cells but not *Ent. faecalis* cells.

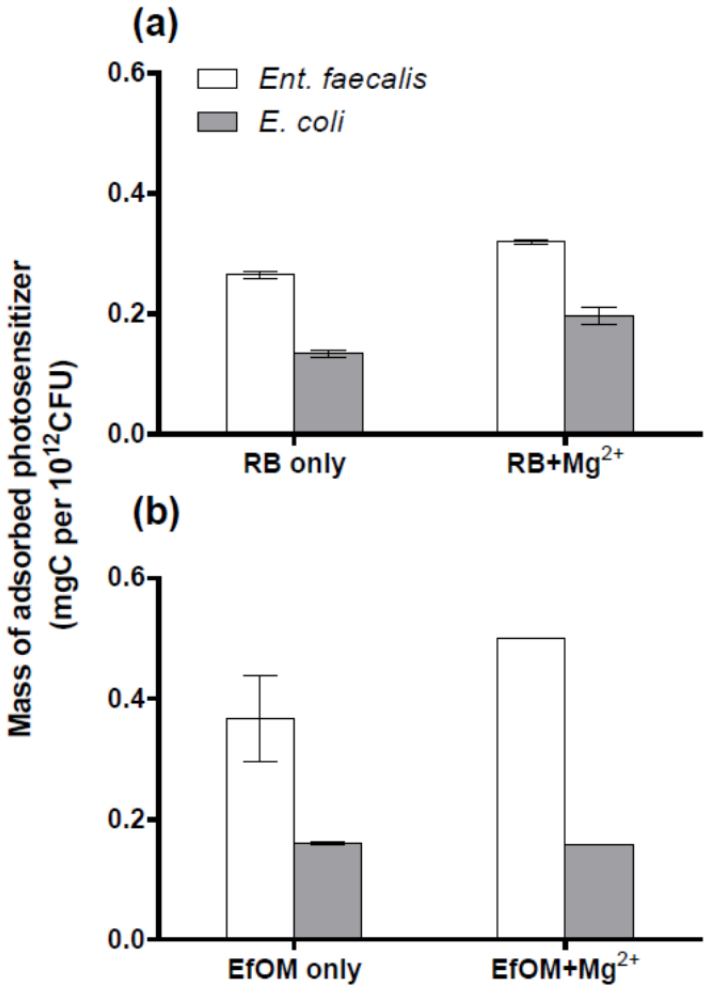

Figure 5.1. Normalized mass of adsorbed photosensitizer onto *Ent. faecalis* (7×10^9 CFU mL^{-1}) and *E. coli* (10^{10} CFU mL^{-1}) in the absence and presence of Mg^{2+} ($[Mg^{2+}]$ = 20 mM). (a) RB solutions ([RB] = 2.5 mgC L^{-1}) and (b) EfOM ([EfOM] = 25 mgC L^{-1}). Error bars indicate ± one standard error for duplicate samples. Error bars of the DOM+Mg^{2+} samples are too small to be seen.

5.3.2 Effect of association between dissolved photosensitizers and bacterial cells on sunlight inactivation

The observed inactivation rates (k_{obs}) of *Ent. faecalis* were higher in the RB and EfOM solutions as compared to clear water (t-test, $p < 0.05$), whereas no significant difference was observed between the inactivation rates of *E. coli* in photosensitizer solutions and in clear water (Figure 5.2), indicating that *Ent. faecalis* is susceptible and *E. coli* is resistant to exogenous inactivation. There was no inactivation observed for either bacterial indicator in the dark (data not shown). These results agree with previous studies on sunlight inactivation of bacteria in water collected from waste stabilization ponds (Davies-Colley et al., 1999; Kadir and Nelson, 2014). The difference in resistance to exogenous inactivation of *E. coli* as compared to *Ent. faecalis* can be explained by the existence of the outer membrane layer, which effectively

protects vital components of the *E. coli* cell from exogenous photosensitizers. In addition, the periplasmic space between the outer membrane and the inner membrane in gram-negative bacteria contains water and possibly other singlet oxygen quenchers (Dahl et al., 1987).

Similar to the adsorption experiments, the concentration of RB used in the inactivation experiments was lower than the EfOM ([RB] = 5×10^{-3} mgC L^{-1} and [EfOM] = 5 mgC L^{-1}). However, the two photosensitizer solutions produced similar steady-state concentrations of singlet oxygen in the bulk phase ($[^1O_2]_{ss,bulk} = 3.10\times10^{-14} \pm 0.06\times10^{-14}$ M in RB solution and $3.5\times10^{-14} \pm 2.4\times10^{-15}$ M in the EfOM solution). The k_{obs} values of *Ent. faecalis* in RB solutions, however, were higher than in EfOM solutions (Figure 5.2a). The result can be explained by the facts that RB was adsorbed more onto *Ent. faecalis* cells and has higher singlet oxygen quantum yield as compared to the EfOM [$\phi_{^1O_2}$(RB) = 0.76 (Lamberts et al., 1984) and $\phi_{^1O_2}$(EfOM) = 0.02 (Chapter 4, Wetland influent DOM)].

The addition of the divalent cation Mg^{2+} appeared to increase the inactivation rates of *Ent. faecalis* and *E. coli* in RB solution, presumably due to greater association of RB with the bacterial cells in the presence of Mg^{2+} (Figure 5.1). However, there was no detectable increase in inactivation of *Ent. faecalis* in EfOM solution in the presence of Mg^{2+}, even though Mg^{2+} increased the adsorption of EfOM onto the bacterial cells. Interestingly, *E. coli* inactivation rate was slightly enhanced in EfOM solution with Mg^{2+} when there was no difference observed for adsorption with EfOM in the presence and absence of Mg^{2+}. A possible explanation for the case of *Ent. faecalis* is that its inactivation rates reach a plateau at certain concentration of EfOM, at which higher concentrations of EfOM do not increase the k_{obs} values. Kohn et al. observed that the values of k_{obs} for MS2 leveled out at around NOM concentration of ~5 mg L^{-1} (Fluka humic acid and Suwannee River humic acid) (Kohn et al., 2007). Results from our previous study also suggest that the increase of EfOM concentration above 5 mgC L^{-1} did not significantly enhance *Ent. faecalis* inactivation rates (Figure 4.10a, Wetland influent DOM samples). For *E. coli*, the change of EfOM molecular structure (Clark and Lucas, 1998) and possibly other photochemical properties in the presence of Mg^{2+} might account for the enhancement of *E. coli* inactivation. More research is needed on the effect of divalent cations on EfOM and the exogenous inactivation of bacteria in EfOM solution.

Except in the EfOM solution with addition of Mg^{2+}, exogenous inactivation of *Ent. faecalis* generally increased with greater adsorption of photosensitizers onto the bacterial cells, suggesting that association with photosensitizers is one of important factors controlling exogenous inactivation of *Ent. faecalis*. This observation agrees with previous studies on photodynamic therapy, showing that the association with photosensitizers of bacterial cells is a prerequisite condition for inactivation of the bacteria (Ehrenberg et al., 1985; Nitzan et al., 1994). The exogenous inactivation of bacteria depends on whether $^1O_2$ produced by exogenous photosensitizers can travel to and interact with vital components of bacterial cells. Given that the diffusion length of $^1O_2$ in water is only ~100 nm (Ogilby, 2010), the dependence of *Ent. faecalis* inactivation to associated photosensitizers observed in this study suggested that the association between photosensitizers and bacterial cells is a key factor contributing to exogenous inactivation of the bacteria. In contrast, due to the resistance to exogenous inactivation of *E. coli*, there was no obvious correlation between the adsorption with photosensitizers onto *E. coli* cells and its inactivation rates. To further investigate the role of association with photosensitizers on

exogenous inactivation of the bacterial indicators, experiments with RB immobilized on polymer beads (RB-Beads) were conducted and described in details in below sections.

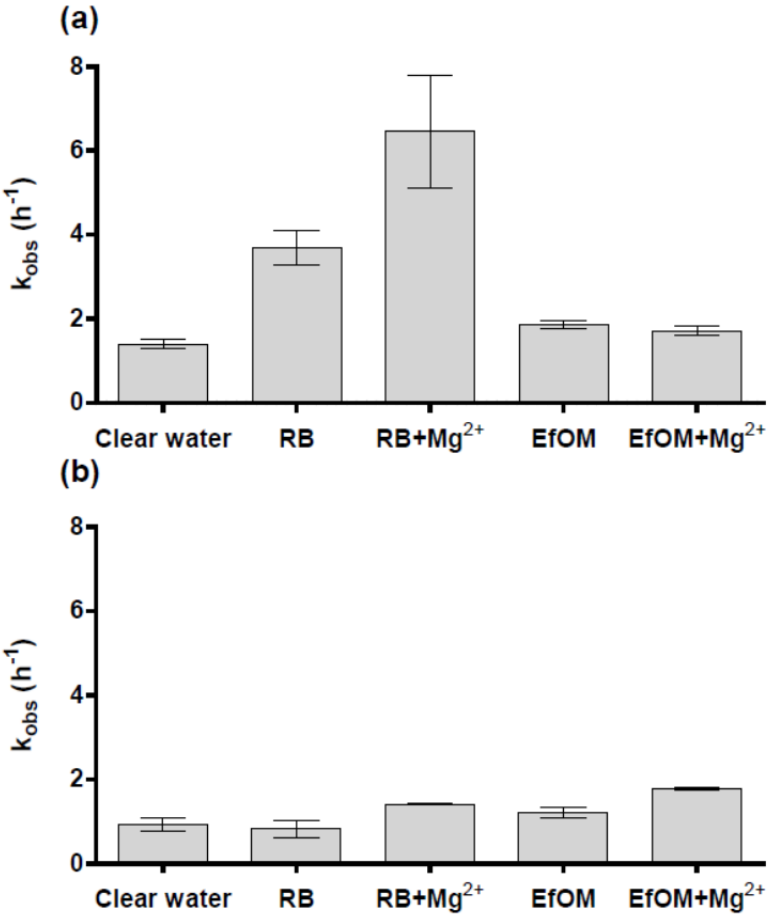

Figure 5.2. Observed inactivation rates of (a) *Ent. faecalis* and (b) *E. coli* in RB solutions ([RB] = 5×10^{-3} mgC L^{-1}) and the EfOM solutions ([EfOM] = 5 mgC L^{-1}) with or without the addition of Mg^{2+} ([Mg^{2+}] = 20 mM). Error bar indicate ± one standard error of duplicate samples.

5.3.3 Inactivation of indicator microorganisms in clear water with addition of RB-Beads

Experiments were conducted with RB-Beads and *Ent. faecalis*, *E. coli* or MS2 in clear water under UVB-blocked simulated sunlight to determine the role of photosensitizer adsorption on exogenous inactivation of the indicator microorganisms. Measurements for trace amount of RB in clear water contained RB-Beads after 8 h showed no detection of dissolved RB (data not shown), suggesting that it was unlikely that RB detached from the RB-Beads. Thus, the immobilized RB was responsible for the production of $^1O_2$ and any inactivation observed in experiments with RB-Beads. The steady-state concentration of $^1O_2$ in the bulk phase increased with the increase in the mass of RB-Beads, indicating that immobilized RB was effective at producing $^1O_2$ under UVB-blocked simulated sunlight (Figure 5.3a). Experiments with MS2 showed that the addition of RB-Beads increased the inactivation rates of MS2 in clear water (Figure 5.3b). In contrast, the inactivation rates of *Ent. faecalis* and *E. coli* did not increase in the

presence of RB-Beads, suggesting that immobilized RB did not cause exogenous inactivation of the bacteria (Figure 5.3c and d). Samples with uncoated beads under simulated sunlight as well as RB-Beads and uncoated beads in the dark did not produce $^1O_2$ or increase inactivation of any of the three indicator organisms.

The finding that RB-beads did not inactivate of *Ent. faecalis* and *E. coli* is different than a previous study, which found that RB-Beads significantly enhanced inactivation rates of *E. coli* under white light emitted from 15-W fluorescence bulbs (Bezman et al., 1978). The observed discrepancy in *E. coli* inactivation could be due to differences in the experimental setups. In Bezman et al.'s study, the suspensions of RB-Beads, *E. coli* and clear water were supersaturated with pure oxygen, whereas there was no addition of oxygen in this study. Higher concentration of dissolved oxygen in the suspension could increase the production of singlet oxygen produced by immobilized RB and enhance inactivation of *E. coli*. The difference in light source could also account for the discrepancy in *E. coli* inactivation: k_{obs} in clear water without addition of beads in Bezman et al.'s study was 1 h^{-1} (Bezman et al., 1978), five times higher than this study (0.2 h^{-1}). In addition, Bezman et al. had higher concentrations of RB-Beads (13 mg mL^{-1}) and bacteria (10^9 CFU mL^{-1}) than this study (1.3 mg mL^{-1} for RB-Beads and 10^7 CFU mL^{-1}), which could increase the possibility for interaction between RB-Beads and bacterial cells, leading to the enhancement in inactivation of *E. coli*.

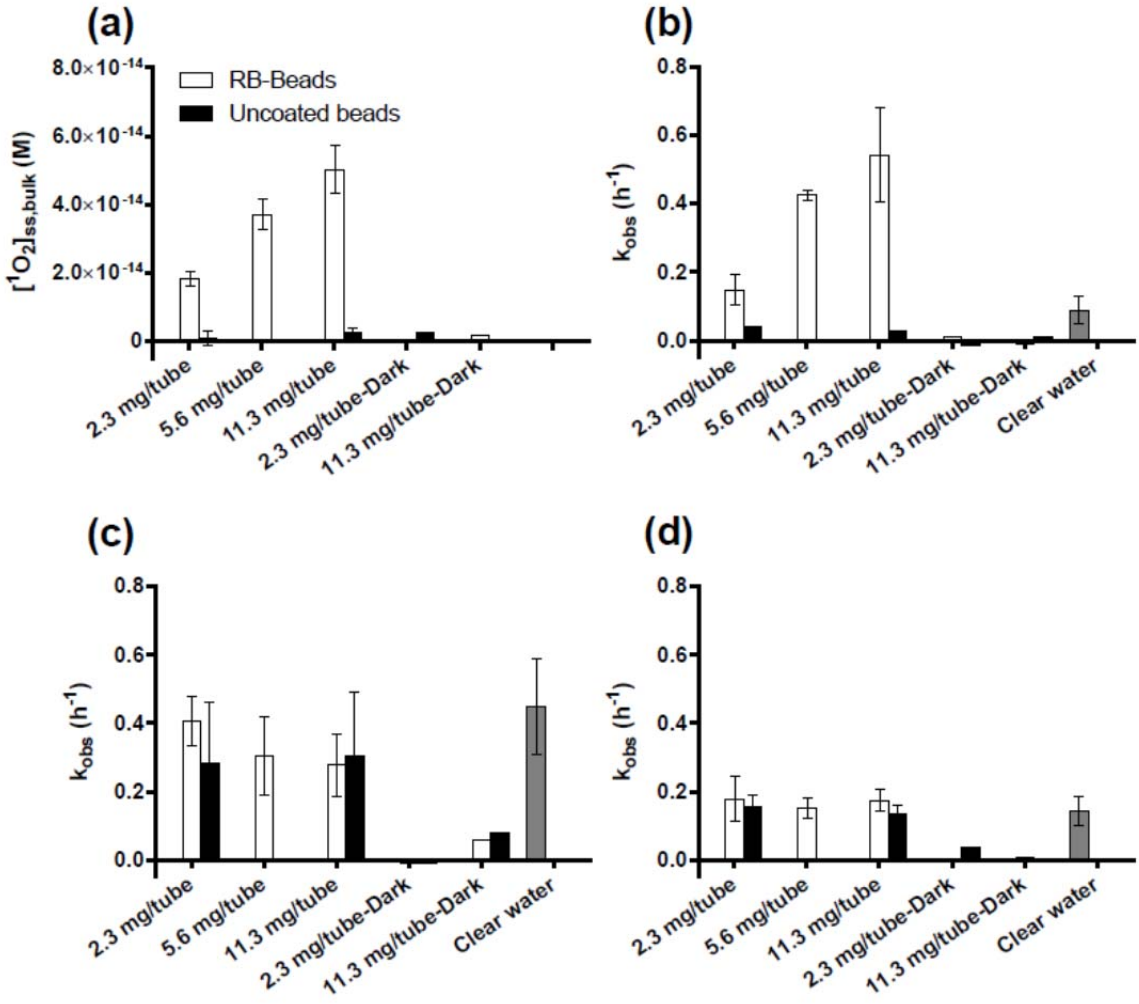

Figure 5.3. (a) Steady-state concentration of singlet oxygen produced in clear water with addition of RB-Beads or uncoated beads under UVB-blocked simulated sunlight or dark condition. Inactivation rates of (b) MS2, (c) *Ent. faecalis* and (d) *E. coli* in clear water with addition of RB-Beads or uncoated beads under UVB-blocked simulated sunlight or dark condition. Amounts of RB-Beads added in each tube 2.3, 5.6, and 11.3 mg are approximately equal to 20 µM, 50 µM, and 100 µM of immobilized RB, respectively. Error bars indicate ± one standard error of replicates. No samples were analyzed for 5.6 mg/tube of uncoated beads.

Effects of exogenous singlet oxygen and association with RB-Beads on inactivation of the indicators

Results from experiments measuring the association between the indicators and RB-Beads indicate that only a small percentage of the organisms were associated with the RB-Beads and membrane filter (3% for *Ent. faecalis* and *E. coli*, 5% for MS2, Figure 5.4). The number of the indicators associated with filters and RB-Beads was slightly higher than with filters only, but the difference was not significant for all three indicators. If only the MS2 associated with RB-Beads was inactivated, we would only have seen 5% inactivation instead of 96% inactivation as

observed in the experiment with 11.3 mg RB-Beads (Figure 5.3b). Thus, any inactivation of the indicators observed in the RB-Bead solutions (Figure 5.3b) was mainly due to the effect of $^1O_2$ produced in the bulk-phase solution. This is the first study to provide direct evidence that $^1O_2$ produced in the bulk solution, rather than by sensitizers attached to the virus, can cause inactivation of MS2. The apparent second-order rate constant of MS2 with $^1O_2$ produced by RB-Beads in the bulk phase (k_2) is $9.5\times10^{12} \pm 2.2\times10^{12}$ M^{-1} h^{-1}, which is similar to the value measured in water from an open-water wetland, but higher than most k_2 values in environmental waters (Silverman et al., 2015). The value of k_2 of MS2 measured from these RB-Beads experiments was even higher than in RB solution [3.4×10^{12} M^{-1} h^{-1}(Kohn and Nelson, 2007) and 1.26×10^{12} $M^{-1}h^{-1}$ (Mattle et al., 2015)]. Such high value of k_2 measured in RB-Bead solution as compared to in dissolved RB solution could be because FFA as a hydrophilic chemical is not a good probe to measure concentration of $^1O_2$ produced by amphiphilic macromolecular species like RB-Beads (Latch and McNeill, 2006). The value of $^1O_2$ concentration in the bulk phase measured using FFA in the RB-Bead solution could be much lower than the actual $^1O_2$ concentration that MS2 particles exposed to, leading to the high value of k_2.

To understand the *Ent. faecalis* and *E. coli* results, we can compare the inactivation observed in the RB solution (5×10^{-3} mgC L^{-1}) and the RB-bead solution (5.6 mg of RB-Beads/tube). These two solutions produced similar $[^1O_2]_{ss,bulk}$ values, but increased inactivation of *Ent. faecalis* was only observed in RB solution; k_{obs} = 3.7 h^{-1} in RB solution, 0.3 h^{-1} in RB-Bead solution, and 0.4 h^{-1} in clear water. This observation agrees with results from previous studies showing that association with photosensitizers is required for photodynamic inactivation of both gram positive and negative bacteria (Dahl et al., 1989a; Demidova and Hamblin, 2005; Hamblin et al., 2002; Nitzan et al., 1992).

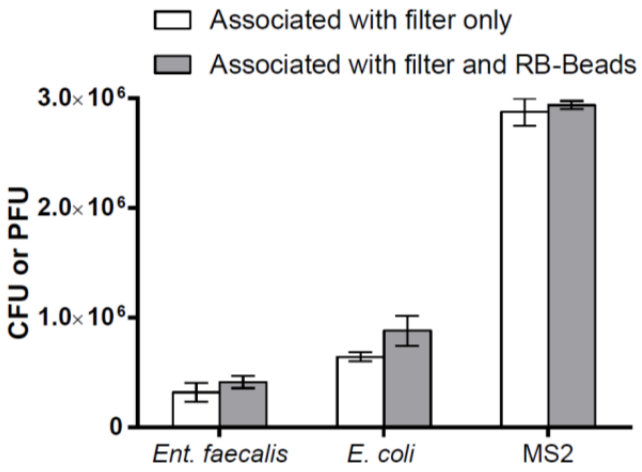

Figure 5.4. Number of microorganisms associated with membrane filter and RB-Beads (11.3 mg per tube) in clear water. The total average number of *Ent. faecalis, E. coli*, and MS2 in clear water is 1×10^7 CFU, 3×10^7 CFU, and 6×10^7 PFU, respectively. Error bars indicate ± one standard error of duplicate samples.

5.3.4 Implication for exogenous inactivation of bacteria

Using RB as a model for natural photosensitizers, this study showed that association with photosensitizers is the one of the requirements for exogenous inactivation of bacterial indicators. Singlet oxygen formed by photosensitizer molecules associated with bacterial cell walls caused exogenous inactivation of *Ent. faecalis*, whereas $^1O_2$ produced in bulk solution did not cause exogenous inactivation. This finding helps to explain the varied effectiveness of different natural photosensitizers to cause sunlight inactivation of *Ent. faecalis*. *E. coli*, on the other hand, was found to be generally resistant to exogenous inactivation even when the photosensitizers were adsorbed to the cells.

CHAPTER 6. Conclusions

6.1 Summary

The ability of an open-water wetland cell to promote sunlight inactivation of fecal indicator bacteria from wastewater effluent was evaluated. Monitoring a pilot-scale system over one year showed that sunlight inactivation was the key process contributing to inactivation of *E. coli* and enterococci. To gain a better understanding of sunlight inactivation mechanisms, laboratory experiments were conducted using water from the open-water wetland and lab-cultured bacteria under simulated sunlight. Results from laboratory experiments suggested that endogenous mechanisms were the main contributor to the inactivation of *E. coli*, and exogenous mechanisms contributed slightly more than endogenous mechanisms to the inactivation of the tested *Enterococcus* spp. Lab-cultured bacteria were more susceptible to sunlight inactivation than indigenous wastewater bacteria in DOM-free water under simulated sunlight. To predict sunlight inactivation of the indicators in open-water wetlands and other sunlit water bodies, a model was developed to predict endogenous and exogenous inactivation rates. The model was evaluated using results from laboratory experiments and monitoring data from the pilot-scale open-water wetland. The exogenous inactivation mechanism was further studied using DOM isolated from different cells in the pilot-scale unit process wetlands. A positive correlation was observed between the steady-state concentration of singlet oxygen produced in the bulk phase of the DOM solutions and the MS2 exogenous inactivation rate. The inactivation of *Ent. faecalis* was strongly dependent on the degree of association between *Ent. faecalis* and the DOM isolates. The association between photosensitizers (Rose Bengal and EfOM) and bacterial cells was also determined to be a prerequisite requirement for the exogenous inactivation of *Ent. faecalis*.

6.2 Sunlight inactivation of indicators in open-water wetlands

In Chapter 2, a photoaction spectrum (PAS) model for predicting endogenous inactivation of MS2 bacteriophage was evaluated using results from experiments with the bacteriophage in photosensitizer-free water under simulated and natural sunlight. There was generally good agreement between observed and modeled MS2 inactivation using the PAS model under natural sunlight and at different depths in a column of strongly humic-colored wetland water under simulated sunlight. Comparison between observed and modeled data suggested that the PAS model could be used to predict changes in inactivation rates due to diurnal and seasonal changes in natural sunlight irradiance, and spectrally-selective sunlight attenuation in the water column. However, a major source of uncertainty in the predictions was the ability to accurately measure or model the comparatively weak and highly variable solar irradiance between 280 and 300 nm – a range to which the inactivation rate is very sensitive. The ability to use total UVB as a simplified model parameter was also tested with these experimental results. The total UVB model was shown to have the potential to be used for estimating endogenous inactivation of organisms for which PAS does not exist, although this approach will be less accurate for light sources whose UVB spectrum differs substantially from the light source used to develop the UVB model.

To determine the ability of open-water unit process wetlands to remove fecal indicator bacteria from wastewater effluent, a pilot-scale open-water wetland was monitored for one year and found to be effective in enhancing sunlight inactivation of fecal indicator bacteria (Chapter 3). The removal of *E. coli* and enterococci in the open-water wetland receiving non-disinfected secondary municipal wastewater reached 3 logs and 2 logs in summer time, respectively.

Pigmented enterococci were found to be significantly more resistant to sunlight inactivation than non-pigmented enterococci. A descriptive model, which accounted for endogenous and exogenous sunlight inactivation mechanisms and dark processes, was developed to predict the inactivation of *E. coli* and pigmented and non-pigmented enterococci. Endogenous inactivation rates were predicted using the total UV model. Exogenous inactivation was only significant for enterococci, and was modeled as a function of steady-state singlet oxygen concentration in the bulk phase. The rate constants were determined from lab experiments and an empirical correction factor was used to account for differences between lab and field conditions. The model was used to predict removal rate constants for the indicators in the pilot-scale wetland. Considering the variability of the monitoring data, there was general agreement between the modeled values and those determined from field measurements. Using the model, open-water wetlands at 40° latitude with practical sizes were predicted to achieve 3-log (99.9 %) removal of *E. coli* and non-pigmented enterococci throughout the year (5.5 ha and 7.0 ha per million gallons of wastewater effluent per day, respectively). Differences in sunlight inactivation rates observed between pigmented and non-pigmented enterococci, as well as between lab-cultured and indigenous wastewater bacteria, highlighted the challenges of using fecal indicator bacteria as model organisms for actual pathogens in natural sunlit environments.

6.3 Effects of photosensitizers on exogenous inactivation

In Chapter 4, the role of DOM as a natural photosensitizer was investigated to provide insight into the exogenous inactivation mechanism. Solid-phase extraction (SPE) resulted in 46.8% to 58.8% recovery of DOM from the influent (nitrified wastewater) and effluent of open-water, cattail, and bulrush wetland cells. Characteristics of wetland DOM isolate solutions and wetland waters, including spectroscopic properties, reactive intermediates formation, and association to bacterial indicator cells were quantified in comparison with two standard DOMs (SRFA and PLFA). Spectroscopic data indicated that vegetated wetland DOM had higher aromaticity and molecular size than DOM from the influent, whereas DOM from the open-water wetland had lower aromaticity and molecular size than the influent DOM. Cattail and open-water DOM isolates associated to the greatest degree with *Ent. faecalis* cells, followed by the influent, bulrush, and two standard DOM isolates. The role of wetland DOM isolates and standard DOM isolates in sunlight inactivation rates of MS2 and *Ent. faecalis* was evaluated based on the characteristics of the DOM isolates and results from sunlight experiments under UVB-blocked simulated sunlight. There was a positive correlation between MS2 inactivation rates and DOM concentrations, as well as $[^1O_2]_{ss,bulk}$, indicating that the DOM isolates enhanced MS2 inactivation. The inactivation rates of MS2 increased the most (compared to sensitizer-free water) in solutions of the influent DOM isolate and PLFA, followed by the open-water isolate, bulrush isolate, cattail wetland effluent isolate, and SRFA. Results of inactivation experiments with *Ent. faecalis* showed that while photosensitizing was dominant in the wetland DOM isolates and PLFA solutions, light screening was significant in SRFA solution. The open-water and cattail DOM isolates were more effective at increasing exogenous inactivation of *Ent. faecalis* than the influent, bulrush DOM isolates, and PLFA. A positive correlation was observed between greater association with the DOM isolates and the inactivation rate of *Ent. faecalis.* The recoverable DOM isolates using the SPE method had similar effect on *Ent. faecalis* inactivation as the whole wetland waters, whereas the non-recoverable components of DOM in the whole wetland waters had an important role in MS2 inactivation.

The role of association of photosensitizers with fecal indicator bacteria on exogenous inactivation was furthered investigated in Chapter 5. The association of *Ent. faecalis* (gram-positive) and *E. coli* (gram-negative) with Rose Bengal (RB) and DOM isolated from secondary municipal wastewater effluent (EfOM) were quantified in the presence and absence of Mg^{2+}. Results showed that the mass of adsorbed RB and EfOM onto *Ent. faecalis* cells was greater than *E. coli* either with or without Mg^{2+}. The presence of Mg^{2+} caused more RB and EfOM to associate with *Ent. faecalis* cells, but only RB was observed to have greater association with *E. coli* cells. Results from inactivation experiments conducted under simulated sunlight were related to results from the adsorption experiments to determine the role of photosensitizer association on exogenous inactivation of the bacteria. The inactivation rates of *Ent. faecalis* generally increased with greater association between photosensitizers and the bacterial cells, except in the case of EfOM and Mg^{2+}. Due to the resistance of *E. coli* to exogenous inactivation, no obvious correlation between photosensitizer association and inactivation rates was observed although there was association with RB and EfOM; the outer membrane likely protects *E. coli* from reactive species generated by the adsorbed senstizers. Irradiated solutions of RB-Beads as a source of exogenous $^1O_2$ did not increase inactivation of *Ent. faecalis* or *E. coli* (compared to senstizer-free solutions), suggesting that association with photosensitizers is required for the exogenous inactivation of *Ent. faecalis.* Interestingly, RB-Bead solution effectively increased the inactivation rate of MS2, which was included for comparison with the bacterial indicators.

6.4 Future Research

A number of opportunities exist to further improve the accuracy of the model developed to predict the endogenous and exogenous inactivation rates of fecal indicator bacteria. The current model uses PAS or total UVB (or total UV) to estimate the endogenous inactivation rates (Chapters 2 and 3). One major limitation of using PAS or total UVB is uncertainty in light irradiance measurements in the range of 280 – 300 nm for developing PAS coefficient values and the correlation factors between total UVB and the endogenous inactivation rates. The prediction of endogenous inactivation can be improved with better measurement of UVB light irradiance in the 280 to 300 nm range. The current model estimates the exogenous inactivation rates based on an assumption that all exogenous processes scale with $[^1O_2]_{ss,bulk}$ (Chapter 3). It is possible that other reactive species (e.g., $^3DOM^*$) are also involved in the exogenous inactivation (Chapter 4). Additionally, association with DOM was shown to have an important influence on the exogenous inactivation rates of organisms (Chapters 4 and 5). Predictions for exogenous inactivation could be more accurate if the model included the involvement of other reactive species, as well as the association between DOM and microorganisms.

Comparison between lab-cultured and indigenous indicator bacteria showed that lab-cultured bacteria were significantly more susceptible to sunlight inactivation than indigenous wastewater bacteria (Chapter 3). The difference between lab-cultured and indigenous indicator bacteria highlighted the challenges with extrapolating results from experiments using lab-cultured indicators to understanding inactivation of indigenous indicators. While it is more convenient to do research with lab-cultured indicator organisms, it is recommended to use indigenous indicator organisms in studies involved with field work. In addition, future work using human pathogens should be conducted to develop a better understanding of differences that may exist between inactivation of lab-cultured indicators and field indicators as compared with human pathogens.

DOM hydrophobicity and molecular size were the primary properties that appeared to influence the ability of DOM to associate with microorganisms (Chapter 4). Results also suggested that several types of interaction might be involved in the association between DOM and microorganisms (e.g., hydrophobicity, electrostatic, and steric interactions). More research is needed to quantify these interations to provide insight into exogenous inactivation mechanism and methods to enhance exogenous inactivation rates.

A demonstration-scale open-water unit process wetland receiving approximately 0.3 MGD of water from the effluent-dominated Santa Ana River was built in the Prado Wetlands in Orange County, CA. The removal performance of pathogens and indicator organismss in the demonstration-scale wetlands has been monitored since it began operation in December 2013. Knowledge on the design, operation, and performance of the Prado open-water wetlands will provide further insight into the utility of open-water wetland cells. The future construction and operation of open-water cells in different locations and receiving diverse influent waters will provide further evidence of the feasibility and viability of the novel open-water wetland design.

References

Barber, L.B., Leenheer, J.A., Noyes, T.I., Stiles, E.A., 2001. Nature and Transformation of Dissolved Organic Matter in Treatment Wetlands. Environ. Sci. Technol. 35, 4805–4816.

Berney, M., Weilenmann, H.-U., Ihssen, J., Bassin, C., Egli, T., 2006a. Specific Growth Rate Determines the Sensitivity of Escherichia Coli to Thermal, UVA, and Solar Disinfection. Appl. Environ. Microbiol. 72, 2586–2593.

Berney, M., Weilenmann, H.-U., Simonetti, A., Egli, T., 2006b. Efficacy of solar disinfection of Escherichia coli, Shigella flexneri, Salmonella Typhimurium and Vibrio cholerae. J. Appl. Microbiol. 101, 828–836.

Bernhard, G., Seckmeyer, G., 1999. Uncertainty of measurements of spectral solar UV irradiance. Journal of Geophysical Research: Atmospheres 104, 14321–14345.

Bezman, S.A., Burtis, P.A., Izod, T.P.J., Thayer, M.A., 1978. Photodynamic Inactivation of E. Coli by Rose Bengal Immobilized on Polystyrene Beads. Photochemistry and Photobiology 28, 325–329.

Bitton, G., 2010. Wastewater Microbiology, Fourth Edition.

Blough, N.V., Zepp, R.G., 1995. Reactive Oxygen Species in Natural Waters, in: Foote, C.S., Valentine, J.S., Greenberg, A., Liebman, J.F. (Eds.), Active Oxygen in Chemistry, Structure Energetics and Reactivity in Chemistry Series (SEARCH Series). Springer Netherlands, pp. 280–333.

Bodhipaksha, L., MacKay, A.A., 2014. Impact of Effluent Discharges on Photochemical Reactive Species Formation in River Waters.

Bodrato, M., Vione, D., n.d. APEX (Aqueous Photochemistry of Environmentally occurring Xenobiotics): a free software tool to predict the kinetics of photochemical processes in surface waters. Environmental Science: Processes & Impacts.

Boehm, A.B., Grant, S.B., Kim, J.H., Mowbray, S.L., McGee, C.D., Clark, C.D., Foley, D.M., Wellman, D.E., 2002. Decadal and Shorter Period Variability of Surf Zone Water Quality at Huntington Beach, California. Environ. Sci. Technol. 36, 3885–3892.

Boehm, A.B., Soetjipto, C., Wang, D., 2012. Solar inactivation of four Salmonella serovars in fresh and marine waters. J Water Health 10, 504–510.

Boehm, A.B., Yamahara, K.M., Love, D.C., Peterson, B.M., McNeill, K., Nelson, K.L., 2009. Covariation and Photoinactivation of Traditional and Novel Indicator Organisms and Human Viruses at a Sewage-Impacted Marine Beach. Environ. Sci. Technol. 43, 8046–8052.

Bonde, G.J., 1963. Bacterial indicators of water pollution : a study of quantitative estimation. Teknisk Forlag, Copenhagen.

Boreen, A.L., Edhlund, B.L., Cotner, J.B., McNeill, K., 2008. Indirect Photodegradation of Dissolved Free Amino Acids: The Contribution of Singlet Oxygen and the Differential Reactivity of DOM from Various Sources. Environ. Sci. Technol. 42, 5492–5498.

Canonica, S., Jans, U., Stemmler, K., Hoigne, J., 1995. Transformation Kinetics of Phenols in Water: Photosensitization by Dissolved Natural Organic Material and Aromatic Ketones. Environ. Sci. Technol. 29, 1822–1831.

Canonica, S., Laubscher, H.-U., 2008. Inhibitory effect of dissolved organic matter on triplet-induced oxidation of aquatic contaminants. Photochemical & Photobiological Sciences 7, 547.

Chaplin, G., Jablonski, N.G., 2009. Vitamin D and the Evolution of Human Depigmentation. Am. J. Phys. Anthropol. 139, 451–461.
Clark, M.M., Lucas, P., 1998. Diffusion and partitioning of humic acid in a porous ultrafiltration membrane. Journal of Membrane Science 143, 13–25.
Cooper, W.J., Zika, R.G., Petasne, R.G., Fischer, A.M., 1989. Sunlight-Induced Photochemistry of Humic Substances in Natural Waters: Major Reactive Species. Water Research 219, 333–362.
Cory, R.M., Cotner, J.B., McNeill, K., 2008. Quantifying Interactions between Singlet Oxygen and Aquatic Fulvic Acids. Environ. Sci. Technol. 43, 718–723.
Craggs, R.J., Zwart, A., Nagels, J.W., Davies-Colley, R.J., 2004. Modelling sunlight disinfection in a high rate pond. Ecological Engineering 22, 113–122.
Cunningham, M.L., Krinsky, N.I., Giovanazzi, S.M., Peak, M.J., 1985. Superoxide anion is generated from cellular metabolites by solar radiation and its components. Journal of Free Radicals in Biology & Medicine 1, 381–385.
D'Andrilli, J., Foreman, C.M., Marshall, A.G., McKnight, D.M., 2013. Characterization of IHSS Pony Lake fulvic acid dissolved organic matter by electrospray ionization Fourier transform ion cyclotron resonance mass spectrometry and fluorescence spectroscopy. Org. Geochem. 65, 19–28.
Dahl, T.A., Midden, W.R., Hartman, P.E., 1987. Pure singlet oxygen cytotoxicity for bacteria. Photochem. Photobiol. 46, 345–352.
Dahl, T.A., Midden, W.R., Hartman, P.E., 1989a. Comparison of killing of gram-negative and gram-positive bacteria by pure singlet oxygen. J Bacteriol 171, 2188–2194.
Dahl, T.A., Valdes-Aguilera, O., Midden, W.R., Neckers, D.C., 1989b. Partition of rose bengal anion from aqueous medium into a lipophilic environment in the cell envelope of Salmonella typhimurium: implications for cell-type targeting in photodynamic therapy. J. Photochem. Photobiol. B, Biol. 4, 171–184.
Davies, M.J., 2003. Singlet oxygen-mediated damage to proteins and its consequences. Biochem. Biophys. Res. Commun. 305, 761–770.
Davies, M.J., Truscott, R.J., 2001. Photo-oxidation of proteins and its role in cataractogenesis. J. Photochem. Photobiol. B, Biol. 63, 114–125.
Davies-Colley, R.J., 2005. Pond disinfection, in: Pond Treatment Technology. IWA Publishing, London, UK, pp. 101–135.
Davies-Colley, R.J., Donnison, A.M., Speed, D.J., 1997. Sunlight wavelengths inactivating faecal indicator microorganisms in waste stabilisation ponds. Water Science and Technology 35, 219–225.
Davies-Colley, R.J., Donnison, A.M., Speed, D.J., 2000. Towards a mechanistic understanding of pond disinfection. Water Science Technology 42, 149–158.
Davies-Colley, R.J., Donnison, A.M., Speed, D.J., Ross, C.M., Nagels, J.W., 1999. Inactivation of faecal indicator micro-organisms in waste stabilisation ponds: interactions of environmental factors with sunlight. Water Research 33, 1220–1230.
Demidova, T.N., Hamblin, M.R., 2005. Effect of Cell-Photosensitizer Binding and Cell Density on Microbial Photoinactivation. Antimicrob Agents Chemother 49, 2329–2335.
Denyer, S.P., Maillard, J., 2002. Cellular impermeability and uptake of biocides and antibiotics in Gram negative bacteria. Journal of Applied Microbiology 92, 35S–45S.

Dittmar, T., Koch, B., Hertkorn, N., Kattner, G., 2008. A simple and efficient method for the solid-phase extraction of dissolved organic matter (SPE-DOM) from seawater. Limnology and Oceanography: Methods 6, 230–235.

Dong, M.M., Rosario-Ortiz, F.L., 2012. Photochemical Formation of Hydroxyl Radical from Effluent Organic Matter. Environ. Sci. Technol. 46, 3788–3794.

Dulin, D., Mill, T., 1982. Development and evaluation of sunlight actinometers. Environ. Sci. Technol. 16, 815–820.

Ehrenberg, B., Malik, Z., Nitzan, Y., 1985. Fluorescence spectral changes of hematoporphyrin derivative upon binding to lipid vesicles, Staphylococcus aureus and Escherichia coli cells. Photochem. Photobiol. 41, 429–435.

Facklam, R.R., Collins, M.D., 1989. Identification of Enterococcus species isolated from human infections by a conventional test scheme. J Clin Microbiol 27, 731–734.

Fein, J.B., Boily, J.-F., Güçlü, K., Kaulbach, E., 1999. Experimental study of humic acid adsorption onto bacteria and Al-oxide mineral surfaces. Chemical Geology 162, 33–45.

Fisher, M.B., Iriarte, M., Nelson, K.L., 2012. Solar water disinfection (SODIS) of Escherichia coli, Enterococcus spp., and MS2 coliphage: effects of additives and alternative container materials. Water Research (Oxford) 46.

Fisher, M.B., Love, D.C., Schuech, R., Nelson, K.L., 2011. Simulated Sunlight Action Spectra for Inactivation of MS2 and PRD1 Bacteriophages in Clear Water. Environ. Sci. Technol. 45, 9249–9255.

Fleming-Singer, M.S., Horne, A.J., 2006. Balancing wildlife needs and nitrate removal in constructed wetlands: The case of the Irvine Ranch Water District's San Joaquin Wildlife Sanctuary. Ecol. Eng. 26, 147–166.

Florida Department of Environmental Protection, 2011. Orlando Easterly Wetlands.

Fout, G.S., Dahling, D.R., Safferman, R.S., 2001. Concentration and processing of waterborne viruses by positive charge 1MDS cartridge filters and organic flocculation, in: USEPA Manual of Methods for Virology.

Frost, P.C., Maurice, P.A., Fein, J.B., 2003. The effect of cadmium on fulvic acid adsorption to Bacillus subtilis. Chemical Geology 200, 217–224.

George, S., Hamblin, M.R., Kishen, A., 2009. Uptake pathways of anionic and cationic photosensitizers into bacteria. Photochem Photobiol Sci 8, 788–795.

Gonsior, M., Zwartjes, M., Cooper, W.J., Song, W., Ishida, K.P., Tseng, L.Y., Jeung, M.K., Rosso, D., Hertkorn, N., Schmitt-Kopplin, P., 2011. Molecular characterization of effluent organic matter identified by ultrahigh resolution mass spectrometry. Water Res. 45, 2943–2953.

Guerard, J.J., Miller, P.L., Trouts, T.D., Chin, Y.-P., 2009. The role of fulvic acid composition in the photosensitized degradation of aquatic contaminants. Aquatic Sciences 71, 160–169.

Gueymard, C.A., 2003. User Interface: Simple Model of Atmospheric Radiative Transfer of Sunshine.

Gueymard, C.A., 2005. Interdisciplinary applications of a versatile spectral solar irradiance model: A review. Energy 30, 1551–1576.

Gueymard, C.A., 2008. Prediction and validation of cloudless shortwave solar spectra incident on horizontal, tilted, or tracking surfaces. Solar Energy 82, 260–271.

Haag, W.R., Hoigne, J., 1986. Singlet Oxygen in surface waters - Part III: Photochemical formation and steady-state concentrtaions in various types of waters. Environ. Sci. Technol. 20, 341–348.

Haag, W.R., Hoigne´, J., Gassman, E., Braun, A., 1984. Singlet oxygen in surface waters — Part I: Furfuryl alcohol as a trapping agent. Chemosphere 13, 631–640.

Hamblin, M.R., O'Donnell, D.A., Murthy, N., Rajagopalan, K., Michaud, N., Sherwood, M.E., Hasan, T., 2002. Polycationic photosensitizer conjugates: effects of chain length and Gram classification on the photodynamic inactivation of bacteria. J. Antimicrob. Chemother. 49, 941–951.

Hancock, R.E., 1997. The bacterial outer membrane as a drug barrier. Trends Microbiol. 5, 37–42.

Helms, J.R., Stubbins, A., Ritchie, J.D., Minor, E.C., Kieber, D.J., 2008. Absorption spectral slopes and slope ratios as indicators of molecular weight, source and photobleaching of chromophoric dissolved organic matter. Limnology and Oceanography 53.

Horne, A.J., Fleming-Singer, M., 2005. Phytoremediation Using Constructed Treatment Wetlands: An Overview. Bioremediation of aquatic and terrestrial ecosystems 329.

Jablonski, N.G., Chaplin, G., 2010. Human skin pigmentation as an adaptation to UV radiation. Proceedings of the National Academy of Sciences 107, 8962–8968.

Jagger, J., 1985. Solar-UV actions on living cells. Praeger.

Jasper, J.T., Jones, Z.L., Sharp, J.O., Sedlak, D.L., 2014a. Biotransformation of Trace Organic Contaminants in Open-Water Unit Process Treatment Wetlands. Environ. Sci. Technol. 48, 5136–5144.

Jasper, J.T., Jones, Z.L., Sharp, J.O., Sedlak, D.L., 2014b. Nitrate Removal in Shallow, Open-Water Treatment Wetlands. Environ. Sci. Technol. 48, 11512–11520.

Jasper, J.T., Nguyen, M.T., Jones, Z.L., Ismail, N.S., Sedlak, D.L., Sharp, J.O., Luthy, R.G., Horne, A.J., Nelson, K.L., 2013. Unit Process Wetlands for Removal of Trace Organic Contaminants and Pathogens from Municipal Wastewater Effluents. Environmental Engineering Science 30, 421–436.

Jasper, J.T., Sedlak, D.L., 2013. Phototransformation of Wastewater-Derived Trace Organic Contaminants in Open-Water Unit Process Treatment Wetlands. Environ. Sci. Technol.

Kadir, K., 2010. Sunlight-Mediated Inactivation Mechanisms of Enteroccocus faecalis and Escherichia coli in Waste Stabilization Ponds.

Kadir, K., Nelson, K.L., 2014. Sunlight mediated inactivation mechanisms of Enterococcus faecalis and Escherichia coli in clear water versus waste stabilization pond water. Water Research 50, 307–317.

Kadlec, R.H., 2009. Comparison of free water and horizontal subsurface treatment wetlands. Ecol. Eng. 35, 159–174.

Kadlec, R.H., Wallace, S., 2009. Treatment Wetlands, 2nd ed. CRC Press, Boca Raton.

Kirk, J.T.O., 1980. Relationship between nephelometric turbidity and scattering coefficients in certain Australian waters. Mar. Freshwater Res. 31, 1–12.

Kirk, J.T.O., 1981. Monte Carlo study of the nature of the underwater light field in, and the relationships between optical properties of, turbid yellow waters. Marine and Freshwater Research 32.

Kirk, J.T.O., 2010. Light and Photosynthesis in Aquatic Ecosystems. Cambridge University Press.

Kohn, T., Grandbois, M., McNeill, K., Nelson, K.L., 2007. Association with natural organic matter enhances the sunlight-mediated inactivation of MS2 coliphage by singlet oxygen. Environ. Sci. Technol. 41, 4626–4632.

Kohn, T., Nelson, K.L., 2007. Sunlight-mediated inactivation of MS2 coliphage via exogenous singlet oxygen produced by sensitizers in natural waters. Environ. Sci. Technol. 41, 192–197.

Lambert, P.A., 2002. Cellular impermeability and uptake of biocides and antibiotics in Gram-positive bacteria and mycobacteria. Journal of Applied Microbiology 92, 46S–54S.

Lamberts, J.J.M., Schumacher, D.R., Neckers, D.C., 1984. Novel rose bengal derivatives: synthesis and quantum yield studies. J. Am. Chem. Soc. 106, 5879–5883.

Latch, D.E., McNeill, K., 2006. Microheterogeneity of Singlet Oxygen Distributions in Irradiated Humic Acid Solutions. Science 311, 1743 –1747.

Lee, E., Shon, H.K., Cho, J., 2014. Role of wetland organic matters as photosensitizer for degradation of micropollutants and metabolites. J. Hazard. Mater. 276, 1–9.

Leenheer, J.A., Croué, J.-P., 2003. Peer Reviewed: Characterizing Aquatic Dissolved Organic Matter. Environ. Sci. Technol. 37, 18A–26A.

Leifer, A., 1988. The kinetics of environmental aquatic photochemistry: theory and practice. American Chemical Society.

Lightbody, A.F., Avener, M.E., Nepf, H.M., 2008. Observations of short-circuiting flow paths within a free-surface wetland in Augusta, Georgia, U.S.A. Limnology and Oceanography 53, 1040–1053.

Love, D.C., Silverman, A., Nelson, K.L., 2010. Human Virus and Bacteriophage Inactivation in Clear Water by Simulated Sunlight Compared to Bacteriophage Inactivation at a Southern California Beach. Environ. Sci. Technol. 44, 6965–6970.

Madigan, M.T., Martinko, J.M., Clark, D.P., Stahl, D.A., 2010. Brock Biology of Microorganisms. Pearson.

Maier, R.M., Pepper, I.L., Gerba, C.P., 2009. Environmental Microbiology. Academic Press.

Malik, Z., Ladan, H., Nitzan, Y., 1992. Photodynamic inactivation of Gram-negative bacteria: problems and possible solutions. J. Photochem. Photobiol. B, Biol. 14, 262–266.

Maraccini, P.A., Ferguson, D.M., Boehm, A.B., 2011. Diurnal Variation in Enterococcus Species Composition in Polluted Ocean Water: A Potential Role for the Enterococcal Carotenoid in Protection Against Photoinactivation. Appl. Environ. Microbiol.

Mattle, M.J., Vione, D., Kohn, T., 2015. Conceptual Model and Experimental Framework to Determine the Contributions of Direct and Indirect Photoreactions to the Solar Disinfection of MS2, phiX174, and Adenovirus. Environ. Sci. Technol. 49, 334–342.

Maurice, P.A., Manecki, M., Fein, J.B., Schaefer, J., 2004. Fractionation of an Aquatic Fulvic Acid upon Adsorption to the Bacterium, Bacillus subtilis. Geomicrobiology Journal 21, 69–78.

McGuigan, K.G., Conroy, R.M., Mosler, H.-J., Du Preez, M., Ubomba-Jaswa, E., Fernandez-Ibañez, P., 2012. Solar water disinfection (SODIS): a review from bench-top to roof-top. J. Hazard. Mater. 235-236, 29–46.

Mostafa, S., Rosario-Ortiz, F.L., 2013. Singlet Oxygen Formation from Wastewater Organic Matter. Environ. Sci. Technol. 47, 8179–8186.

Nitzan, Y., Gutterman, M., Malik, Z., Ehrenberg, B., 1992. Inactivation of Gram-negative bacteria by photosensitized porphyrins. Photochemistry and Photobiology 55, 89–96.

Nitzan, Y., Pechatnikov, I., 2011. Chapter 3. Approaches to Kill Gram-negative Bacteria by Photosensitized Processes, in: Hamblin, M.R., Jori, G. (Eds.), Comprehensive Series in Photochemical & Photobiological Sciences. Royal Society of Chemistry, Cambridge, pp. 45–67.

Nitzan, Y., Wexler, H.M., Finegold, S.M., 1994. Inactivation of anaerobic bacteria by various photosensitized porphyrins or by hemin. Curr. Microbiol. 29, 125–131.
Ogilby, P.R., 2010. Singlet oxygen: there is indeed something new under the sun. Chem Soc Rev 39, 3181–3209.
Orange County Water District, 2008. Prado Wetlands.
Paul, A., Hackbarth, S., Vogt, R.D., Röder, B., Burnison, B.K., Steinberg, C.E.W., 2004. Photogeneration of singlet oxygen by humic substances: comparison of humic substances of aquatic and terrestrial origin. Photochem. Photobiol. Sci. 3, 273–280.
Pedersen, S., Bloch, P.L., Reeh, S., Neidhardt, F.C., 1978. Patterns of protein synthesis in E. coli: a catalog of the amount of 140 individual proteins at different growth rates. Cell 14, 179–190.
Pellieux, C., Dewilde, A., Pierlot, C., Aubry, J.-M., 2000. [18] Bactericidal and virucidal activities of singlet oxygen generated by thermolysis of naphthalene endoperoxides, in: Singlet Oxygen, UV-A, and Ozone. Academic Press, pp. 197–207.
Pilarek, M., Glazyrina, J., Neubauer, P., 2011. Enhanced growth and recombinant protein production of Escherichia coli by a perfluorinated oxygen carrier in miniaturized fed-batch cultures. Microbial Cell Factories 10, 50.
Quiñónez-Díaz, M.J., Karpiscak, M.M., Ellman, E.D., Gerba, C.P., 2001. Removal of pathogenic and indicator microorganisms by a constructed wetland receiving untreated domestic wastewater. J. Environ. Sci. Health. Part A Toxic/Hazard. Subst. Environ. Eng. 36, 1311–1320.
Reed, R.H., 2004. The inactivation of microbes by sunlight: solar disinfection as a water treatment process. Adv. Appl. Microbiol. 54, 333–365.
Richard, C., Canonica, S., 2005. Aquatic Phototransformation of Organic Contaminants Induced by Coloured Dissolved Natural Organic Matter, in: Boule, P., Bahnemann, D.W., Robertson, P.K.J. (Eds.), Environmental Photochemistry Part II, The Handbook of Environmental Chemistry. Springer Berlin Heidelberg, pp. 299–323.
Rosado-Lausell, S.L., Wang, H., Gutiérrez, L., Romero-Maraccini, O.C., Niu, X.-Z., Gin, K.Y.H., Croué, J.-P., Nguyen, T.H., 2013. Roles of singlet oxygen and triplet excited state of dissolved organic matter formed by different organic matters in bacteriophage MS2 inactivation. Water Res. 47, 4869–4879.
Rose, R.K., Matthews, S.P., Hall, R.C., 1997. Investigation of calcium-binding sites on the surfaces of selected gram-positive oral organisms. Arch. Oral Biol. 42, 595–599.
Schaap, A.P., Thayer, A.L., Blossey, E.C., Neckers, D.C., 1975. Polymer-based sensitizers for photooxidations. II. J. Am. Chem. Soc. 97, 3741–3745.
Sengupta, M.E., Thamsborg, S.M., Andersen, T.J., Olsen, A., Dalsgaard, A., 2011. Sedimentation of helminth eggs in water. Water Res. 45, 4651–4660.
Sharpless, C.M., Aeschbacher, M., Page, S.E., Wenk, J., Sander, M., McNeill, K., 2014. Photooxidation-Induced Changes in Optical, Electrochemical, and Photochemical Properties of Humic Substances. Environ. Sci. Technol. 48, 2688–2696.
Sherman, J.M., 1938. The Enterococci and Related Streptococci1. J Bacteriol 35, 81–93.
Shon, H.K., Vigneswaran, S., Snyder, S.A., 2006. Effluent Organic Matter (EfOM) in Wastewater: Constituents, Effects, and Treatment. Critical Reviews in Environmental Science and Technology 36, 327–374.

Silverman, A.I., Nguyen, M.T., Schilling, I.E., Wenk, J., Nelson, K.L., 2015. Sunlight Inactivation of Viruses in Open-Water Unit Process Treatment Wetlands: Modeling Endogenous and Exogenous Inactivation Rates. Environ. Sci. Technol.

Silverman, A.I., Peterson, B.M., Boehm, A.B., McNeill, K., Nelson, K.L., 2013. Sunlight Inactivation of Human Viruses and Bacteriophages in Coastal Waters Containing Natural Photosensitizers. Environ. Sci. Technol. 47, 1870–1878.

Sinton, L., Hall, C., Braithwaite, R., 2007. Sunlight inactivation of Campylobacter jejuni and Salmonella enterica, compared with Escherichia coli, in seawater and river water. Journal of Water and Health 5, 357.

Sinton, L.W., Finlay, R.K., Lynch, P.A., 1999. Sunlight Inactivation of Fecal Bacteriophages and Bacteria in Sewage-Polluted Seawater. Appl. Environ. Microbiol. 65, 3605–3613.

Sinton, L.W., Hall, C.H., Lynch, P.A., Davies-Colley, R.J., 2002. Sunlight Inactivation of Fecal Indicator Bacteria and Bacteriophages from Waste Stabilization Pond Effluent in Fresh and Saline Waters. Appl. Environ. Microbiol. 68, 1122–1131.

Twardowski, M.S., Boss, E., Sullivan, J.M., Donaghay, P.L., 2004. Modeling the spectral shape of absorption by chromophoric dissolved organic matter. Marine Chemistry 89, 69–88.

US EPA, 2001. The Living Machine (R) Wastewater Treatment Technology- An Evaluation of Performance and System| US EPA [WWW Document]. URL http://yosemite.epa.gov/water/owrccatalog.nsf/9da204a4b4406ef885256ae0007a79c7/5d2a6584de0e37df85256b06007254a3!OpenDocument (accessed 8.18.14).

US EPA, R. 9, 2004. NPDES Wastewater & Stormwater Permits - Water | Pacific Southwest | US EPA [WWW Document]. URL http://www.epa.gov/region9/water/npdes/index.html (accessed 9.28.14).

Valduga, G., Bertoloni, G., Reddi, E., Jori, G., 1993. Effect of extracellularly generated singlet oxygen on gram-positive and gram-negative bacteria. J. Photochem. Photobiol. B, Biol. 21, 81–86.

Vione, D., Falletti, G., Maurino, V., Minero, C., Pelizzetti, E., Malandrino, M., Ajassa, R., Olariu, R.-I., Arsene, C., 2006. Sources and Sinks of Hydroxyl Radicals upon Irradiation of Natural Water Samples. Environ. Sci. Technol. 40, 3775–3781.

Vymazal, J., 2011. Constructed Wetlands for Wastewater Treatment: Five Decades of Experience†. Environ. Sci. Technol. 45, 61–69.

Wehner, J.F., Wilhelm, R.H., 1956. Boundary conditions of flow reactor. Chemical Engineering Science 6, 89–93.

Weishaar, J.L., Aiken, G.R., Bergamaschi, B.A., Fram, M.S., Fujii, R., Mopper, K., 2003. Evaluation of Specific Ultraviolet Absorbance as an Indicator of the Chemical Composition and Reactivity of Dissolved Organic Carbon. Environ. Sci. Technol. 37, 4702–4708.

Wilkinson, F., Brummer, J.G., 1981. Rate constants for the decay and reactions of the lowest electronically excited singlet state of molecular oxygen in solution. Journal of Physical and Chemical Reference Data 10, 809.

Zepp, R.G., Cline, D.M., 1977. Rates of direct photolysis in aquatic environment. Environ. Sci. Technol. 11, 359–366.